12-15-2014

Novel Biofabrication Technologies to Recapitulate *In Vivo* Geometries in Collagen Hydrogels

Veronica Rodriguez-Rivera
University of South Carolina - Columbia

NOVEL BIOFABRICATION TECHNOLOGIES TO RECAPITULATE *IN VIVO* GEOMETRIES IN COLLAGEN HYDROGELS

by

Veronica Rodriguez-Rivera

Bachelor of Science
University of Puerto Rico-Mayaguez, 2007

Submitted in Partial Fulfillment of the Requirements

For the Degree of Doctor of Philosophy in

Chemical Engineering

College of Engineering and Computing

University of South Carolina

2014

Accepted by:

John W. Weidner, Major Professor

Michael J. Yost, Major Professor

Richard L. Goodwin, Committee Member

Ehsan Jabbarzadeh, Committee Member

Mark J. Uline, Committee Member

Francis Gadala-Maria, Committee Member

Lacy Ford, Vice Provost and Dean of Graduate Studies

ACKNOWLEDGEMENT

I am truly grateful to my family: Mom (Cecy), Dad (Emilio), and my sister (Vanessa). This work would not be possible without their support and guidance. I would like to express my deepest gratitude to my mentor Dr. Michael J. Yost for his excellent guidance, caring, patience, providing an excellent atmosphere for doing research and above all for being an extraordinary friend. I would like to thank my lab co-workers over the years: Mary O. Morales, Alexander Wagner, Eric Yost, Jeffery Gardner, Heather Bainbridge, Dr. Stephen Fann, Dr. Bennett W. Calder, and Dr. J Matthew Rhett for their collaboration and their input at every stage of this dissertation work. I would like to thank Michael Gore and Jeffrey Davis from the School of Medicine at the University of South Carolina for their help and collaboration for this project. Also, I wish to thank my advisor Dr. John W Weidner and Dr. Francis Gadala-Maria, Dr. Mark Uline, Dr. Richard L. Goodwin, and Dr. Ehsan Jabbarazeh for serving as committee members and providing advice on this work.

This work was supported by Alfred P. Sloan Foundation , the South East Alliance for Graduate Education and the Professoriate (SEAGEP), NIH-NIDCR IRO1DE019355 (MJ Yost, PI) , and NSF-EPSCoR(EPS-0903795).

ABSTRACT

Tissue engineering and regenerative medicine aims to restore form and function to tissues that have been lost or damaged due to disease, congenital defect, or trauma. Biomaterials suitable to restore these complex tissues need to provide a balance between chemical and mechanical properties, providing accurate cell-matrix interaction and induce in vivo behaviors such as proliferation, differentiation and migration. It also requires that physical and chemical cues be presented to the body in the proper temporal and spatial pattern. The extracellular matrix exerts forces that are transmitted through focal adhesion causing changes in the cell behavior. The hypothesis for this dissertation work was that by using the ideal substrate composition, the geometrical features and the proper elasticity of the substrate, we can recapitulate the microenviroments of the in vivo niche and control cell behavior.

The self renewal capabilities of muscle stem cells, satellite cells, are lost once they are culture in a rigid environment where they commit to become skeletal myocytes. In our studies, we tuned the elasticity of a collagen hydrogel to their in vivo elastic modulus and we maintain the quiescence phenotype. We developed reaction electrospinning, which is a technique that combines two processes: electrospinning and fibrillogenesis. For the first time in literature, we show that as we spin collagen monomers and microfibrils using benign solvents, they undergo fibrillogenesis resulting

in fibrous collagen scaffolds. Also, we developed a sacrificial material, BSA rubber, which can deliver specific geometrical templates to a collagen material, recapitulating the internal three-dimensional architectures. Our prototype consist of a 3D branched architecture using type I collagen.

Overall, we developed fabrication techniques that allow us to tune the elasticity of the matrix, create fibrous scaffolds, and incorporate the geometrical features into an in vitro collagen scaffold. These techniques combine state of the art imaging, micromachining and selective enzymatic activity to create three dimensional biomaterials. The overall goal of this work is to fabricate custom made tissue scaffolds that replicate in vivo tissue composition, architecture, and cell population for broad application in tissue engineering. These new biomaterials will enable the modulation of cell potential, and thus, accelerate discovery in the field of regenerative medicine.

TABLE OF CONTENTS

LIST OF TABLES

LIST OF FIGURES

CHAPTER 1:

INTRODUCTION AND BACKGROUND

1.1 INTRODUCTION

Tissue engineering and regenerative medicine aims to restore form and function to tissues that have been lost or damaged due to disease, congenital defect, or trauma. Restoration of these complex tissues requires ideal communication between cells, as well as between cell and extracellular matrix. It also requires that physical and chemical cues be presented to the body in the proper temporal and spatial pattern. The extracellular matrix is responsible for providing the adequate balance between physical features, chemical composition, and mechanical forces that influence the cells. Recently, growing evidence shows that mechanical forces have a more profound effect that previous researcher realized, generating a cascade of intracellular events that causes changes in cell behavior [1, 2]. The microenvironment exerts forces that are transmitted through focal adhesion causing changes in the cell behavior from maintaining quiescence to inducing activation of cells.

We have developed several fabrication techniques that allow us to tune the elasticity of the matrix, create fibrous scaffolds, and incorporate the geometrical features into an in vitro scaffold. Using our newly developed biofabrication techniques, we are able to control the composition of the matrix, the forces that exert on the cells, and the topography that dictates the internal structure of the native tissue. The aim of this dissertation work was to create the next generation of biomaterials that are biocompatible, contain specific 3D architectural features, promotes in vivo cell behaviors, and are functional, making them ideal candidates for tissue transplantation. We use collagen as scaffold material and change the elasticity of it in order to control cellular behavior. We developed reaction electrospinning, which is a technique that

allows us to mimic the collagen fibrous nature of the microenvironments by combining two processes: electrospinning and fibrillogenesis. Also, we developed a sacrificial material that can deliver specific geometrical templates to a collagen material, recapitulating the voids and inside three-dimensional architectures. The overall goal of this work is to fabricate custom made tissue scaffolds that replicate in vivo tissue composition, architecture, and cell population for numerous applications in tissue engineering such as modeling, drug therapeutics, and replacement of lost or damaged tissue (figure 1.1).

The aim of this chapter is to present the many factors that affect the cellular behavior and specific techniques in which we can control them. We examined how the mechanical forces translates into changes at the cellular level. As seen in literature, the extracellular matrix components play a crucial role in the cell behavior. Collagen is a natural component of the extracelllular matrix that has been shown to induce in vivo cell behaviors[3, 4]. We showed the importance of this protein, how the molecule is produced and the extracellular events that lead to the production of collagen fibers. We introduce several biofabrication techniques that have been implemented in order to control the physical and mechanical properties of the matrix, as well as the spatial arragement of natural matrix components and cell population.

1.2 MECHANICAL FORCES

Cells respond to the mechanical environment by mechanotransduction, inducing changes in protein composition, morphology, phenotype, and lineage [2, 5, 6]. Cells can sense and respond to mechanical forces such as shear stress, mechanical strain, matrix topography, and rigidity (figure 1.2)[6]. In this section, we show how the stimulus provided by each of the mechanical forces translated into a specific cellular response.

1.2.1 Mechanical Strain

There is a balance of forces between cells and ECM though the actin cytoskeleton. Any external strain that they sense on the matrix is transfer to the cell by the surface molecules such as integrins causing changes in the organization of their cytoskeleton, and sends signals in which they can switch between cell growth and differentiation. This effect has been well documented in different cell lineages such as osteogenic[7], vascular[8], and myogenic[9].

Riha et al showed that embryonic stem cells subjected to periodic cyclic strain induces vascular smooth muscle cell differentiation[8]. They showed a spindle shaped morphology and parallel alignment compared to a round shape as seen in the static state. The mechanical strain by itself was strong stimulus to drive differentiation into a specific linage. This behavior has been seen in other cell types such as adipose derived stem cells, where presence of uniaxial strain caused upregulation of skeletal muscle related genes such as MyoD, Myog, and Mysoin heavy chain [9].

These studies showed a synergistic effect between soluble growth factors and mechanical strain forces, but the degree of the differentiation according to mRNA and

protein expression could not be achieved just by chemical factors. It has even been shown that the direction of the strain greatly influences the protein expression [10]. The strain that the substrate is subjected to can be sensed by the cells through the focal adhesions causes rearrangement in the cytoskeleton of the cells and determines the cell lineage.

1.2.2 Shear Stress

The in vivo environment of the cells is constantly exposed to dynamic shear stress caused by liquids such as blood and interstitial fluid. Bone is constantly subjected to forces that produces strain and pressure gradient that induces flow of the interstitial fluid. This movement results in shear stress development. The normal shear stress in the bone marrow is 8-30 dyn/cm^2 [11]. Inside the vasculature, the blood flow causes constant shearing forces of 15 dyn/cm^2 . Previous studies have the constant exposure of the vessel walls to a physiological shear stress creates a protective barrier for the endothelium against the inflammatory response activity and prevents apoptosis of endothelial cells[12].

Wang showed that by exposing embryonic stem cells to a physiological shear stress of 15 dyn/cm^2, the MSC (murine embryonic mesenchymal cells) aligned to flow and differentiated into endothelial cells, which are cells that line the lumen of the vasculature[13]. There was an upregulation of angiogenic growth factors and a downregulation of growth factors associated with smooth muscle cell differentiation.

The shearing environment induces specific behavior depending on the cell type. The endothelial cells located in the vasculature lumen are the most affected by these forces.

The shear stress is responsible for the maintenance of the lumen wall and the increase of angiogenesis and vasculogenesis potential.

1.2.3 Topography

Cells can sense specific features of their environment and regulate their shape, apoptosis, proliferation, or differentiation. The extracellular matrix where cells reside is made of a complex arrangement of molecules organized in fiber and sheets that range in scale size from nanometers to centimeters. The specific spatial arrangement the cells and the extracellular matrix components induce unique responses on cells. Also, there has been well documented that a 3D environment induces behaviors not seen in 2D environments [14-16].

Ankam et al demonstrated that only by changing from an isotropic to anisotropic environment, he obtained two different lineages: neurons and glial cells[17]. Yost et al. showed that the spiral arrangement of the 3D collagen scaffold induce in vivo behavior such as contraction of the myotubes[3].

The topographical cues regulate the cell shape, migration, and proliferation of a wide variety of cells. In our work, we are able to transfer the geometrical features of native tissue into a mold that will be used to deliver the dimensions to a collagen scaffold. Also, we developed the techniques to engineer a fibrous scaffold network that resembles the complex fibrous nature of the extracellular matrix. This three-dimensional fibrous scaffold provides the ideal architectural features that closely resemble the in vivo tissue.

1.2.4 Substrate Rigidity

Another mechanical property that can affect the cell behavior is the substrate stiffness or rigidity which is the ability of the material to undergo deformation in response to an applied force by the cell. If the substrate resists deformation, it results on changes in their cellular behavior. Each tissue has a specific elasticity and the cell response depend strongly on the stiffness that they sense [18].

Gilbert et al showed that the satellite cells or muscle precursor cells, maintained their quiescent phenotype in a PEG hydrogel that mimic the stiffness of the in vivo microenviroment, which has an elastic modulus of 12 KPa. Pax 7, which is a transcription factor that is expressed on quiescent cells, its maintained on cells with elasticity of 12 KPa[19]. Other researchers have found that in using mesechymal stem cells and placing on environment with elasticity of 80 KPa, cells expressed osteogenic differentiation markers [20].

The rigidity of the matrix has an effect in the quiescence and differentiation of cells. Following Glibert et al work, we create collagen hydrogel that mimic the satellite cell niche. We determined that the elasticity by itself was the dominant factor in maintaining the specific phenotype expression. The relationship between the elasticity of the substrate and the stem cell is an important factor in the development of therapeutic biomaterials.

Overall, the ability of cells to sense forces, internalize them by transmitting them to their interior or to other cells, and transduce them into biochemical signals is vital in the control of cell responses such as differentiation, proliferation and/or motility[21].

These mechanical forces govern the functionality of the tissue and are vital in the development of functional grafts.

1.3 THE EXTRACELLULAR MATRIX (ECM) COMPONENTS

The components of the matrix affects also the cell behavior. The extracellular matrix of the connective tissues is composes of diverse proteins that provide structural integrity and physiological functions. The different arragements of the fibrillar components and soluble proteins dictates the biological and physical characteristics. The cell-matrix interactions dictates proliferation, migration and differentiation of the cell [1, 9, 22, 23]. There is a wide variety of materials that has been studied that aims to mimic the microenvironment. They are mostly divided into synthetic and natural materials. Natural materials, such as collagen, have been shown to provide the necessary cues to adopt in vivo behaviors [3, 4, 23].

There are many different types of collagen that vary in function, size, composition, and tissue distribution. This family is composed of about 26 genetically distint collagen types. Collagen is the most abundant structural protein in all animals extracellular matrix, being the primary component of the connective tissue [6]. It comprises three quarters of the dry weight of human skin[24]. Collagen is present in 30% of the total protein and about 90% of that is represented by Type I collagen[25]. This protein has wide variety of applications in the cosmetic, biomedical, pharmaceutical, and leather industry [26]. Its natural abundance and its ability to provide the necessary biological cues to direct cell behavior have prompted the development of collagen as a biomaterial [3, 4].

Collagens are triple helical proteins which are distributed throughout the body and are vital for many functions such as cell adhesion, migration, tissue scaffolding, and tissue repair among others[27]. It contains three polypeptides (α) chains, each one forms an extended left-handed helix with 18 amino acids per turn[28]. All three chains are staggered by one residue and supercoiled in a right handed form to produce the triple helix. Each polypeptide chain has a repeating sequence of Gly-X-Y triplet, in which every glycine residues occupies every third position and X and Y are frequently proline and hydroproline respectively. Glycine is small enough to be packed into the core of the helix. The three α chains are held together by hydrogen bonds[29].

1.3.1 Collagen Synthesis

The collagen fibers appear early during embryonic development. They become responsable for the functionality of the tissues such as bone, skeletal muscle, and skin and contibute to the integrity of blood vessels . The biosynthesis of the collagen that starts with gene transcription of the genes and formation of mRNA in the nucleus followed by postraslational modifications, secretion and extracellular processing to form the collagen fibers is a very dynamic and complex process[6]. Initially, the procollagen α chains that are made of approximatekly 1000 amino acids of length are synthesized [30]. The procollagen contains N and C terminal ends (propeptides). The C-propetide plays a role in the initiation of the triple helix formation. [6, 31]. It contains chain recognition sites that controls which three α-chain come together to form the triple helix structure[32].

The composition and the aggregation of the α –chains vary depending on the collagen type, and can be classified as heterotrimers (have two or more different α-

chains) and homotrimers (have three identical α –chains). Collagen type I has two α1 and one α2. The collagen tye I molecule contints five domains: N-propeptide, N-telopeptide, triple helix, C-telopeptide, and C-propeptide. The triple helical part of the molecule is composed of Gly-X-Y, that repeats along the structure. The collagen molecules are packaged in the golgi compartment within the cells into secretory vesicles that can travel and be release in the extracellular matrix[6].

1.3.2 Collagen Fibrillogenesis

Fibrillogenesis is the process responsible for the formation of filamentous fibrils by orderly self- assembly of the collagen molecules. This process starts when the molecules are secreted into the extracellular matrix. The fibril forming collagens are the only ones that undergo this process. These type of collagen are type I, II, III, and V, which they can spontanously aggregate after being processed in the extracelular matrix. The ability to self assemble is encoded in the molecular strcuture. The enzymatic cleavage of the C-propetides and N-propetides is an essential step for inducingng the fibril formation. The hydrophobic and electrostatic interaction of collagen monomers are responsible for the formation of the quarter-staggered arrangement of collagen microfibrils, which then aggregate into five-stranded fibrils and further proceed to form larger fibrils (figure 1.3) [28, 33]. The molecular arrangement of the fibrils is stabilized by the formation of covalent cross-links in their N-telopeptide and C-telopeptide by hydroxylation of the lysine residues. The nonhelical telopeptides of type I collagen contains the specific residue involved in the aldehyde-mediated covalent crosslinking of the fibrils. Crosslinks between the molecules is vital to stabilize the structure and make it resitant to physical forces and enzymatic attacks. The fiber formation process produces

collagen fibrils that have a characteristic D periodic cross striated fibrils (D=67 nm, axial periodicity) (figure 1.4).

In vitro fibrillogenesis in a multistep assembly process[34]. In in vitro fibrillogenesis, the collagen is acidified to break the hydrophobic and ionic interactions. This way, we generate a combination of collagen momoners and microfibrils that are stacked in a 4D conformation.There are three routes used to raise the temperature and pH of the acidified collagen and induce fibrillogenesis[35]. By neutralizing and warming up the solution, molecules aggregate into lateral to end to end formation. Then, the fibrils can be covalent crosslinks and produce the collagen fibers.

There are some difference between the in vivo and in vitro self assembly process. One of the main differences between both systems are the prescence of other components such as non collagenous proteins, glycoproteins, and other components are normally abscense in the purified collagen. Fibroblast also control the specific spatial orientation of the fibrils that they deposit. These cells are the responsible of depositing the right tissue specific orientation, either parallel or random. The cells localizes the binding sites of the collagen and regulates the fibril formation in vivo which is essential to the formation of a long range of specific packing assemblies that are tissue specific [25]. In vivo fibril formation is influence by others molecules as well, such as collagen Type V and XI, fibronectin, and proteglycans that infuluences the nucleation, growth, quality, quantity and diameter of the fibrils and this behavior is seem to be tissue specific [27, 36-39] For example, in the tendon the fibrils assemble in parallel bundles while in the conrea they assemble into orthagonal lattices[39]. Another difference is the initial stage of aggregation of the collagen molecules. The solutions in the starting product are

polydisperse, containing dilute collagen molecules of monomers, dimers, higher aggegates and a small presence of covalently cross link fibrils. In the in vivo process, the fibroblast secrete the collagen moleclues in high concentration of procollagen which is the precursor form of collagen[33].

Collagen has been shown to have the ideal properties to become an integral component of tissue scaffolds. By understanding its molecular properties, as well as the fibrillogennessis process, we can manipulate the protein and mimic the microenviroments.

1.4 BIOFABRICATION

Taking in consideration the factors that affect the cell behavior, researchers have develop techniques to account for all this parameters. The goal of the biofabrication techniques is to engineer tissue scaffolds where we can control spatial orientation of cells and extracellular matrix component, mimic the architectural features, elasticity, and cell population to create a reasonable mimic of the native tissue.

Various fabrication techniques have been developed. Each technique has its advantages and disadvantages in producing tissue scaffolds. The fabrication techniques fall under two categories: conventional and advanced. The conventional techniques include the use of synthetic and natural traditional materials to make porous structures. Some examples are solvent-casting [40], freeze drying, and melt molding. These techniques have difficulties in the structure porosity and creating interconnected channels within the scaffold. Advanced techniques include sterolitography [17], molding, 3D

printing[41, 42], and electrospinning [43, 44] among others[45, 46]. These techniques made used of computer aid interface to direct the specific spatial arrangement of the cells and extracellular matrix.

Among these techniques, electrospinning and 3D printing at the moment are the most successful techniques that mimic the fibrous nature of the extracellular matrix and control the placement of extracellular matrix component and cells, respectively.

The combination of composition of the substrate, the geometrical features and the elasticity of the substrate, we can recapitulate the microenvironments and see in vivo behaviors. We developed several biofabrication techniques to deliver the necessary instructive to collagen scaffold. Overall, these biofabrication techniques combines imaging of tissue of interest, 3D printing, and selective enzymatic activity to create the new generation of 3D biomaterials for research and clinical application.

The next five chapters explain in depth the different biofabrication techniques and how they contribute to the production of tissue scaffolds. The second chapter, "*Extraction and Characterization of Collagen from Bovine Calf Hide*" presents an investigation of the effectiveness of the extraction of non collagenous material and the integrity of the collagen structure in each of the collagen extraction steps. It also shows several factors that influence the collagen structure and fibrillogenesis process from an acidified collagen solution. The third paper "*Reaction Electrospinning: A Novel Technique for the Fabrication of Collagen Scaffolds"* introduces a novel technique that combines the process of electrospinning and fibrillogenesis to create fibrous collagen scaffolds. The fourth paper "*Designer Collagen Hydrogels to Regulate Satellite Cell Phenotype"*

investigates the effect of the elasticicity of the matrix in the control of the quiescent phenotype expression of the satellite cells or muscle precursor cells.

The next two papers show a novel biofabrication technique that consists of imaging of the tissue of interest, 3D printing, and selective enzymatic activity to 3D biomaterials. The fifth paper "*Three-Dimensional Biomimetic Technology: Novel Biomaterials to Create Defined Architectures in Hydrogels"* characterizes our developed sacrificial material, "BSA rubber" which we used to transfer specific architectural features to a scaffold material. The last chapter, "*Three-Dimensional Printing: Mimicking In Vivo Environments*" demonstrates how we can translate the architectural features from Renal CT angiograms images into a PLA mold. Then, using the BSA rubber, we can deliver the geometrical features to a collagen scaffold.

1.5 REFERENCES

1. Moore, K.A. and I.R. Lemischka, *Stem cells and their niches.* Science, 2006. 311(5769): p. 1880-5.

2. Kshitiz, et al., *Control of stem cell fate and function by engineering physical microenvironments.* Integrative Biology, 2012. 4(9): p. 1008.

3. Yost, M.J., et al., *A novel tubular scaffold for cardiovascular tissue engineering.* Tissue Eng, 2004. 10(1-2): p. 273-84.

4. Whelan, M.C. and D.R. Senger, *Collagen I initiates endothelial cell morphogenesis by inducing actin polymerization through suppression of cyclic AMP and protein kinase A.* J Biol Chem, 2003. 278(1): p. 327-34.

5. Orr, A.W., et al., *Mechanisms of Mechanotransduction.* Developmental Cell, 2006. 10(1): p. 11-20.

6. Gelse, K., *Collagens—structure, function, and biosynthesis.* Advanced Drug Delivery Reviews, 2003. 55(12): p. 1531-1546.

7. Ward, D.F., Jr., et al., *Mechanical strain enhances extracellular matrix-induced gene focusing and promotes osteogenic differentiation of human mesenchymal stem cells through an extracellular-related kinase-dependent pathway.* Stem Cells Dev, 2007. 16(3): p. 467-80.

8. Riha, G.M., et al., *Cyclic strain induces vascular smooth muscle cell differentiation from murine embryonic mesenchymal progenitor cells.* Surgery, 2007. 141(3): p. 394-402.

9. Bayati, V., et al., *The evaluation of cyclic uniaxial strain on myogenic differentiation of adipose-derived stem cells.* Tissue Cell, 2011. 43(6): p. 359-66.

10. Park, J.S., et al., *Differential effects of equiaxial and uniaxial strain on mesenchymal stem cells.* Biotechnol Bioeng, 2004. 88(3): p. 359-68.

11. Weinbaum, S., S.C. Cowin, and Y. Zeng, *A model for the excitation of osteocytes by mechanical loading-induced bone fluid shear stresses.* J Biomech, 1994. 27(3): p. 339-60.

12. Partridge, J., et al., *Laminar shear stress acts as a switch to regulate divergent functions of NF-kappaB in endothelial cells.* FASEB J, 2007. 21(13): p. 3553-61.

13. Wang, H., et al., *Shear stress induces endothelial differentiation from a murine embryonic mesenchymal progenitor cell line.* Arterioscler Thromb Vasc Biol, 2005. 25(9): p. 1817-23.

14. Tian, X.F., et al., *Comparison of osteogenesis of human embryonic stem cells within 2D and 3D culture systems.* Scand J Clin Lab Invest, 2008. 68(1): p. 58-67.

15. Cukierman, E., et al., *Taking cell-matrix adhesions to the third dimension.* Science, 2001. 294(5547): p. 1708-12.

16. Baker, B.M. and C.S. Chen, *Deconstructing the third dimension: how 3D culture microenvironments alter cellular cues.* J Cell Sci, 2012. 125(Pt 13): p. 3015-24.

17. Ankam, S., et al., *Substrate topography and size determine the fate of human embryonic stem cells to neuronal or glial lineage.* Acta Biomater, 2013. 9(1): p. 4535-45.

18. Engler, A.J., et al., *Matrix elasticity directs stem cell lineage specification.* Cell, 2006. 126(4): p. 677-89.

19. Gilbert, P.M., et al., *Substrate elasticity regulates skeletal muscle stem cell self-renewal in culture.* Science (New York, N.Y.), 2010. 329(5995): p. 1078-81.

20. Rowlands, A.S., P.A. George, and J.J. Cooper-White, *Directing osteogenic and myogenic differentiation of MSCs: interplay of stiffness and adhesive ligand presentation.* Am J Physiol Cell Physiol, 2008. 295(4): p. C1037-44.

21. Li, D., et al., *Role of mechanical factors in fate decisions of stem cells.* Regen Med, 2011. 6(2): p. 229-40.

22. Chen, S.S., et al., *Cell-cell and cell-extracellular matrix interactions regulate embryonic stem cell differentiation.* Stem Cells, 2007. 25(3): p. 553-61.

23. Kihara, T., et al., *Exogenous type I collagen facilitates osteogenic differentiation and acts as a substrate for mineralization of rat marrow mesenchymal stem cells in vitro.* Biochem Biophys Res Commun, 2006. 341(4): p. 1029-35.

24. Kotch, F.W. and R.T. Raines, *Self-assembly of synthetic collagen triple helices.* Proc Natl Acad Sci U S A, 2006. 103(9): p. 3028-33.

25. Di Lullo, G.A., et al., *Mapping the ligand-binding sites and disease-associated mutations on the most abundant protein in the human, type I collagen.* J Biol Chem, 2002. 277(6): p. 4223-31.

26. Benjakul, S., et al., *Extraction and characterisation of pepsin-solubilised collagens from the skin of bigeye snapper (Priacanthus tayenus and Priacanthus macracanthus).* J Sci Food Agric, 2010. 90(1): p. 132-8.

27. Kadler, K.E., et al., *Collagens at a glance.* Journal of Cell Science, 2007. 120(12): p. 1955-1958.

28. Hofmann, H., P.P. Fietzek, and K. Kuhn, *The role of polar and hydrophobic interactions for the molecular packing of type I collagen: a three-dimensional evaluation of the amino acid sequence.* J Mol Biol, 1978. 125(2): p. 137-65.

29. Shoulders, M.D. and R.T. Raines, *Collagen structure and stability.* Annu Rev Biochem, 2009. 78: p. 929-58.

30. Exposito, J.Y., et al., *The fibrillar collagen family.* Int J Mol Sci, 2010. 11(2): p. 407-26.

31. Malone, J.P., K. Alvares, and A. Veis, *Structure and assembly of the heterotrimeric and homotrimeric C-propeptides of type I collagen: significance of the alpha2(I) chain.* Biochemistry, 2005. 44(46): p. 15269-79.

32. Khoshnoodi, J., et al., *Molecular recognition in the assembly of collagens: terminal noncollagenous domains are key recognition modules in the formation of triple helical protomers.* J Biol Chem, 2006. 281(50): p. 38117-21.

33. Veis, A. and K. Payne, *Collagen fibrillogenesis*. Collagen. Biochemistry. 1988, Boca Raton: CRC Press. 113.

34. Kadler, K.E., et al., *Collagen fibril formation.* Biochemical Journal, 1996. 316: p. 1-11.

35. Holmes, D.F., M.J. Capaldi, and J.A. Chapman, *Reconstitution of collagen fibrils in vitro; the assembly process depends on the initiating procedure.* International Journal of Biological Macromolecules, 1986. 8(3): p. 161-166.

36. Wenstrup, R.J., et al., *Regulation of collagen fibril nucleation and initial fibril assembly involves coordinate interactions with collagens V and XI in developing tendon.* J Biol Chem, 2011. 286(23): p. 20455-65.

37. Wenstrup, R.J., et al., *Murine model of the Ehlers-Danlos syndrome. col5a1 haploinsufficiency disrupts collagen fibril assembly at multiple stages.* J Biol Chem, 2006. 281(18): p. 12888-95.

38. Li, Y., et al., *A fibrillar collagen gene, Col11a1, is essential for skeletal morphogenesis.* Cell, 1995. 80(3): p. 423-430.

39. Kadler, K.E., A. Hill, and E.G. Canty-Laird, *Collagen fibrillogenesis: fibronectin, integrins, and minor collagens as organizers and nucleators.* Curr Opin Cell Biol, 2008. 20(5): p. 495-501.

40. Cao, H. and N. Kuboyama, *A biodegradable porous composite scaffold of PGA/beta-TCP for bone tissue engineering.* Bone, 2010. 46(2): p. 386-95.

41. Bose, S., S. Vahabzadeh, and A. Bandyopadhyay, *Bone tissue engineering using 3D printing.* Materials Today, 2013. 16(12): p. 496-504.

42. Kolesky, D.B., et al., *3D bioprinting of vascularized, heterogeneous cell-laden tissue constructs.* Adv Mater, 2014. 26(19): p. 3124-30.

43. Hasan, A., et al., *Electrospun scaffolds for tissue engineering of vascular grafts.* Acta Biomater, 2014. 10(1): p. 11-25.

44. Zheng, W., W. Zhang, and X. Jiang, *Biomimetic Collagen Nanofibrous Materials for Bone Tissue Engineering.* Advanced Engineering Materials, 2010. 12(9): p. B451-B466.

45. Zhu, N. and X. Chen, *Biofabrication of Tissue Scaffolds*. Advances in Biomaterials Science and Biomedical Applications. 2013.

46. Kundu, J., et al., *Chapter 2 - Biomaterials for Biofabrication of 3D Tissue Scaffolds*, in *Biofabrication*, G. Forgacs and W. Sun, Editors. 2013, William Andrew Publishing: Boston. p. 23-46.

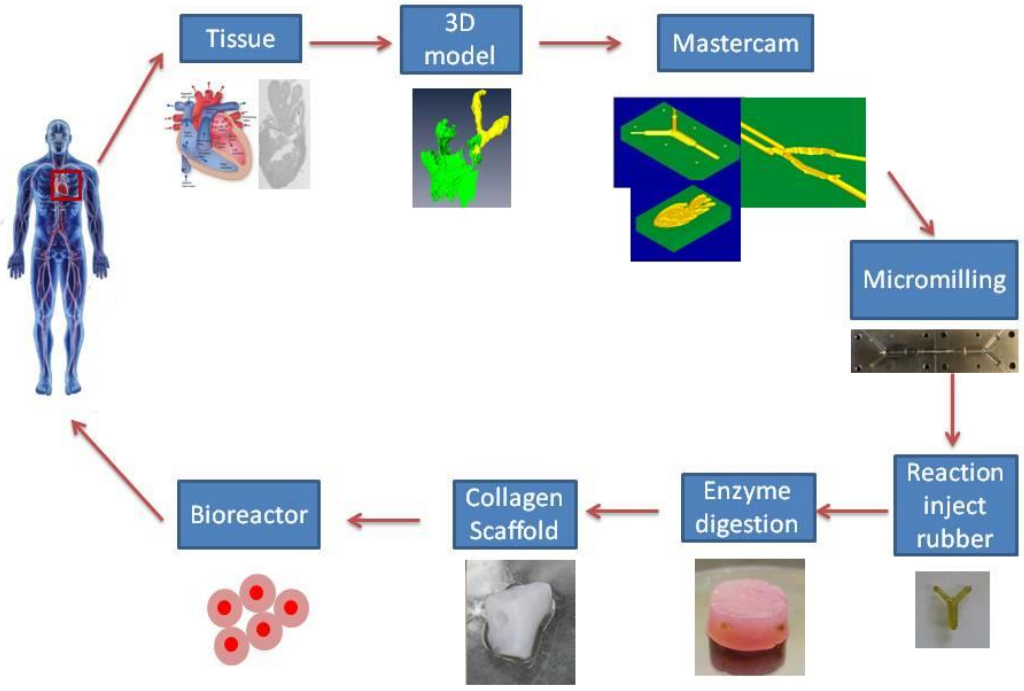

Figure 1.1: Novel Biofabrication Scheme. By obtaining images from the tissue of interest, we create a 3D model that upholds the specific geometries. Then, we create a negative mold of that model, and reaction injected our newly developed BSA rubber. Collagen is casted around the BSA rubber, and then by enzymatic digestion, we produce a 3D collagen scaffold. Then, we seed it with cells that are present in the original tissue, and we can deliver it to the patient.

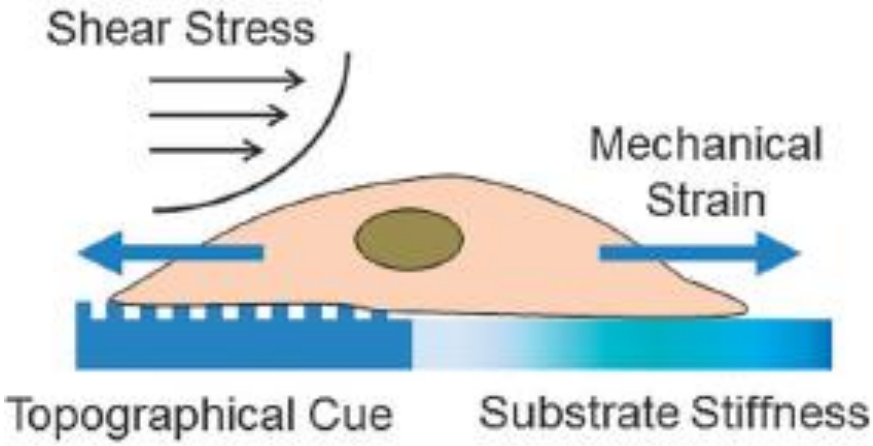

Figure 1.2: Mechanical Forces that regulates the stem cell behaviors. The main forces that the cells are subjected in their in vivo environments are shear stress, mechanical strain, substrate stiffness, and topographical cues. These forces are internalized by mechanotransduction and the cell responds to the changes in their cytoskeleton by changing its behavior. Image from Kshitiz et al.[2].

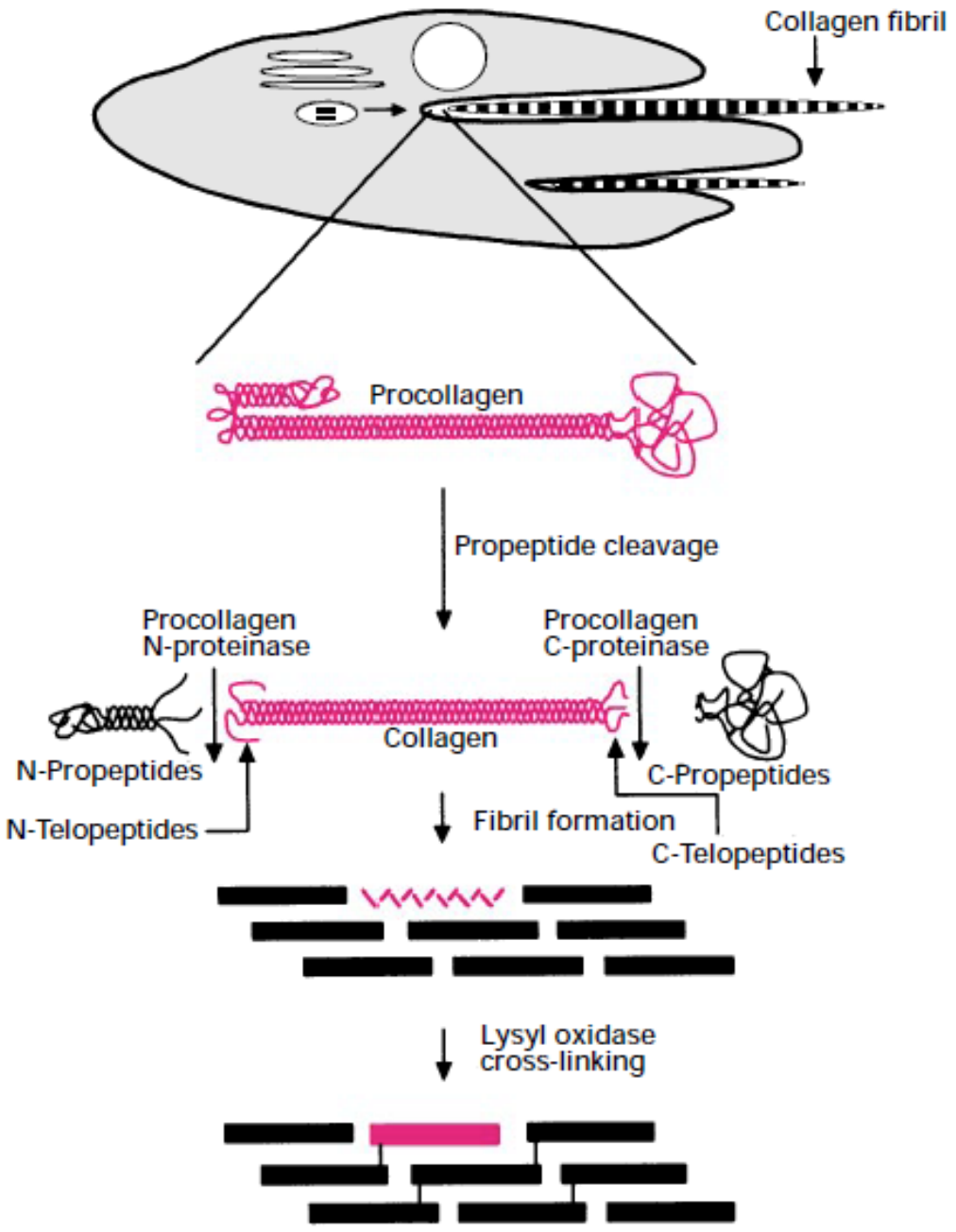

Figure 1.3: Collagen fibrillogenesis. After the collagen molecule is release from the cells to the extracellular matrix, specific enzymes cleave the propeptides at each end, inducing the self assembly process. Image from Kadler et al. [34].

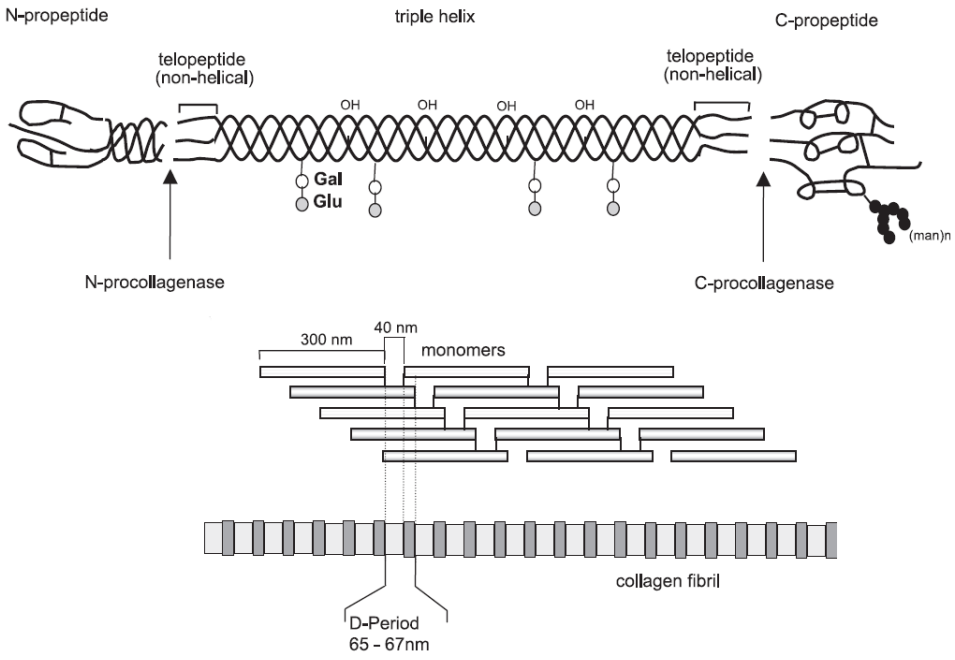

Figure 1.4: Molecular structure of the collagen type I. When the N- and C- propeptides are removed, the collagens can aggregate into fibrils. The self assembly process produces a quarter-staggered formation, producing a periodic pattern characteristic of the collagen. Image modified from Gelse et al.[6]

CHAPTER 2:

EXTRACTION AND CHARACTERIZATION OF COLLAGEN FROM BOVINE CALF HIDE

2.1 ABSTRACT

Collagen is the most abundant protein in the body. It is of significant importance in the medical and biotechnology field. In the tissue engineering field, collagen is used as a scaffold material to facilitate growth and maintenance of the cells, as well as to provide the necessary mechanical and topography cues to control cell behavior. The optimal scaffold for biomedical applications should be biocompatible, biodegradable, mechanical stable and porous. We introduce a protocol in which we can obtain a large amount of purified collagen. This process adopts some of the steps used in the leather industry and modifies them to preserve the integrity of the collagen. We developed a method in which we can standarlize the collagen extraction protocol by testing the raw material at each step of the process. We obtain highly purified collagen that can undergo fibrillogenesis and become a biodegradable scaffold material.

2.2 INTRODUCTION

Collagen is the major structural protein in the connective tissue. It has a wide variety of applications in the cosmetic, biomedical[1, 2], food[3], and leather industries[4]. It has many special characteristics such as being biodegradable and containing weak antigencity[5, 6]. Collagen is composed of three coiled subunits composed of two alpha (I) chain and one alpha 2 (I) chain. Each one consists of 1050 amino acids twisted around in the characteristic right handed triple helix structure. Type I is the most studied fibrillar collagen and is widely used in biomedical field[7]. Purified

type I collagen has been used for several clinical application such as dermal repair, plastic surgery, and drug delivery[8].

The most common source of collagen is rat tail tendon[9], skin (bovine, porcine, and fish)[10], and cell culture[11]. The leather industry is the leading market concerning the processing of skin or hides of animals, which then become leather. This market generates considerable amount of waste product, called splits, which can be use for biomedical applications [12]. Currently the most common methods to extract collagen are using neutral salt extraction, low concentration acid extraction, and enzymatic solution extraction. Overall, there is lack of standards among the different procedures of collagen extraction that contributes to a lot of variation in kinetics, shear data, and compressibility that makes the comparison between findings in literature difficult. There needs to be standards for the extraction process in order to fully investigate according to the type of extraction how efficient is, the integrity of the collagen molecule, and detail of kinetics of the fibrillogenesis. Unfortunately, it hasn't been documented how each step of the extraction process modifies the collagen and its effectiveness in the removal of unwanted material.

We describe a collagen extraction protocol from bovine hide that is quality controlled by monitoring each step by molecular testing. The goal of the collagen processing is to remove all noncollagenous material and maintain its integrity. In every process, there are certain factors that are controlled such as pH, ionic strength, time, and temperature. We have adopted some of the steps in the leather production. The quality of the collagen product is important in order to create fibrous scaffolds that don't have any immunoresponse[13] and allows the momomers and microfibrils to undergo

fibrillogenesis. We are interested in obtaining the highest yield of collagen, maintaining the integrity of the protein structure, and obtaining high collagen concentrations. We examined each step of the extraction protocol. Also, we tested the final product to determine the ability of the collagen to be acidified and reconstituted into collagen fibers. Our product generates high collagen concentration solution. This extraction process produces high quality collagen suitable for tissue scaffolds that mimic the microenvironments in which the biochemical and biophysical parameters can be controlled.

2.3 MATERIALS AND METHODS

2.3.1 Collagen Extraction Process

The collagen extraction protocol follows the flow chart shown in figure 2.1.

2.3.1.1 Initial Processing

Collagen is prepared from hide of an 18 month old bovine steer (Caughman's in Lexington, SC). Briefly, the hide was cut in pieces averaging 12" x 12" . The hides were stored at -20˚C for preservation until processed. Then, selected pieces were thawed overnight on 4˚C fridge overnight.

2.3.1.2 Hair removal

After the hide was thawed, we proceeded to remove the superficial epidermis including hair, follicles pits, and facias using a surgical scalpel. The top grain layer was removed because of the highly non acidic dissociation crosslinks, it not unsuitable for biomedical applications[14]. The hides were weighted and washed three times with DI water to remove all lose hair.

2.3.1.3 Liming

The hides become chemical modified and swelled to allow the hydrolysis and diffusion of non collagenous material. $Ca(OH)_2$ solution is used to open up the hide. This solution maintains a pH close to 12.6. If it reaches 13, there is rapid hydrolytic damage of collagen[4]. The unwanted material was removed using a lime solution bath composed of 2% $Ca(OH)_2$ (Sigma) per hide weight. The solution was mixed well and placed on a tub with the hides. Every hour, we mix well and added DI water if necessary to maintain the hide submerged in solution. We could see the hide swelling up and becoming stiff. The hides were incubated for 6 days at 4˚C.

2.3.1.4 Deliming

The purpose of this step is to solubilize any residual lime and unswell the hide by lowering the pH. The hide was washed twice in DI water and placed in tumbler with 1M NaCl solution to facilitate the removal of the $Ca(OH)_2$ from the hides. The pH of the

solution was adjusted to 5 with 1M HCl solution added slowly, allowing time to equilibrate. This was done every 2 hr for approximately 2 weeks, while keeping the hides cold at 4˚C. We checked the internal pH of the hides using a pH probe. The target internal pH was 6. The hides were washed three times with DI water.

2.3.1.5 Enzymatic Treatment

To increase the collagen yield and remove any other noncollagenous materials, we treated the hides with pepsin. After the deliming process, the conductivity was monitored to ensure the removal of salts. They were placed in the tumbler with cold DI water and the conductivity was monitored every hr until it reached 100 µS/cm (it took approximately 4 days). The hide was then cut into 1" x 1" and placed in cold 0.5 M Acetic Acid solution. Pepsin (Fisher) was added in a 50:1 hide weight:pepsin and placed in a tub for 2 hrs. Then, we placed it on a tumbler (DVTS15, Daniel Food Equipment) at 4˚C for 3 days.

2.3.1.6 Mixing and Homogenizing the collagen

To obtain a collagen suspension, we homogenize the collagen pieces. The collagen was grinded using a clean and lubricated meat grinder (Model 4612, Hobart). Then, 0.5 M Acetic Acid was added and mixed (Kitchen Aid, Professional 6) until we obtained a liquid consistency. We verified that the pH was within 3-4.5. The collagen was left to swell overnight at 4˚C. The next day, we added enough acetic acid to have a liquid consistency and pressed the collagen through a mesh filter (12 ton Hydraulic Press, Central Hydraulics). The suspension was centrifuge at 7500 rpm for 30 min to remove

any insoluble particle. The bottom layer was removed which had tiny hairs and other particles.

2.3.1.7 Collagen Precipitation and Dialysis

We precipitate the collagen using salt to further purify and obtain the highest collagen concentration. First, we measured the volume of collected collagen. We added NaCl to a concentration of 1 M until the collagen came out of solution. The solution was placed in mixer at 4˚C. The collagen was spun down to get rid of the water at 5000-7000 rpm (4676-9343 rcf) for 30 minutes at 4 ˚C. This took several spins to collect all of the collagen. The collagen must be kept at 4˚C. After collecting the collagen, we added 0.3% sodium bicarbonate (Sigma) solution pH 8 until we got a paste consistency.

We proceeded to drop the ionic strength of the collagen. The ionic strength affects the ability of fibrillogenesis process. The collagen solution was placed in dialysis bags. We added 1% sodium bicarbonate in the solution where the dialysis tubes are going to be submerged and modify the pH to 8. Once the surrounding liquid has a pH of 7, we switched to DI water and continually change the water until the conductivity reaches 50µS/cm. Then we placed the collagen in 50 mL conical tubes, centrifuge at 7000 rpm (9343 rcf) for 30 minutes at 4 ˚C , remove the supernatant, and stored at -20 ˚C.

2.3.2 Sample Analysis

After each step, a piece of the hide material was taken. The sample was lyophilized (Lyophilizer, Labcono Free Zone) and grounded. Approximately, 20 mg of the tissue was weighed and placed on 2 mL eppendorf tubes. The overall procedure for the extraction of soluble protein, testing the integrity of collagen, and the digestion of collagen can be seen in figure 2.2 and 2.3.

2.3.2.1 Extraction of Soluble Protein

The amount of soluble protein was extracted from the hides using a radioimmunoprecipitation assay buffer (RIPA). RIPA is a rapid and effective cell lysis buffer that allows the extraction of soluble proteins. RIPA is composed of 50 mM Tris-HCl (Fisher Scientific), 150 mM NaCl(Fisher Scientific), 1% NP-40 (Thermo Scientific), 0.5% Sodium Deoxycholate (Sigma-Aldrich), and 1% SDS (Sigma). We added 26 µL of RIPA per mg of lyophilized tissue. We also added a protease inhibitor (Halt protease and phosphate single use inhibitor, Thermo Scientific). The samples were vortex and place on sonicator with ice for 90 min. Every 10 min, the samples were vortex and place back in the sonicator bath. After sonication, the samples were spun down at 4˚C 15000 rpm (21130 rcf) for 20 min. The supernatant was extracted and stored at -20˚C. The pellet was lyophilized overnight.

2.3.2.2 Enzyme digestion

The integrity of the collagen was determined by a trypsin digestion assay. Native triple helices are characterized by the protease resistant and can only degrade by collagenase [15-17]. The lyophilized pellet after RIPA extraction was weighted, and the same amount of RIPA added was added of the enzyme solution. The pellet was incubated with 0.25% Trypsin solution (pH 7.8) for 24 hr at 30˚C. After 24 hr, the samples were spun down at 4˚C 15000 rpm (21130 rcf) for 20 min. The supernatant was extracted and stored at -20˚C. The pellet was lyophilized overnight and weight the next day.

2.3.2.3 Protein Quantification

The amount of soluble protein was quantified using a bicinchoninic acid assay (BCA, Pierce). Briefly, BSA (Sigma) and gelatin (Sigma) solutions were made and used as standard for each sample. Gelatin, which is a degraded stated of collagen, was ideal for these samples.

2.3.2.4 Sodium docecyl sulfate-polyacrylamide gel electrophoresis (SDS-PAGE)

RIPA, Trypsin, and collagenase digestion samples were taken to identify the proteins in solution. Three samples were taken from three independent test samples.. The samples were mixed with 10X Protein loading buffer that is composed of 1 M Tris-HCl (Fisher), pH 6.8, 10% SDS(Sigma), 0.2% Brillianr Blue R-250 (Fisher), 25% β-mercaptoethanol(Sigma), and 50% glycerol (Alfa Aesar) in a 9:1 (sample:sample buffer)

ratio. Ten micrograms of protein was loaded to each well and was done in triplicate. Samples were run using 1X Buffer made from 10X Tris/Glycine/SDS Buffer (Biorad). The samples were heated for 5 min at 95˚C. After being heated, 40 µL of each sample was loaded in the wells of a 4-20% Mini Protean TGX Gel (Biorad), and electrophoresis was performed at 100V. After electrophoresis, the gel was fixed with a mixture of 50%(v/v) methanol(Fisher) and 10% (v/v) acetic acid(Fisher) for 30 min at room temperature, followed by staining with 0.01%(w/v)Brilliant Blue R-250(Fisher) in 20%(v/v) methanol and 10%(v/v) acetic acid overnight in shaker at 4 C. Finally, the gel was destained with a mixture of 30% methanol and 10% acetic acid for 1 hr in shaker at 4˚C, and destained again twice for 30 min with same solution. Precision Dual Color Standards (Biorad) was used to estimate the molecular weight of the protein.

2.3.2.5 Fibrillogenesis

We tested the ability of our collagen extracted product to undergo fibrillogenesis. We thawed the collagen and determined the percentage of solids. We proceeded to acidify the collagen to pH 3. The collagen was left at 4˚C to stabilize. The next day, the collagen concentration was adjusted to 1.75% collagen and the pH was adjusted to 3. To polymerize the collagen, media and HEPES were added in an 8:1:1 ratio[18]. We tested four different medias: DMEM/High Glucose that contains sodium piruvate (HyClone) (Media 1), DMEM/High Glucose without sodium piruvate (HyClone) (Media 2), MEM 10X with no L-glutamine and sodium bicarbonate (Gibco) (Media 3), and Dulbecco modified eagle (Sigma) (Media 4). The gels were casted to cylindrical molds (12 well

plate, Corning). Plates were loaded into a pre heated (37˚C) multi mode microplate reader (Biotel) and absorbance at 405 (A_{405}) was measured every min for two hours.

2.4 RESULTS

2.4.1 Protein quantification

The non collagenous protein content in the hide decreased after each treatment. As expected, there was more soluble protein in the non process samples than the limed samples. After lyophilizing the pellet that was subjected to trypsin digestion, we saw that there was more protein dissolved than shown in the BCA assay. We used BSA and gelatin standards to quantify the protein concentration of each sample. The protein concentration was determined using the gelatin standard curve (table 2.1).

2.4.2 Sodium docecyl sulfate-polyacrylamide gel electrophoresis (SDS-PAGE)

The non processed samples showed a band at around 60 KDa (figure 2.4). This can be indicative of bovine albumium (MW 66 KDa). Also, there is a small smear below 50 KDa that could be hydrolyzed collagen. In the trypsin treatment, there are no collagen bands. There is a very faint band at 45 KDa, but most of the protein in the supernatant corresponds to trypsin and some of its autloysis amino acid products that contain smaller amino acids below 15 KDa.

The limed process samples show a very small amount of soluble protein at about 10 KDa (figure 2.5). Sample 1 of the RIPA extraction sample shows negligible collagen bands. It was not seen in the other two samples. After the pellet was subject to trypsin digestion, we only saw trypsin on the gels.

2.4.3 Fibrillogenesis

The percentage of collagen solids was high, fluctuating between 3-7% (wt/wt). The general procedure was to mix the collagen solution with buffer solution, heat to physiological temperature, and monitor the absorbance with respect time. In the first two media, we could see a layer of liquid on top of the fibers. This is indicative of collagen precipitation due to high salt concentration that prevents the fiber formation process. Fiber produce from media 3, produce a good consistency gel that had a slightly pink color, indicative of the neutral pH. Collagen gel produce by fiber using media 4, produce a softer gel compare to the one produce with media 3, but it had a yellow color, indicative of acid gel (figure 2.6).

The typical absorbance curve for fibrillogenesis consist of three distinct phases: a lag, growth, and plateau phase. When the collagen was mixed with the buffer solution, the absorbance increased with time (figure 2.7). The samples prepared using media 3 and 4 showed a sigmoidal shaped polymerization curve with characteristic growth and plateau region. The lack of the lag phase on the turbimetric curve can be caused due to delay of placing the plate into the microplate reader. We have an exponential growth period that's indicative of the higher order assemblies. The media 4 sample showed

higher absorbance values compared to 3. The sample 4 seems to have a delay in reaching the plateau region compared to sample 3. The first two samples didn't seem to aggregate into fibrils.

2.5. DISCUSSION

Collagen is the most abundant protein in the connective tissue. It is present on the body as insoluble fibers surrounded by interstinal fluid. The collagen microstructure is vital for diffusion, mechanical strength, and degradation/ remodeling capabilities. This protein, which composed the majority of the extracellular matrix, is responsible of providing the necessary mechanical, biological, and physical cues though the cell-surface receptors that are mediated through the integrins. The balance between a cell and the extracellular matrix determines the cell morphology as well as induces changes in cell behavior from quiescent to initializing cell differentiation. To maximize its full potential, a standardized collagen extraction protocol needs to be implemented in which each step of the extraction process is thoroughly analyzed and provides high collagen yield. In this way, we can determine the efficiency of the removal of the non collagenous materials and ensure that the process doesn't affect the molecular structure of the collagen.

There are several differences between the starting product used for tanning and the extraction of collagen for biomedical applications. Compared to the tanning industry, we are not interested in the upper layer called top grain, which produces the high quality leather. This layer is not suitable for biomedical applications. For our purposes, we are interested in the layer below that, the corium layer. This portion is also referred to as

splits. For the proper collagen extraction, this layer needs to be stripped from any flesh, fats, or subdermal tissues.

In the liming process, the treatment with base causes drastic changes on the characteristic of the collagen. This process is referred to as opening of the hide. The swelling of the hide facilitates the diffusion and proteolysis of cellular and non collagenous material such as albumiun and globular proteins by hydrolysis of the peptide bonds. The collagen becomes chemically modified as it swells, leaving an open structure by the separation of fibres and the fibrils from one another[4, 19]. Ammonia is released from the glutamine and asparagine, forming carboxyl groups. This can also be observed in the amino content, showing a decrease of amines after the base treatment[19, 20]. At this step, there is a shift in the isoelectric point of the collagen from pH 7.4 to 5-6. There is also osmotic swelling of the hide. There is osmotic swelling of the hide which causes changes to the fiber network. The fiber shows different shapes and the fibrils tend to slightly twist. The fibrils increase in thickness and decrease in length. In our studies, we saw soluble proteins available on the unprocessed hide that were not present after the liming process. This is indicative that the liming process successfully cause swelling in the hide, allowing at the same time diffusion of all non collagenous materials. The first sample in the liming processed hide shows collagen bands due to accidental aspiration of the pellet. This provided insight of the integrity of collagen. Future analysis will be performed on the pellet to further validate this point.

The deliming process consists of preparing the hide for the enzymatic treatment by removing the solid lime. To do this, the hide has to be neutralized in order to liberate all the calcium that binds to the carboxyl group and to return the hide to its original state.

Salts are added to increases the ionic strength of the solution, allowing quick penetration into the hide. The most common salts used are NaCl and NH_4Cl. At this step, acid swelling must be prevented because it can cause non-reversible disruption of the structure of collagen. They will swell on the outside, trapping calcium. The change in pH favors the enzymatic activity of pepsin. The conductivity needs to be reduced in order to have a more effective enzymatic activity. We used this enzyme, which will partially cleave the telopeptides allowing a higher yield of extracted collagen. The collagen triple helix structure is not affected by proteases. However, the telopeptides, which are non helical peptide chains at the each end of the helical portion, is not resistant to the enzymatic attack. There is controversy in literature about the extraction of the collagen using pepsin. Pepsin attacks selectively the telopetides. The telopeptides are non triple helical extensions from the polypeptide chain. Previous researches have stated that the telopetides are needed in order to induce fibrillogenesis[21, 22]. However, it has been established that the telopeptides play a role in the kinetics of self-assembly of collagen momomers and microfibrils but does not mean that they contain the "code" necessary to induce the appropriate packing of collagen into fibers. The telopeptides accelerate the nucleation compared to the collagen without the telopeptides[23, 24].

After the enzymatic extraction, we proceeded to homogenize, purify, and reduce the ionic strength of the collagen. The salt allows the precipitation of the collagen, further isolating the collagen from the solution. The collagen was subjected to slow dialysis and adjustment to neutral pH. The conductivity of the collagen aids the fibrillogenesis process. A conductivity of 50µS/cm is equivalent to a salt concentration of 500 mM[25].

It has been established that this is the ideal salt concentration to create the D-banding in the collagen fibers.

By generating a mass balance on the protein, it looks like we should use the BSA standards to determine the protein concentration in the RIPA extraction. It seems that using the gelatin standard for determining soluble proteins underestimates the actually protein concentration in solution. We should use the BSA standard curve to quantify the amount of protein for the RIPA extracted proteins and the gelatin standards for the typsin and collagenase treatment. The amino acids residues of gelatin cause much less reduction of Cu^{2+} to Cu^{+} than the residues of BSA in the BCA assay. Using BSA standard will underestimate the amount of collagen dissolved after enzymatic treatment. Using the gelatin standard curve for the enzymatic treatment, we have an accurate quantification of protein if there is collagen in the solution after the enzymatic treatment. Using this information, we should repeat the SDS gels to correlate the results. Our result already show that compared to the non process sample, the liming step is effective in removing non collagenous proteins indicated by the lack of soluble proteins in solution after treatment.

The self-assembly of collagen fibrils is affected by ionic strength, temperature, pH and ions in the solvent [20, 26]. Fibrillogenesis, or the process on where collagen molecules assemble into collagen fibers, is governed by covalent bonds, electrostatic forces, hydrophobic and hydrophilic interactions. The addition of NaCl to acidified collagen and adjusted to pH 7.0 produced the formation of D-banded fibrils [25]. Using different medias we determined that the sodium bicarbonate that is present in media 1 and 2, affect the fibrillogenesis process preventing the aggregation of the microfibrils. We

showed that using a media that neutralizes the collagen, we see a sigmoidal shaped polymerization curve with characteristic growth and plateau region. In this way, we are conditioning the collagen hydrogel for its interaction with cells.

Future work will be done to further identify the effectiveness of this isolation protocol. The procedures of quantifying and identifying the proteins available on the pellet at each of the steps will provide insights of the stability of the unsoluble material.

2.6 CONCLUSION

This collagen extraction protocol generates collagen with the highest concentration. We can manipulate this collagen to the desired mechanical properties and it is capable of undergoing fibrillogenesis, making this product suitable for the tissue engineering and the regeneration field.

2.7 REFERENCES

1. Doillon, C.J., *Skin replacement using collagen extracted from bovine hide.* Clin Mater, 1992. 9(3-4): p. 189-93.

2. Oliveira, M.R., et al., *Tissue Engineering: Using Collagen Type I Matrix for Bone Healing of Bone Defects.* Journal of Craniofacial Surgery, 2013. 24(4): p. E394-E396.

3. Pritikin, W.B., *Microscopic structure of small diameter reconstituted collagen sausage casings.* Microscope, 1975. 23(2): p. 103-108.

4. Beghetto, V., et al., *The Leather Industry: A Chemistry Insight Part 1: an Overview of the Industrial Process.* Science at Ca'Foscari, 2013: p. 13-22.

5. Rauterbe.J, R. Timpl, and Furthmay.H, *Structural characterization of n-terminal antigenic determinants in calf and human collagen.* European Journal of Biochemistry, 1972. 27(2): p. 231-&.

6. Bunyaratavej, P. and H.L. Wang, *Collagen membranes: A review.* Journal of Periodontology, 2001. 72(2): p. 215-229.

7. Berglund, J.D., et al., *A biological hybrid model for collagen-based tissue engineered vascular constructs.* Biomaterials, 2003. 24(7): p. 1241-1254.

8. Kadler, K.E., et al., *Collagens at a glance.* Journal of Cell Science, 2007. 120(12): p. 1955-1958.

9. Xiong, X., et al., *A new procedure for rapid, high yield purification of Type I collagen for tissue engineering.* Process Biochemistry, 2009. 44(11): p. 1200-1212.

10. Benjakul, S., et al., *Extraction and characterisation of pepsin-solubilised collagens from the skin of bigeye snapper (Priacanthus tayenus and Priacanthus macracanthus).* J Sci Food Agric, 2010. 90(1): p. 132-8.

11. Kadler, K.E., Y. Hojima, and D.J. Prockop, *Assembly of type-I collagen fibrils denovo - between 37-degrees and 41-degrees-C the process is limited by micro-unfolding of monomers.* Journal of Biological Chemistry, 1988. 263(21): p. 10517-10523.

12. Li, D., W. Yang, and G.Y. Li, *Extraction of native collagen from limed bovine split wastes through improved pretreatment methods.* Journal of Chemical Technology and Biotechnology, 2008. 83(7): p. 1041-1048.

13. Badylak, S.F. and T.W. Gilbert, *Immune response to biologic scaffold materials.* Semin Immunol, 2008. 20(2): p. 109-16.

14. Michael, J.Y., T. Louis, and L.P. Robert, *Collagen Processing*, in *Encyclopedia of Biomaterials and Biomedical Engineering*. 2013, Taylor & Francis. p. 348-354.

15. Zhang, Z.K., G.Y. Li, and B. Shi, *Physicochemical properties of collagen, gelatin and collagen hydrolysate derived from bovine limed split wastes.* Journal of the Society of Leather Technologists and Chemists, 2006. 90(1): p. 23-28.

16. Keech, M.K., *The effect of collagenase and trypsin on collagen-an electron microscopic study* Anatomical Record, 1954. 119(2): p. 139-159.

17. Drake, M.P., et al., *Action of proteolytic enzymes on tropocollagen and insoluble collagen.* Biochemistry, 1966. 5(1): p. 301-312.

18. Elsdale, T. and J. Bard, *Collagen substrata for studies on cell behavior.* J Cell Biol, 1972. 54(3): p. 626-37.

19. Yost, M.J., L. Terracio, and R.L. Price, *Collagen Processing*, in *Encyclopedia of Biomaterials and Biomedical Engineering*. 2013, Taylor & Francis. p. 348-354.

20. Veis, A. and K. Payne, *Collagen fibrillogenesis*. Collagen. Biochemistry. 1988, Boca Raton: CRC Press. 113.

21. Kadler, K.E., et al., *Collagen fibril formation.* Biochemical Journal, 1996. 316: p. 1-11.

22. Holmes, D.F., M.J. Capaldi, and J.A. Chapman, *Reconstitution of collagen fibrils in vitro; the assembly process depends on the initiating procedure.* International Journal of Biological Macromolecules, 1986. 8(3): p. 161-166.

23. Kreger, S.T., et al., *Polymerization and matrix physical properties as important design considerations for soluble collagen formulations.* Biopolymers, 2010. 93(8): p. 690-707.

24. Kuznetsova, N. and S. Leikin, *Does the triple helical domain of type I collagen encode molecular recognition and fiber assembly while telopeptides serve as catalytic domains? Effect of proteolytic cleavage on fibrillogenesis and on collagen-collagen interaction in fibers.* J Biol Chem, 1999. 274(51): p. 36083-8.

25. Harris, J.R., A. Soliakov, and R.J. Lewis, *In vitro fibrillogenesis of collagen type I in varying ionic and pH conditions.* Micron, 2013. 49: p. 60-8.

26. Trelstad, R.L., D.E. Birk, and F.H. Silver, *Collagen fibrillogenesis in tissues, in solution and from modeling - a synthesis.* Journal of Investigative Dermatology, 1982. 79: p. S109-S112.

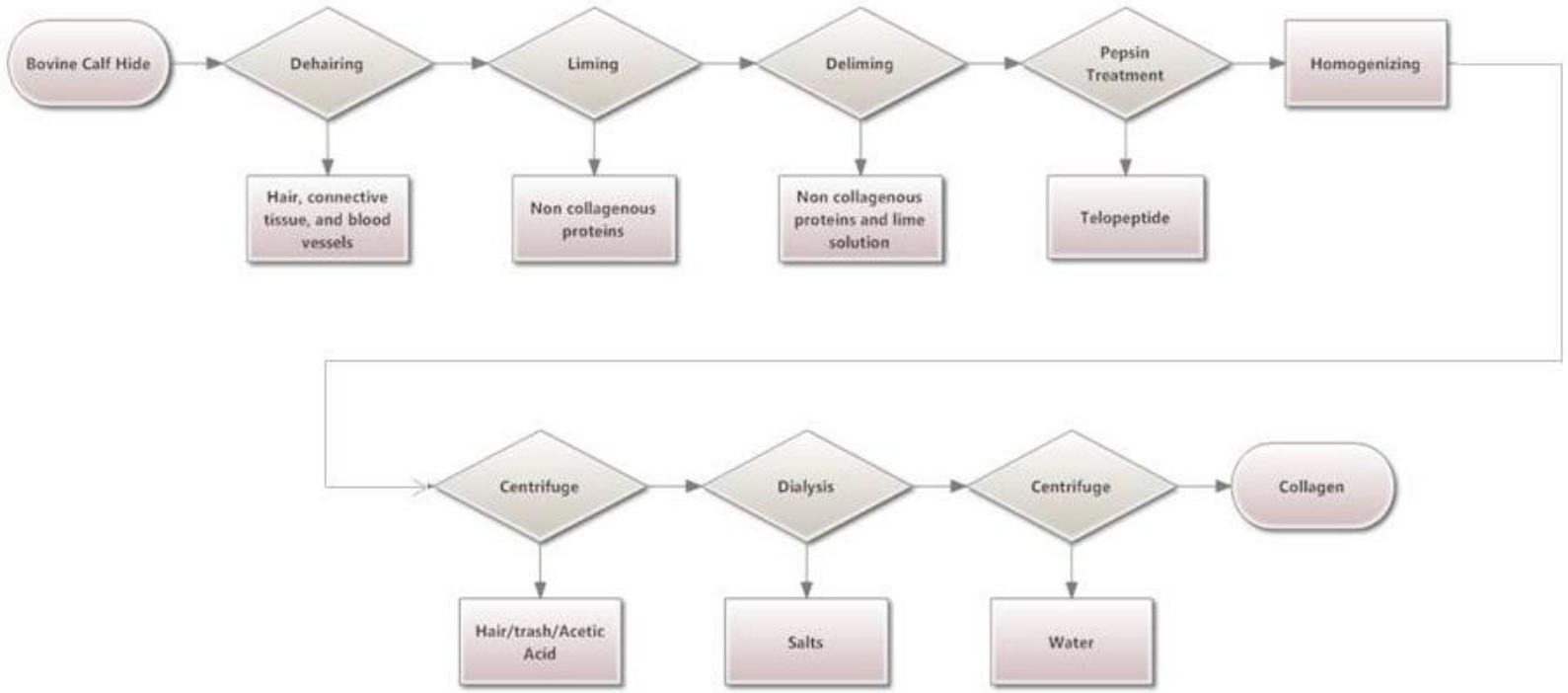

Figure 2.1 : Collagen extraction protocol.

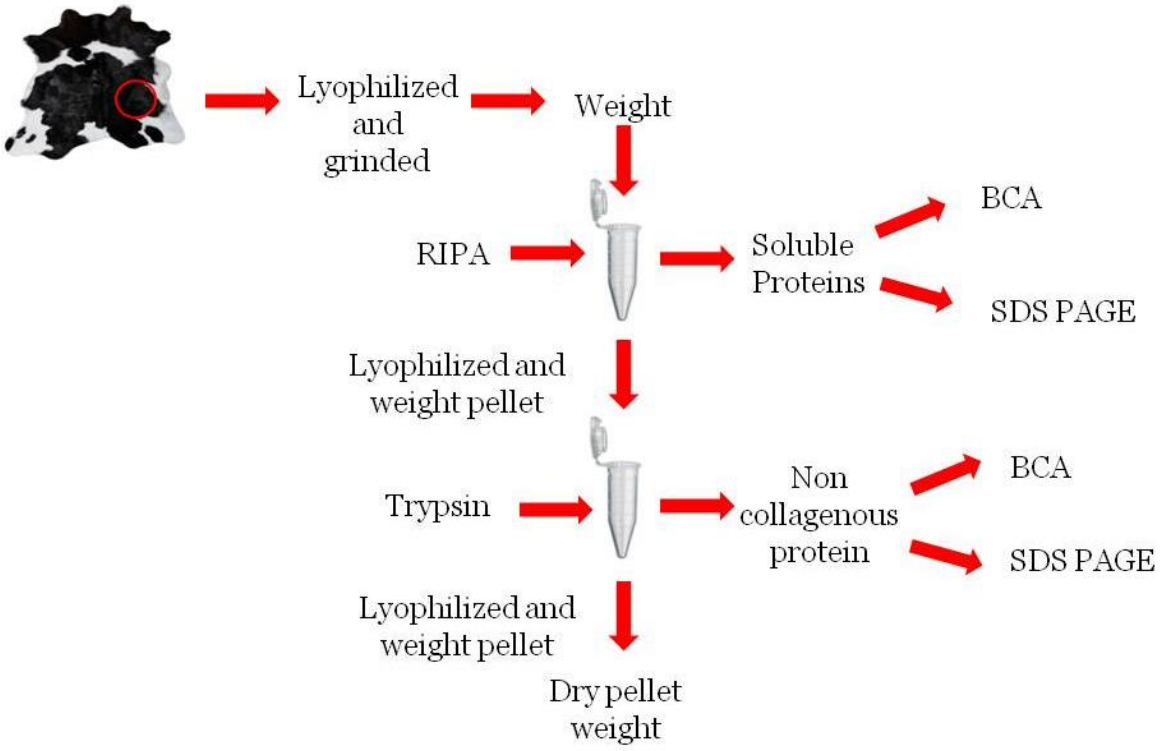

Figure 2.2: Extraction of Soluble protein using RIPA buffer and testing the integrity of the collagen by a trypsin assay. The soluble proteins were removed from the hide using RIPA buffer. After removing the supernatant and lyophilizing the pellet, a trypsin solution was added. The collagen is resistant to trypsin. The presence of collagen in the supernatant indicates that collagen molecule has been damaged, making it not resistant to enzymatic attack. The supernatant was analyzed by quantifying and identifying the proteins in solution.

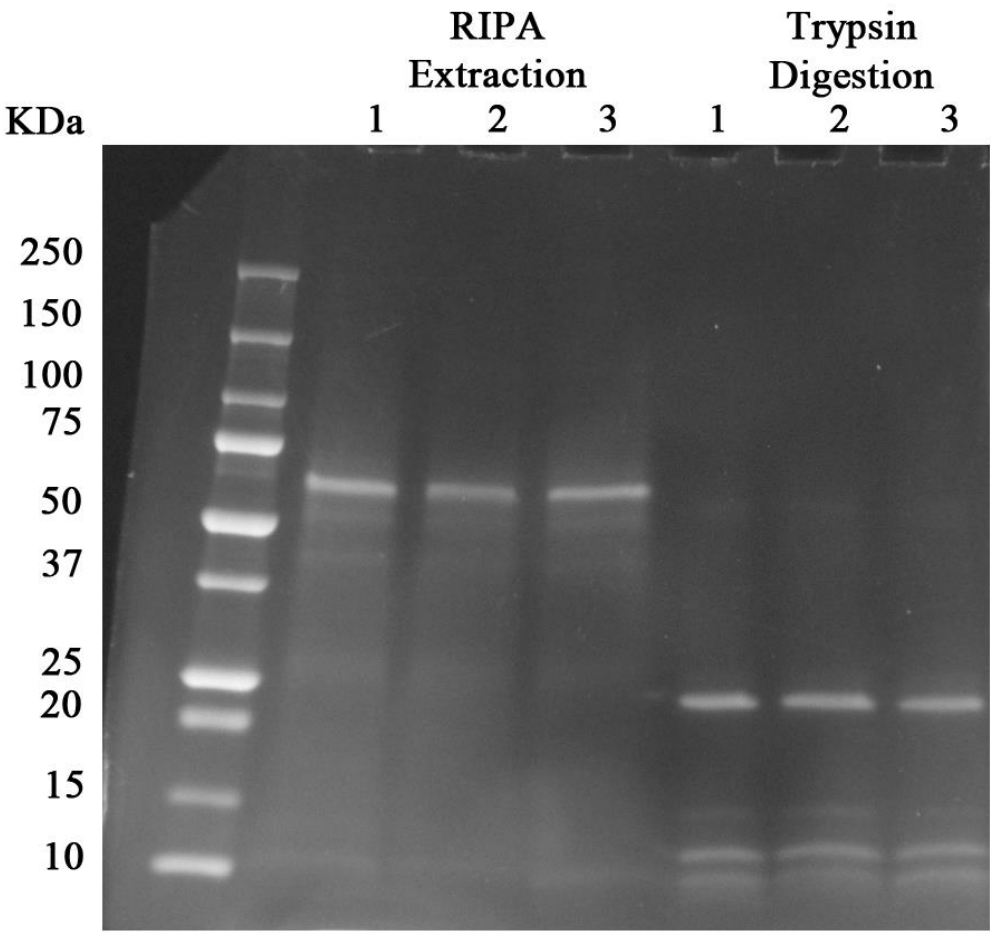

Figure 2.3: SDS PAGE analysis of the non processed hide. Using RIPA we can see a band at around 70 KDa in all three samples. After trypsin digestion, we saw that there was only trypsin in solution, indicating that the collagen is resistant to the enzyme.

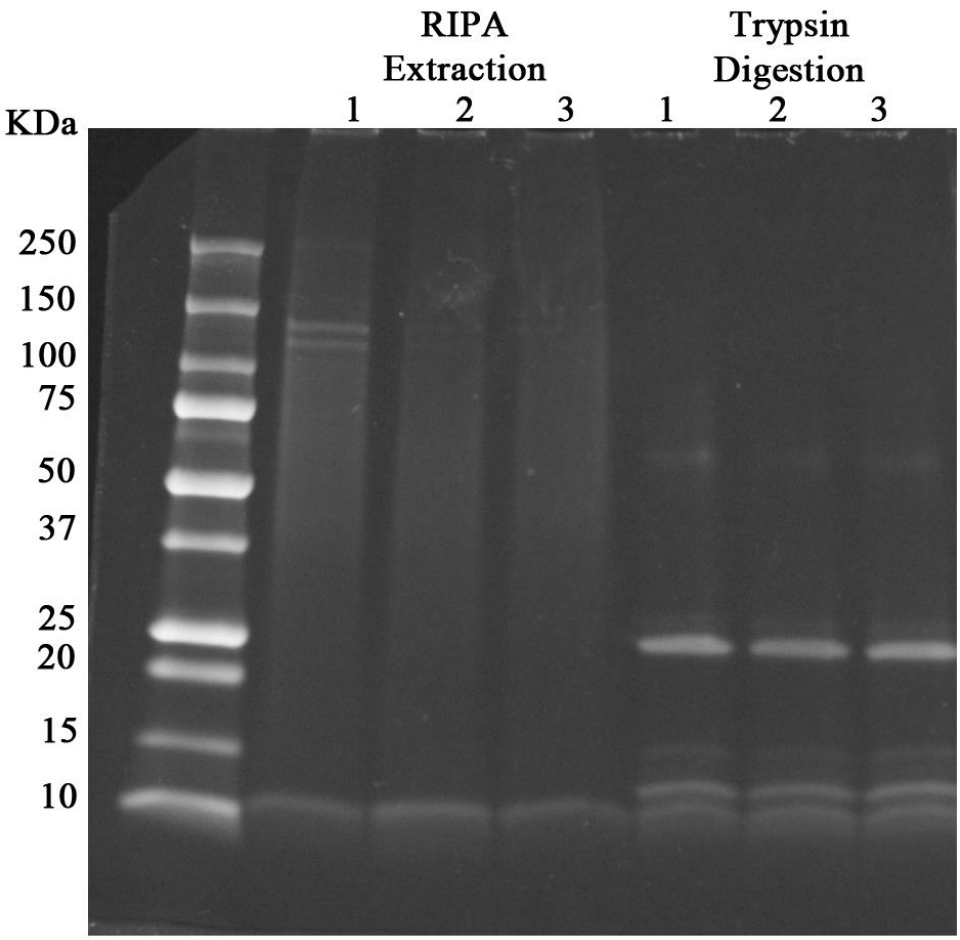

Figure 2.4: SDS PAGE analysis of the hide after liming treatment. Using RIPA we can see a faint band above 250 KDa and two bands below 150 KDa on sample 1. This is due to accidental aspiration of the pellet. The other two samples show bands at 10 KDa indicative of broken down polypeptide chains. In the tryspin treatment, we only see a band around 25 KDa that correspond to trypsin and some of its autolysis products below 15 KDa.

Figure 2.5: Fibrillogenesis. Collagen gels were castes on 12 well plates and its kinetics was determined using four different cell culture medias. Each number corresponds to a media used (see description in Materials and Method section)

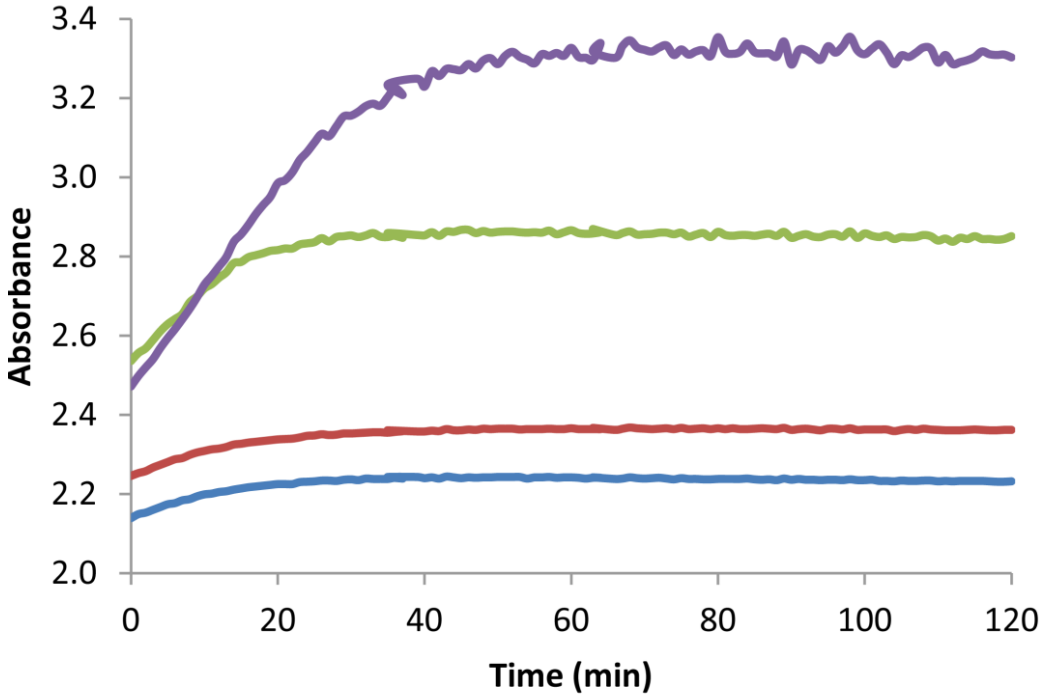

Figure 2.6: Turbidimetry Curves. The acidified collagen was mixed with media and placed on a pre heated microplate reader to determine the absorbance. We can see a growth and plateau phase. Blue- Media 1, Red- Media 2, Green- Media 3, and Purple-Media 4.

Table 2.1: RIPA and trypsin digestion based on gelatin standards. N1-N3 corresponds to the non process samples and L1-L3 corresponds to hide samples after liming treatment.

Sample	Start Tissue Weight (mg)	BCA (RIPA) ug/uL	Total Protein (mg)	Tissue after RIPA extraction (mg)	Difference (mg)	BCA (Trypsin) ug/uL	Total Protein (mg)	Tissue after trypsin (mg)	Difference (mg)
N1	18.8	2.7329	1.3	18.6	0.2	1.6790	0.8	15.9	2.7
N2	21.0	3.7772	2.1	20.4	0.6	1.7155	0.9	18.2	2.2
N3	20.4	2.6737	1.4	19.7	0.7	1.7885	0.9	17.1	2.6
L1	18.9	1.2070	0.6	16.9	2.0	1.7317	0.9	14.4	2.5
L2	21.2	0.8241	0.5	19.1	2.1	1.7844	1.0	16.9	2.2
L3	18.9	1.0097	0.5	16.7	2.2	1.3102	0.6	15.1	1.6

CHAPTER 3:

REACTION ELECTROSPINNING: A NOVEL TECHNIQUE FOR THE FABRICATION OF COLLAGEN SCAFFOLDS[1]

[1] Rodriguez-Rivera, V; Weidner, JW and Yost, MJ. Submitted to *Biofabrication*, 08/26/14

3.1 ABSTRACT

Demand for the development of biofibrous materials has increased enormously due to their potential applications in the medical, industrial, and filtration fields. Having control of the fiber structure is ideal for medical applications. A successful in vitro material needs to balance its chemical and mechanical properties, providing an accurate cell-matrix interaction and inducing in vivo behaviors such as proliferation, differentiation, migration, and regeneration. The optimal scaffold for biomedical applications should be biocompatible, biodegradable, mechanically stable, and porous. Currently used solvents for collagen fiber electrospinning denature the structure of the collagen. We introduced a modification of this technique using benign solvents, called reaction electrospinning, and we obtained quarter-staggered assemblies that were characteristic of native collagen. Using trypsin digestion in combination with SDS-PAGE and western blot analysis, we confirmed the integrity of the collagen structure. Additionally, we determined that, for our range of parameters, the flow rate and the electrical field correlated to the collagen fiber diameter. This technique allows fibrillogenesis to occur in vitro as the fibers are being collected, resulting in collagen fibers suitable for the fabrication of biomimetic scaffolds mimicking the architecture of the extracellular matrix.

3.2 INTRODUCTION

There is a growing demand for biodegradable polymer materials that mimic extracellular matrix components and architecture for application in tissue engineering and

regenerative medicine [1-5]. There is a vast amount of research focusing on synthetic materials such as polylactic acid (PLA), polyglycolic acid (PGA), and poly(ethylene glycol)(PEG). Although great advances have been made in adapting these materials into a bioinstructive scaffold [6-8], these materials have limited potential when placed in contact with natural tissues [9]. Type I collagen is the most widely distributed protein in our bodies, accounting for 70-90% of the collagen found in the form of elongated fibers. Collagen plays a critical structural role in soft tissues, organs, and bone, and it determines a wide range of mechanical and biological properties. This biomaterial contains the necessary cues to direct cells in their in vivo behaviors [10-14]. Collagen consists of three α peptide chains, containing a Gly-X-Y amino acid repeat along the chain where X and Y are most frequently proline and hydroxylated proline, which individually form a left handed coil that intertwines into a right-handed triple helix structure. Native collagen fibrils range from 30-130 nm in diameter [2]. Collagen contains two globular domains that require enzymatic cleavage to reduce them to soluble monomers, triggering the packing to ordered fibrils and inducing the self-assembly process called fibrillogenesis. The processing of collagen and bio-derived materials has been of great interest for the fabrication of fibrous natural scaffolds that mimic the extracellular matrix architecture that ranges in the nanometer to millimeter scale.

Electrospinning is considered to be among the most successful fabrication techniques for producing fibrous materials. Over the past decade, this technique has received growing attention due to its ability to create scaffolds that closely resemble the native extracellular matrix [1, 2, 15, 16]. Nanometer scale materials are crucial in biological systems to provide functional interactions between the molecules inside and

outside of cells [17]. In the electrospinning process a polymeric solution is placed on a syringe that is held by surface tension to the end of the capillary tube. The tip of the syringe is connected to a voltage source, and the collector is grounded to allow the collection of charged polymer. With no voltage, the polymer will be dispensed as droplets or as a single jet. As the polymer is subjected to the electric field, the repulsion forces act opposite to the surface tension. As the intensity of the field increases, the solution at the tip of the tube elongates, forming a conical shape known as a Taylor cone. At this point in the process, the droplet is held by its surface tension. When the electrostatic forces overcome the surface tension, a polymer solution emerges from the Taylor cone as a jet. As the jet accelerates, the solvent evaporates and thins in the electrical field. Radial charge repulsions result in an instability region on which it seems as if there is a splitting of the primary jet into multiple filaments or spraying, but the process actually creates a very fast whipping jet [1, 2, 18]. To create the ideal fiber dimensions several operational parameters must be controlled such as the polymer solution (viscosity, solvent, and concentration), the electrical field, the needle dimensions, and the feed rate. There are a wide variety of electrospun materials that includes natural proteins, synthetic peptides, and blends with synthetic organic polymers [17].

Commonly used solvents include fluoroalchohols such as 1,1,1,3,3,3 hexanofluoro-2-propanol (HFP). These solvents cause conformational changes to the native structure of collagen. HFP is a highly fluorinated alcohol that destabilizes the native triple helical structure of the protein and promotes alpha helix formation [19, 20]. These fibers contain low denaturation temperatures similar to gelatin and can lose up to

99% of the triple helical structure under pepsin treatment [21]. Researchers have found that approximately 45% of proline helical content of collagen is denatured using this solvent [19].

Our hypothesis is that by using our modified reaction electrospinning process, we will produce electrospun collagen fibers that reform their native structure. Using benign solvents such as water and ethanol at low pH, we can reduce the surface tension, which is one of the factors that affects the electrospinning, without damaging the protein structure. To verify our hypothesis, we conducted a series of experiments to allow us to assess the structure and integrity of the electrospun collagen fibers. We used scanning electron microscopy (SEM) to determine the fiber diameter and transmission electron microscopy (TEM) to determine the banding pattern. Trypsin digestion assays were performed to determine the stability of the triple helical structure. We called our newly developed technique, which combines the fiber formation process of electrospinning and fibrillogenesis, "reaction electrospinning". We can make collagen scaffolds with varying fiber diameters and varying size of voids and openness of the woven structure. In reaction electrospinning swollen dissociated collagen monomers and microfibrils are formed into thin fibers by the electric field, spun into an anhydrous ammonia atmosphere and into a solution of ammonium sulfate. The fibrils undergo fibrillogenesis and reprecipitate native banded collagen fibrils within the spun fibers. Our method produced electrospun collagen fibers that contained an average periodicity of 65.4 ± 2.6 nm. These collagen fibrous constructs allowed the adhesion of endothelial and fibroblast cells. Most importantly, the electrospun collagen was resistant to trypsin, which indicates that the triple helical

structure present in the native collagen structure is also contained in the electrospun collagen fibers.

3.3 MATERIALS AND METHODS

3.3.1 Nanofiber fabrication though reaction electrospinning

An electrospinning apparatus was built in our laboratory (Figure 3.1). A high-voltage power supply (Spellman CZE 1000R, Spellman High Voltage Electronics Corp., Hauppauge, NY, USA) was used to charge the polymeric solution, which is contained in a syringe. The syringe was connected so that at the tip of the needle or nozzle delivers a charged polymer jet. The collection target was grounded and conductive to allow fiber deposit. For this setup the collection target was stationary, providing a random fiber orientation. Previous researchers have used several collectors, such as mesh screens, by using either a rotational or stationary mandrel [2]. The syringe and syringe pump (Digital Servo Motor, Emerson Industrial Automation, Control Techniques Americas, LLC, Eden Prairie, MN, USA) were placed vertically. The interphase between the syringe pump and the driver (Epsilon EP 204 Driver -240 VAC, Single Phase, 50/60Hz, 4 Amps Continuous, 8 Amp Peak, Emerson Industrial Automation) allowed the controlled delivery of the optimal volume at a controlled volumetric-flow rate to cover the collection target.

We extracted the collagen from steer hide using a method previously described [10]. The collagen solution was adjusted to a pH of 3 using very small amounts of 12M HCl, incubated overnight, and checked the next day. The collagen was diluted with DI

water to the desired collagen concentration. The solution was then diluted with 70% ethanol to create a 1:1 EtOH:H_2O mixture and acidified to pH 3. The solution was aliquotted into 3-cc syringes and briefly centrifuged to remove air bubbles. The syringe piston was then replaced and adjusted to the 3-cc mark on top. We used a 26-gauge needle (BD PrecisionGlide, BD Biosciences, San Jose, CA, USA). The collector target consisted of a glass tissue culture plate containing the collector solution (8 M ammonia sulfate solution at pH 8) and a nylon mesh to recover the fibers. The solution was grounded to create an electrical field. An alligator clip was placed on the syringe tip.

Using a Power Tools Pro v5.1 (Emerson Industrial Automation), we jogged the shaft until it touched the piston. In the first experiments we used 2% collagen and varied the parameters for the electrical field, flow rate, gauge, and gap distance. In the second set of experiments we used 1% and 2.5% collagen concentrations with a 24-gauge needle and a gap distance of 7 cm and varied the electrical field and the flow rate.

Acidified collagen was dispensed and exposed to ammonia vapors in a closed chamber, and the fibers were collected in a stationary, grounded collection target that contained concentrated ammonia sulfate solution at pH 8. The solution contained a nylon mesh to remove the fibers from the solution afterward. The chamber was filled with a 50/50 mixture of nitrogen/ammonia gas for 30 min. The resulting collagen fibers were removed from the solution and placed in 4°C deionized water for 15 min. This was repeated three times and left overnight at 4°C. The following day, the fibers were washed three times more with 4°C deionized water for 15 min and then placed in a 0.3% bicarbonate solution for 15 min. Then, the fibers were submerged in 4°C deionized water for 2 hr and placed overnight at 4°C in a Mosconas solution (136.8 mM NaCl, 28.6 mM

KCl, 11.9 mM $NaHCO_3$, 9.4 mM glucose, 0.08 NaH_2PO_4 , pH 7.4; Sigma-Aldrich, St. Louis, MO, USA). On the 3rd day the fibers were UV irradiated with 6.3×10^5 microjoules per cm^2, and the fibers were divided into samples for SEM, TEM, trypsin digestion, and measurement of dry weights.

3.3.2 SEM

To determine the collagen fiber diameter, samples were prepared for SEM. The method used was the GTA-O-GTA-O-GTA-O method. Fibers were fixed with 2.5% glutaraldehyde in deionized water at 4°C overnight. The sample was washed twice with 1X PBS. Samples were treated with 1% tannic acid/1% glutaraldehyde for 1 hr. The samples were immersed in a 1% aqueous solution of OsO_4 for 1 hr. Samples were rinsed and treated twice with the GTA-O steps: a 1-hr incubation in 1% glutaraldehyde/1% tannic acid at room temperature, followed by a 1-hr rinse in 1% OsO_4. The fibers were then dehydrated in a graded ethanol series, dried to the critical point, mounted on aluminum stubs, and imaged on a JEOL (Tokyo, Japan) JSM-6300V at 10 KV. Using Image J software (NIH, Bethesda, MD, USA), we placed a grid on the images and selected nine intersection points, selected random fibers, and measured the fiber diameters. We calculated the mean and standard deviation (SD) per run.

3.3.3 TEM

To determine the molecular structure of the fibers, the samples were fixed with 2.5% glutaraldehyde in deionized water at 4°C overnight. The samples were washed twice with 1X PBS, and then immersed in 1% tannic acid/1% glutaraldehyde in 1X PBS for 30 min. After rinsing, samples were treated with 1% osmium tetroxide/1.5% K+ ferricyanide in 1X PBS for 1 hr. The samples were rinsed and dehydrated in a series of ascending aqueous ethanol concentrations. Samples were embedded in PolyBed 812. Ultra-thin sections were obtained using the Reinchert Ultracut E ultra-microtome (Leica Microsystem Ltd, Wetzlar, Germany) collected on copper grids. Contrast was added to samples with 2% uranyl acetate (aq) and a Hanaichi lead stain[22] and imaged using a JEM-200CX transmission electron microscope (JEOL Ltd, Tokyo, Japan) at 120 KV.

3.3.4 Trypsin digestion

To determine the integrity of the collagen, a trypsin digestion test was performed [23-25]. Electrospun collagen fibers were exposed to a 0.25% trypsin solution (pH 7.8) overnight at 30°C. The supernatant was extracted and a bicinchoninic acid assay (BCA, Pierce Chemical, Rockford, IL, USA) was performed to quantify the amount of protein in solution. The dry weight of the collagen was determined prior and after the enzyme treatment.

3.3.5 Sodium dodecyl sulfate-polyacrylamide gel electrophoresis (SDS-PAGE)

Trypsin digestion samples were taken to identify the proteins in solution. Three samples were taken from three independent collagen electrospun fibers. Samples were mixed with 10X protein loading buffer (1 M Tris-HCl, pH 6.8, 10% SDS, 0.2% bromophenol blue, 25% β-mercaptoethanol, and 50% glycerol) in a 9:1 (sample:sample buffer) ratio. Samples were run using 1× running buffer made from 10× Tris/Glycine/SDS Buffer (Bio-Rad Laboratories, Hercules, CA, USA). The samples were heated for 5 min at 95°C. After being heated, 40 µL of each sample was loaded in the wells of a 4-20% Mini Protean TGX Gel (Bio-Rad Laboratories), and electrophoresis was performed at 100V. After electrophoresis, the gel was fixed with a mixture of 50% (v/v) methanol and 10% (v/v) acetic acid for 30 min at room temperature, followed by staining with 0.01% (w/v) Brilliant Blue R-250 (ThermoFisher Scientific, Waltham, MA, USA) in 20% (v/v) methanol and 10% (v/v) acetic acid overnight in a shaker at 4°C. Finally, the gel was destained by washing three times with a mixture of 30% methanol and 10% acetic acid for 1 hr in a shaker at 4°C, and destaining with same solution two more times for 30 min. Precision Dual Color Standards (Bio-Rad Laboratories) was used to estimate the molecular weight of the protein. Each band was analyzed using Image J software to quantify the ratio of expression relative to other bands within each sample.

3.3.6 Western blot analysis

To determine the quantities of collagen in the trypsin assay, immunoblots were performed. The supernatants were obtained from the three independent synthesis

reactions of collagen fibers digested with trypsin. Samples were mixed with 4× Laemmli sample buffer (Bio-Rad Laboratories) containing 100 mL/L β-mercaptoethanol (βME) in a 3:1 (sample:sample buffer) ratio. Samples were run using 1× Buffer made from 10X Tris/Glycine/SDS Buffer (Bio-Rad Laboratories). The samples were heated for 5 min at 95°C. After being heated, 40 µL of each sample was loaded in the wells of a 4-20% Mini Protean TGX Gel (Bio-Rad Laboratories), and electrophoresis was performed at 100V. The proteins were transferred to membranes in electroblot transfer buffer (25 mM Tris, pH 6.8, 190 mM glycine, and 20% methanol) at 100V for 80 min. The blots were blocked in 5% nonfat milk in washing buffer (20 mM Tris, pH 6.8, 137 mM sodium chloride, and 0.2% Tween 20) for 1 hr at room temperature. Subsequently, they were exposed to anti-collagen I antibody (Novus Biological, NB600-408, Littleton, CO, USA) at 1:1000 overnight at 4°C. Then, we added a goat anti-rabbit IgG horseradish peroxidase secondary antibody (G2123, Invitrogen, Eugene, OR, USA) at 1:5000 for 1 hr at room temperature. The blot was washed on an orbital shaker for 30 min, changing the washing buffer every 10 min. To detect the bound antibodies, we used an enhanced chemiluminescence detection system (Pierce ECL Western Blot Substrate, Rockford, IL). Images were taken at an 8-min exposure.

3.3.7 Cell Culture

Cells were cultured in 75 cm^2 BioLite culture flasks (ThermoFisher Scientific) at 37°C in 5% CO_2 humidified incubators. Human adipose microvascular endothelial cells (HAMEC; ScienCell Research Laboratories, Carlsbad, CA, USA) were grown in

Endothelial Cell Growth media (EGM-2; Lonza Group Ltd., Basel, Switzerland). Adult normal human dermal fibroblast cells (NHDFs, Lonza Group Ltd.) were cultured in Fibroblast Growth Media (FGM-2; Lonza Group Ltd.). The cells were passaged using 0.05% trypsin in 1X PBS (ThermoFisher Scientific) and harvested when they reached a confluency of approximately 80%.

3.3.8 Generation of collagen constructs

Electrospun collagen fibers were seeded with fibroblasts and endothelial cells. We used a 4:1 ratio of NHDFs and HAMECs, which is reported to be the ideal ratio to promote vasculogenesis [26]. Briefly, we used approximately 4 g of 2.5% electrospun collagen fibers spun at 20 KV at a flow rate of 0.5 cc/min. The fibers were cast on a 12-well plate and seeded with a total of 1-2 million cells. The media used was a 2:1 ratio of FGM-2 and EGM-2. The construct was incubated in cell culture for 2 and 5 days, changing the media after 3 days.

3.3.9 Immunofluorescence labeling

The collagen constructs were washed with PBS and fixed with 4% formaldehyde for 1 hr at room temperature. The sample was washed with PBS and placed on a 12-well plate. The construct was permeabilized using 0.01% Triton X-100/0.01M glycine for 30 min and blocked with 5% BSA solution in 1× PBS overnight at 4°C. The anti-CD-31 (abcam, Cambridge, MA, USA, 1:50) and anti-collagen 1 (abcam, 1:200) primary

antibodies were diluted in a 1% BSA solution and incubated overnight at 4°C. After rinsing, the constructs were incubated for 2 hr at room temperature with Alexa Fluor 546 goat anti-rabbit (Molecular Probes, Eugene, OR, USA, 1:500), Hoechst 33342 (Invitrogen Life Technologies, Carlsbad, CA, USA, 1:1000), monoclonal anti-actin, α-smooth muscle actin-FITC (αSMA; Sigma-Aldrich, 1:200), and Alexa Fluor 633 Phalloidin (Molecular Probes, 1:500) antibodies. Samples were mounted on glass slides with 1-mm coverslips using ProLong Gold antifade reagent (Molecular Probes).

3.3.10 Imaging

Z-stack images were taken (step size averaging 5 μm) using a Leica TCS SP5 AOBS Confocal Microscope System (Leica Microsystems, Inc., Exton, PA, USA) in sequential multichannel mode. The stacks were projected at maximum and leveled using ImageJ and Adobe Photoshop CS5 (Adobe Systems Inc., San Jose, CA, USA).

3.3.11 Statistical Analysis

Data presented are expressed as the mean ± standard deviation (SD). One way analysis of variance (ANOVA) for multiple comparisons was employed to determine the variance of the population of the samples. The threshold for statistical significance was set at $p<0.05$. A Modified Thompson Tau test was used to determine outliers.

3.4 RESULTS

3.4.1 Determination of the parameters affecting the fiber diameter

SEM micrographs (Figure 3.2 and 3.3) of the electrospun collagen fibers were obtained using the parameters described in Table A.1 and A.4. A random fibrous mesh was created by the different parameters with 2% collagen that have diverse orientation of individual fibers averaging 560 ± 167 nm in diameter. A fiber diameter of 625±81 and 644±61 nm were produced by 1% and 2.5% collagen concentration, respectively (Parameters on Table A.4). The fiber diameter distributions among the tested parameters are shown in Supplemental Figures 3.1 and 3.2.

Using Design Expert, we designed an experiment of 22 runs (Table A.1). Regression analysis and ANOVA using the four parameters indicated that there was a significant difference in the fiber diameter produced depending upon the flow rate ($p=0.046$) and the electrical field ($p=0.009$) (Table A.2). These two parameters were the major factors that determined the fiber diameter of the collagen (Figure A.1); whereas, the remaining parameters had minor or insignificant effects on the outcome ($p>0.05$). By removing the gap and gauge parameters from the statistical analysis, these findings became more significant (Table A.3). Because viscosity has been reported to play a role in the electrospun fiber, we designed a second set of experiments using two different collagen concentrations and varied the electric field and the flow rate (Table A.4). We showed that again, for our reaction electrospinning setup, within the range of each parameter tested, the electric field ($p=0.05$) and the flow rate ($p=0.048$) were the only variables that significantly influenced the electrospun collagen fiber diameter (Figure A.2

and Table A.5). By removing the concentration from the statistical analysis, these findings became more significant (Table A.6).

3.4.2 Determination of the collagen structure in the electrospun fibers

The electrospun collagen fibers exhibit the characteristic cross striation pattern of native collagen independent of the collagen concentration. TEM images showed clear banding patterns of approximately 65.4±2.6 nm in width (Figure 3.4). The final run, which correlated to the lowest concentration, lowest flow rate, and highest electric field, produced the loosest collagen fibrils and the one that showed the characteristic banding similar to that of native collagen. The last run banding measurement was considered an outlier. An average periodicity of 67 nm is present in the native hydrated state. The preparation process that is composed of dehydration and shrinking has been shown previously can cause lower values on the TEM images ranging from 55-65 nm. These parameters produced a combination of predominantly fully assembled fibrils as well as a lesser amount of loosely packed collagen bundles. TEM showed that individual fibrils had a diameter of 145±33 nm.

3.4.3 Determination of the integrity of the collagen fibers

Three samples were taken from three independent collagen fibers incubated with trypsin, and the amount of protein dissolved was determined by a BCA assay (Table A.7). The electrospun collagen fibers were mostly resistant to trypsin digestion with only

a minimal amount of soluble collagen. The final dry weight of the collagen was increased by the trypsin residue. Using SDS-PAGE we determined that the majority of the soluble protein was trypsin, accounting for 75%, 72%, and 64% of each sample, respectively (Figure 3.5).

The immunoblot analysis showed that there was very little protein dissolved during the trypsin digestion assay that corresponded to collagen (Figure 3.6). All three samples showed a faint band at approximately 60 KDa, which corresponded to hydrolyzed collagen. Unraveled collagen fibrils are susceptible to trypsin attack to a certain degree. Compared to the overall sample a very negligible amount of protein was dissolved in the trypsin digestion solution.

3.4.4 Cell adhesion to the collagen constructs

To determine the biological compatibility of the reaction electrospun collagen fibers, we cultured endothelial and fibroblast cells for 2 (Figures 3.7-3.8) and 5 (Figure 3.9) days. Immunostaining was performed using three markers: collagen 1, α-smooth muscle actin (myofibroblast cells), and CD31 (endothelial cells). Immunohistochemistry confirmed the presence of these markers on the collagen fibrous scaffolds. Cells were also stained with Hoechst (nuclei) and Phalloidin (f-actin, cytoskeleton).

Figure 3.9 shows the immunostaining of endothelial and fibroblast cells after culturing for 5 days on collagen nanofibers. These images show that cells organized into cluster of cells with sprouting projections extending to another cell cluster - a behavior characteristic of endothelial cell sprouting. Collagen I has been shown to cause

endothelial cells to assume a spindle-shaped morphology, which is similar to precapillary formation, and to align into cord assemblies [11]. Microscopy analysis showed a fiber diameter averaging 450 μm, which indicated some reduction from the original fiber diameter (574 nm). In other areas of the sample, the fiber diameter averaged 1 mm in width, which might indicate merging of two fibers due to cellular contraction (figure 3.7 and 3.8).

3.5 DISCUSSION

The majority of human tissues and organs are attached to a collagen fibrous structure with a fiber size ranging from the nanometer to millimeter scale. Electrospinning is currently the most successful method for the fabrication of nanofiber structures. Unfortunately, common solvents denature the collagen structure. In this study, we demonstrate with collagen, a clinically approved biopolymer, a new technique called reaction electrospinning production of scaffolds that are biocompatible, supporting a submicron fibrous platform for the use of tissue engineering and regenerative medicine. The fibrous nanoscale structures provide the necessary support for cells allowing them to demonstrate typical in vivo behaviors. The similarities between the electrospun collagen fibers and the morphology of the ECM provides an ideal biomimetic niche for seeded cells [2]. Using electrospun fibers researchers have labored to replicate several tissue morphologies including cartilage, bone, vasculature, and nerves [3, 4, 27, 28].

The major novelty of this study is the development and optimization of the reaction electrospinning procedure. This technique combines electrospinning with the fibrillogenesis process. Monomeric native molecules and intermediate aggregates are

soluble and stable at pH 3 at a low ionic strength and temperature. The acidified polymer solution is used as our electrospinning solution. As the collagen solution is electrospun, there is an increase in the temperature and pH caused by contact with the ammonia vapors and solution. This initiates the self-assembly fibrillogenesis process. The aggregation process initiates with a quarter-staggered arrangement of the monomers, which then aggregate into five-stranded fibrils that continue to further assemble to form larger fibrils [29-31]. In our process, we control the diameter of the fibers as they are being precipitated and reconstituted into collagen fibrils that resemble the behavior of native collagen.

Several parameters affect the fibers created by electrospinning. These include the solvent (solution viscosity and conductivity), the strength of the field, the flow rate, and the air gap (the distance between the collector and the syringe tip). The most common types of solvents used for electrospinning are the fluoroalchohols that reduce the surface tension of the solution. This process has been reported to produce scaffolds that are readily soluble in aqueous media. Collagen in its native state and under physiological conditions is a water-insoluble polymer due to its hydrophobic residues residing on the outside of its polypeptide structure. The shift from a water insoluble protein to a water soluble protein entails conformational changes in the protein structure. HFP solubilizes the collagen, but in the process the two trifluoromethyl groups break the hydrophobic interactions and the solvent's acidity assists in breaking the hydrogen bonds [20]. These electrospun collagen scaffolds are soluble in aqueous media due to damage to their secondary structures and are not suitable for use in tissue engineering scaffolds. To compensate for this, researchers have used several crosslinking mechanisms to stabilize

the structure of the electrospun fibers. One of the most common crosslinking reagents is glutaraldehyde. Glutaraldehyde reacts with the amide group of collagen forming crosslinks between the polymer chains, but this approach introduces toxicity, side products, and changes in morphology (porosity and fiber diameter) [32]. Dong et al shows that by using a benign solvent that combines water and ethanol with salt, collagen can be solubilized at a neutral pH, creating a stable electrospinning system. The collagen mats produced are still soluble and additional crosslinking with 1,ethyl-3(3-dimethylaminopropyl)carbodiimidehydrochloride) (EDC) and N-hydroxysuccinimide (NHS) is required [20]. The high concentration of salts destabilizes the collagen, which can cause conformational changes in the protein. In contrast, by using UV irradiation to reconstitute the covalent bonds existing in the native collagen structure, we obtain collagen fibrils that closely mimic what is observed in the native tissue. UV irradiation stabilizes the collagen structure and improves its mechanical properties, making the structure resistant to enzymatic attack. Previous researchers have found that the concentration of the polymeric solution affects the fiber diameter. Shih et al. [33] found that by using collagen concentrations of 4, 8, and 12% in a HFP solvent they obtained fiber diameters of 50-200, 200-500, and 500-1000 nm, respectively. Common electrospinning procedures use 3%-10% collagen solubilized in HFP [2, 21, 34]. Matthews et al. found no evidence of electrospinning at a collagen concentration of 0.0083 g/mL (0.8 wt %) [2]. Failure to electrospin might be caused by the effects of the fluoroalcohols on the collagen, causing loss of the triple helical structure [21]. We selected a collagen range from 1-2.5% collagen, which is lower than previously published data, and we used acidified collagen dissolved in ethanol. This solution contains a

combination of monomers and microfibrils. At lower concentrations, we have the necessary properties to electrospin the collagen. Within the tested range we obtain non-soluble fiber formation at each collagen concentration. The collagen concentration is not correlated to fiber diameter within this range ($p=0.368$). The first set of experiments was designed to determine which parameters - including electrical field, air gap, flow rate, and gauge - affect the fiber diameter. Of these parameters only the electrical field and the flow rate affect the fiber diameter. The same result was found in the second experiment.

One of the most important features of reconstituted collagen fibers is the characteristic D banding. This pattern, which results from the alternating overlapping and gap zones caused by the specific assembly arrangement of the collagen molecules, is called the "fingerprint" of collagen. Fibrillogenesis, or the process by which collagen molecules assemble into collagen fibers, is governed by covalent bonds, electrostatic forces, hydrophobic, and hydrophilic interactions. Previous researchers have shown that the characteristic banding pattern is affected by factors such as the buffer type, ionic strength, and pH affecting the in vitro fibrillogenesis process. This collagen banding pattern is lost by using fluoroalchohols, which is an indication of denaturation of the collagen structure [21]. Our electrospun collagen fibrils that maintain the characteristic banding pattern closely resemble the range of the individual fibrils found in biologically derived collagen. The ability of collagen to form striated fibrils involves hydrophobic and charge interactions. Researchers have argued that in order to fully characterize the fiber diameter, analysis by TEM and SEM should be employed, based on the limitations of each technique. SEM is unable to detect objects smaller than 0.25 μm, but TEM cannot detect fibers larger than 60 μm [35]. The size distribution of the electrospun collagen

fibers is 100-500 nm. This range is close to ideal, mimicking the native ECM (50-500 nm).

As revealed by immunostaining of α-smooth muscle actin and CD31, myofibroblast and endothelial cells adhere to the collagen fibers and maintain their phenotypic expression. There are also signs of contraction of the matrix and common endothelial cell behaviors including forming small clusters of cells and creating sprout extensions on the constructs cultured for longer periods of time.

Additionally, the tight triple helical structure of collagen is resistant to pepsin and trypsin, unless the structure is compromised. Immunoblot analysis shows that there is little protein dissolved when the electrospun collagen fibers are subjected to trypsin digestion. This protein can be attributed to a small amount of loosely packed collagen.

3.6 CONCLUSION

Reaction electrospinning produces collagen fibers that can be reconstituted into mature collagen fibers. Using benign solvents, we eliminate the toxicity attributed to previously established procedures without denaturing the collagen fiber structure. Using this design, we can obtain a triple helical collagen desired to generate fibrous collagen scaffolds.

3.7 REFERENCES

1. Huang, Z.-M., et al., *A review on polymer nanofibers by electrospinning and their applications in nanocomposites.* Composites Science and Technology, 2003. **63**(15): p. 2223-2253.
2. Matthews, J.A., et al., *Electrospinning of Collagen Nanofibers.* Biomacromolecules, 2002. **3**(2): p. 232-238.
3. Hasan, A., et al., *Electrospun scaffolds for tissue engineering of vascular grafts.* Acta Biomater, 2014. **10**(1): p. 11-25.
4. Liu, T., et al., *Nanofibrous collagen nerve conduits for spinal cord repair.* Tissue Eng Part A, 2012. **18**(9-10): p. 1057-66.
5. Prabhakaran, M.P., J. Venugopal, and S. Ramakrishna, *Electrospun nanostructured scaffolds for bone tissue engineering.* Acta Biomaterialia, 2009. **5**(8): p. 2884-2893.
6. Jeong, S.I., et al., *In vivo biocompatibilty and degradation behavior of elastic poly(L-lactide-co-epsilon-caprolactone) scaffolds.* Biomaterials, 2004. **25**(28): p. 5939-46.
7. Kretlow, J.D., L. Klouda, and A.G. Mikos, *Injectable matrices and scaffolds for drug delivery in tissue engineering.* Adv Drug Deliv Rev, 2007. **59**(4-5): p. 263-73.
8. Oh, S., *Fabrication and characterization of hydrophilic poly(lactic-co-glycolic acid)/poly(vinyl alcohol) blend cell scaffolds by melt-molding particulate-leaching method.* Biomaterials, 2003. **24**(22): p. 4011-4021.

9. Nugent, H.M. and E.R. Edelman, *Tissue engineering therapy for cardiovascular disease.* Circ Res, 2003. **92**(10): p. 1068-78.

10. Yost, M.J., et al., *A novel tubular scaffold for cardiovascular tissue engineering.* Tissue Eng, 2004. **10**(1-2): p. 273-84.

11. Whelan, M.C. and D.R. Senger, *Collagen I initiates endothelial cell morphogenesis by inducing actin polymerization through suppression of cyclic AMP and protein kinase A.* J Biol Chem, 2003. **278**(1): p. 327-34.

12. Mason, B.N., et al., *Tuning three-dimensional collagen matrix stiffness independently of collagen concentration modulates endothelial cell behavior.* Acta Biomater, 2013. **9**(1): p. 4635-44.

13. Zheng, W., W. Zhang, and X. Jiang, *Biomimetic Collagen Nanofibrous Materials for Bone Tissue Engineering.* Advanced Engineering Materials, 2010. **12**(9): p. B451-B466.

14. Fann, S.A., et al., *A model of tissue-engineering ventral hernia repairs.* Journal of Investigative Surgery, 2006: p. 193-205.

15. Hofman, K., et al., *Effects of the molecular format of collagen on characteristics of electrospun fibres.* Journal of Materials Science, 2011. **47**(3): p. 1148-1155.

16. Guarino, V., et al., *Polylactic acid fibre-reinforced polycaprolactone scaffolds for bone tissue engineering.* Biomaterials, 2008. **29**(27): p. 3662-3670.

17. Khadka, D.B. and D.T. Haynie, *Protein- and peptide-based electrospun nanofibers in medical biomaterials.* Nanomedicine, 2012. **8**(8): p. 1242-62.

18. Shin, Y.M., et al., *Electrospinning: A whipping fluid jet generates submicron polymer fibers.* Applied Physics Letters, 2001. **78**(8): p. 1149.

19. Yang, L., et al., *Mechanical properties of single electrospun collagen type I fibers.* Biomaterials, 2008. **29**(8): p. 955-962.

20. Dong, B., et al., *Electrospinning of Collagen Nanofiber Scaffolds from Benign Solvents.* Macromolecular Rapid Communications, 2009. **30**(7): p. 539-542.

21. Zeugolis, D.I., et al., *Electro-spinning of pure collagen nano-fibres – Just an expensive way to make gelatin?* Biomaterials, 2008. **29**(15): p. 2293-2305.

22. Hanaichi, T., et al., *A stable lead by modification of sato method.* Journal of Electron Microscopy, 1986. **35**(3): p. 304-306.

23. Zhang, Z.K., G.Y. Li, and B. Shi, *Physicochemical properties of collagen, gelatin and collagen hydrolysate derived from bovine limed split wastes.* Journal of the Society of Leather Technologists and Chemists, 2006. **90**(1): p. 23-28.

24. Keech, M.K., *The effect of collagenase and trypsin on collagen-an electron microscopic study* Anatomical Record, 1954. **119**(2): p. 139-159.

25. Drake, M.P., et al., *Action of proteolytic enzymes on tropocollagen and insoluble collagen.* Biochemistry, 1966. **5**(1): p. 301-312.

26. Czajka, C.A. and C.J. Drake, *Self-Assembly of Prevascular Tissues from Endothelial and Fibroblast Cells under Scaffold-Free, Non-adherent Conditions.* Tissue Eng Part A, 2014.

27. Reznikov, N., R. Shahar, and S. Weiner, *Three-dimensional structure of human lamellar bone: the presence of two different materials and new insights into the hierarchical organization.* Bone, 2014. **59**: p. 93-104.

28. Liu, T., et al., *Photochemical crosslinked electrospun collagen nanofibers: synthesis, characterization and neural stem cell interactions.* J Biomed Mater Res A, 2010. **95**(1): p. 276-82.

29. Trelstad, R.L., K. Hayashi, and J. Gross, *Collagen fibrillogenesis: intermediate aggregates and suprafibrillar order.* Proc Natl Acad Sci U S A, 1976. **73**(11): p. 4027-31.

30. Harris, J.R., A. Soliakov, and R.J. Lewis, *In vitro fibrillogenesis of collagen type I in varying ionic and pH conditions.* Micron, 2013. **49**: p. 60-8.

31. Holmes, D.F., M.J. Capaldi, and J.A. Chapman, *Reconstitution of collagen fibrils in vitro; the assembly process depends on the initiating procedure.* International Journal of Biological Macromolecules, 1986. **8**(3): p. 161-166.

32. Hartman, O., et al., *Microfabricated electrospun collagen membranes for 3-D cancer models and drug screening applications.* Biomacromolecules, 2009. **10**(8): p. 2019-32.

33. Shih, Y.R., et al., *Growth of mesenchymal stem cells on electrospun type I collagen nanofibers.* Stem Cells, 2006. **24**(11): p. 2391-7.

34. Yang, L., et al., *Mechanical properties of single electrospun collagen type I fibers.* Biomaterials, 2008. **29**(8): p. 955-62.

35. MacKinnon, P.A., et al., *Electron microscopy study of refractory ceramic fibers.* Appl Occup Environ Hyg, 2001. **16**(10): p. 944-51.

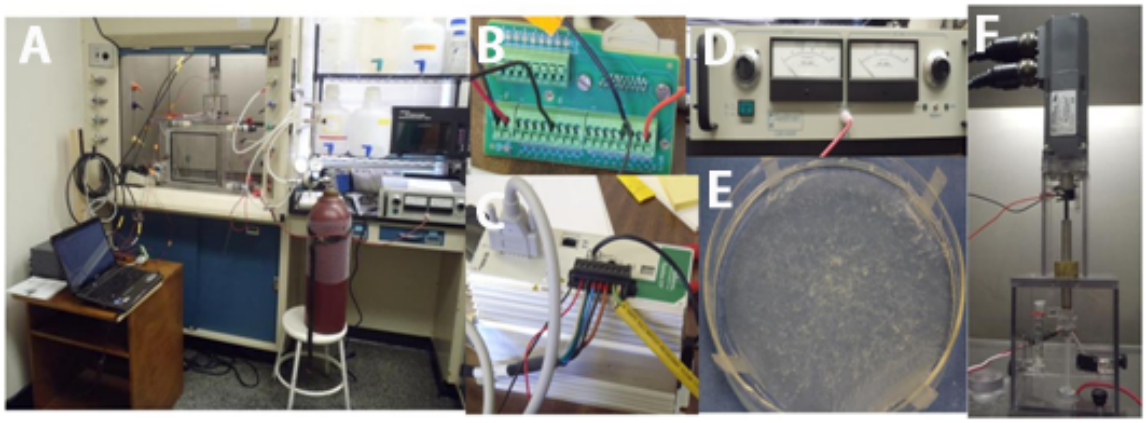

Figure 3.1. The electrospinning setup. We built an electrospinning apparatus (A) that consists of a limit control (B), driver (C), voltage source (D), and syringe pump (F). The electrospun collagen fibers are collected in a grounded solution (E).

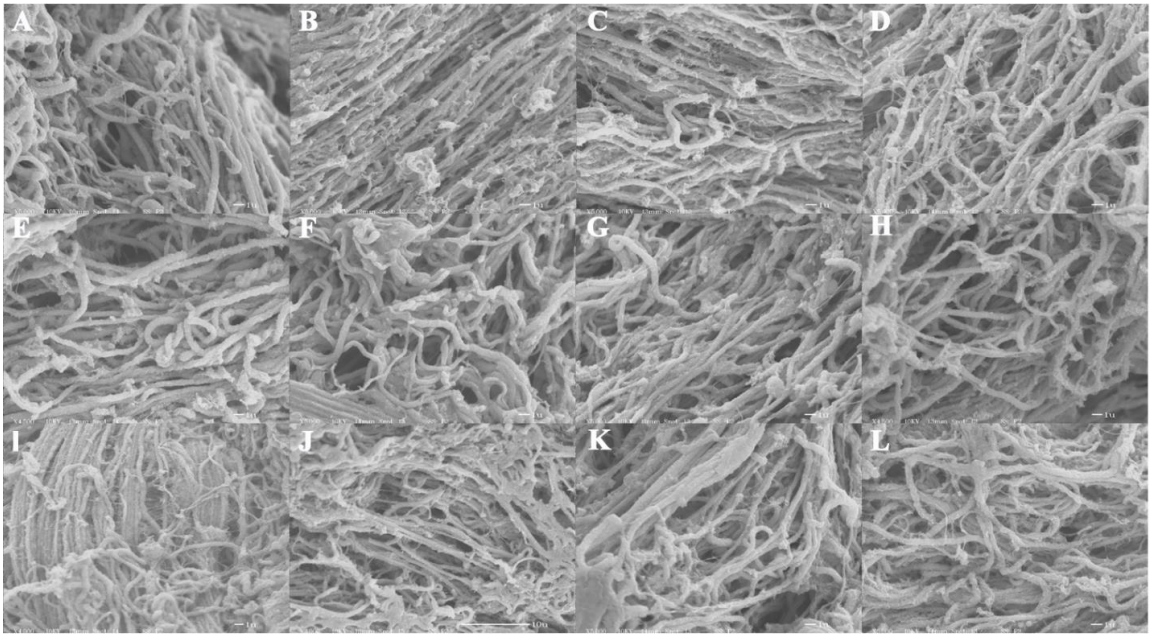

Figure 3.2. SEM images of 2% electrospun collagen fibers using parameters described in Table A.1. Images A-L represent runs 4, 5, 10, and 13-21, respectively (Table A.1). Most of the electrospun collagen fibers produced are randomly oriented; however, there is some apparent alignment in runs 5(B) and 18(I).

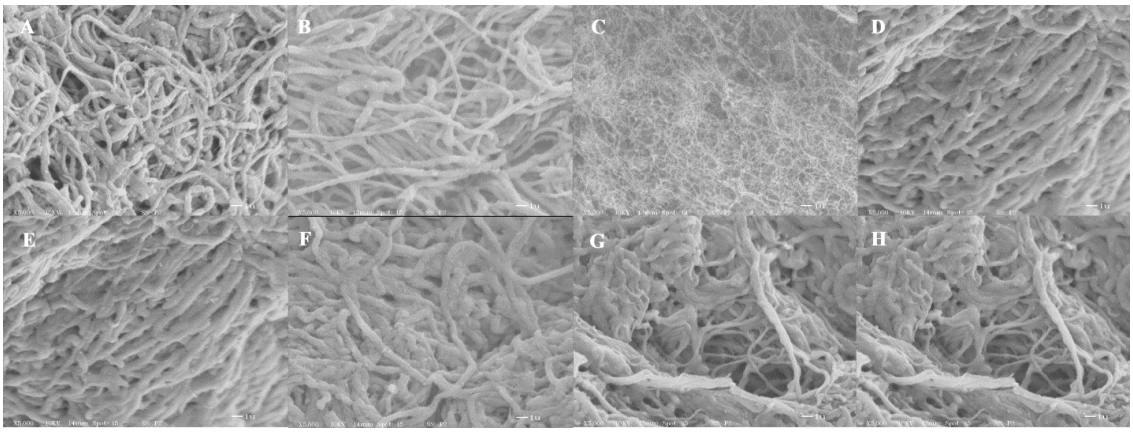

Figure 3.3. SEM images for 1 and 2.5% electrospun collagen fibers using the parameters in Table A.4. Images in A-H correspond to runs 1-8 (Table A.4), respectively. These images show randomly oriented fibers using two different collagen concentrations.

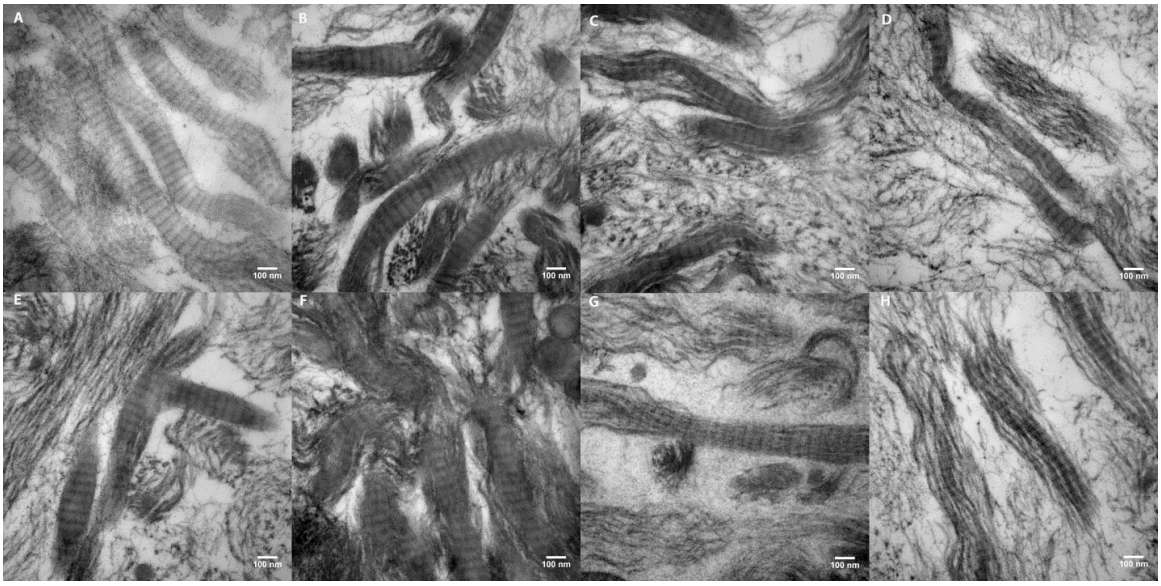

Figure 3.4. TEM images of the 1 and 2% electrospun collagen fibers. Images in A-H correspond to runs 1-8 (Table A.4), respectively. A banding pattern of approximately 65 nm characteristic of native collagen can be seen. (scale bars 100 nm)

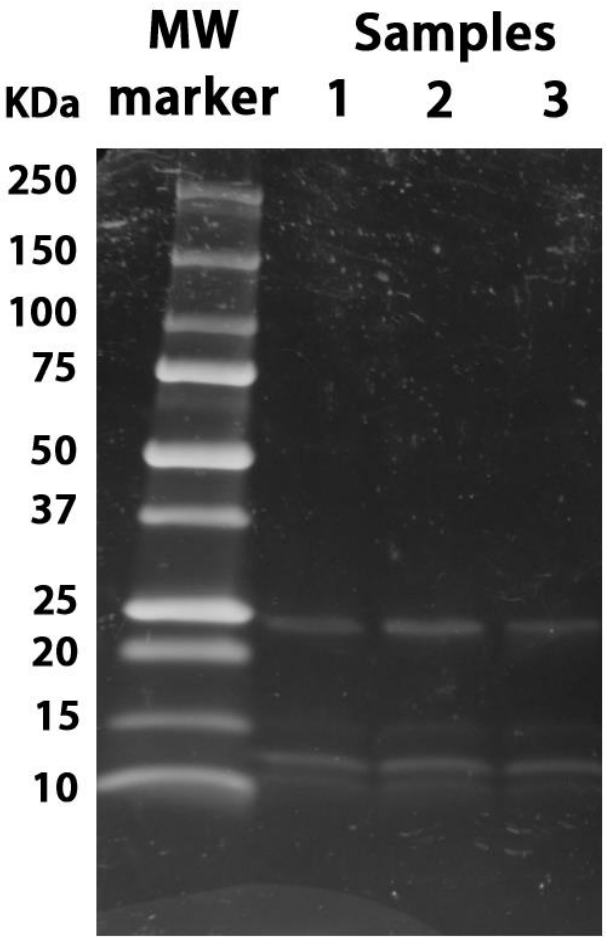

Figure 3.5. The SDS-PAGE of the trypsin digestion assay is shown. The molecular weight marker (lane 1) and the trypsin digestion samples (in lanes 2-4) are shown. There is a band of the expected size for tryspin (MW 23 KDa), showing that very little protein is removed from the collagen spun fibers.

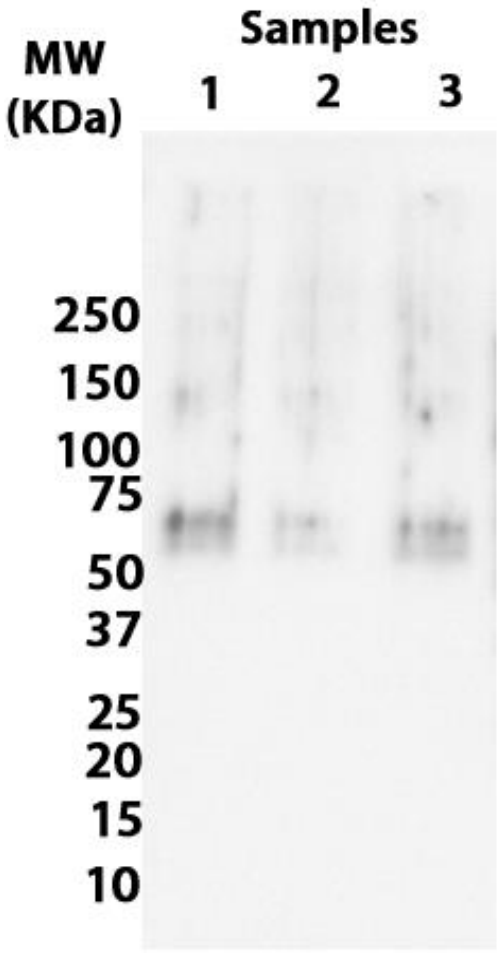

Figure 3.6. Western Blot Analysis. A western blot analysis of the trypsin digestion assay is shown. In the three samples a band ~60 KDa was detected representing a very small amount of hydrolyzed collagen.

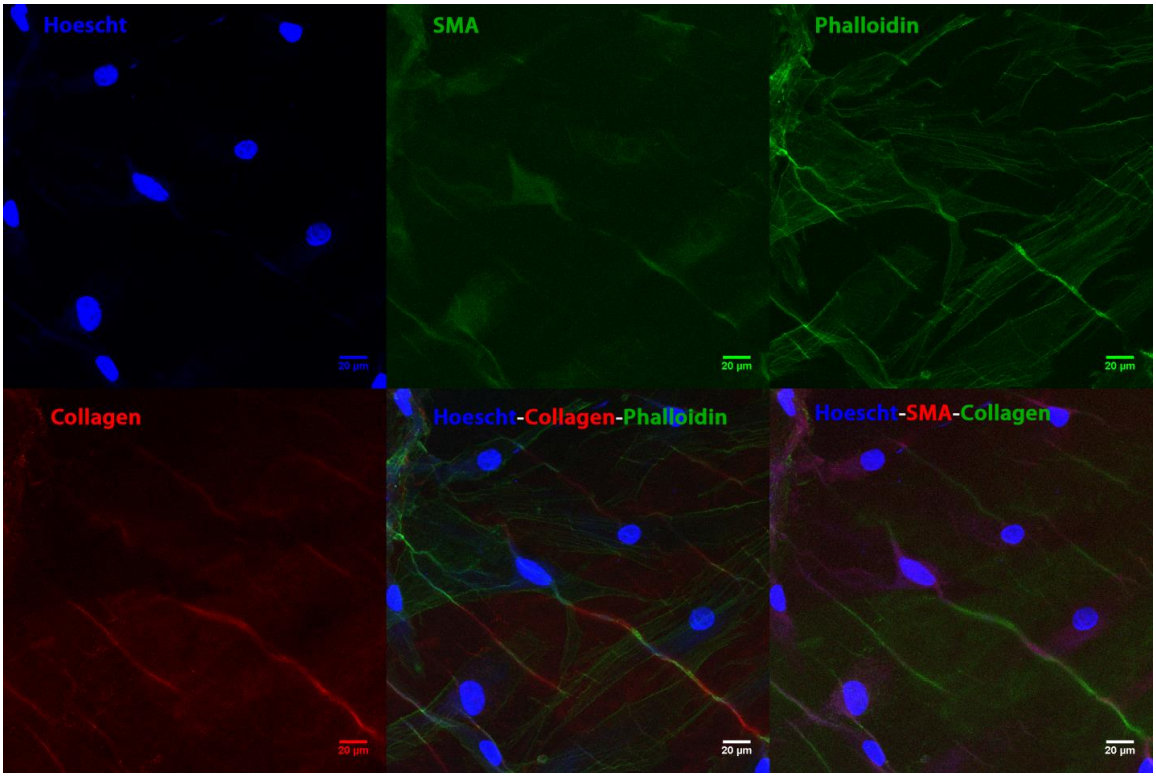

Figure 3.7. Confocal microscopy of the collagen fibers cultured for 2 days with endothelial and fibroblast cells. These images revealed the presence of α-smooth muscle actin and collagen. The cell adhesion and alignment of the fibroblast to the collagen electrospun collagen fiber is shown. (63× magnification, scale bar 20 µm)

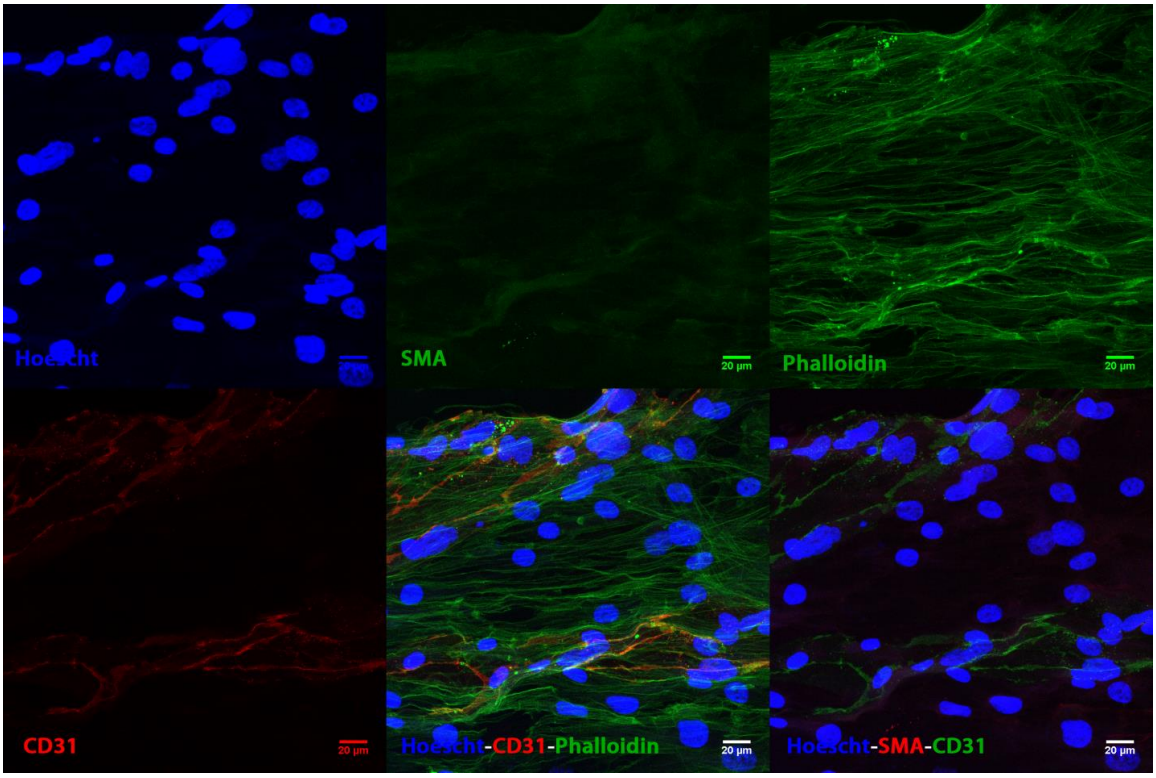

Figure 3.8. Confocal microscopy of the collagen fibers cultured for 2 days with endothelial and fibroblast cells. These images revealed the presence of α-smooth muscle actin and CD31. The phenotypic expression of these markers was maintained when cultured in the electrospun collagen fibers. (63× magnification, scale bar 20 µm)

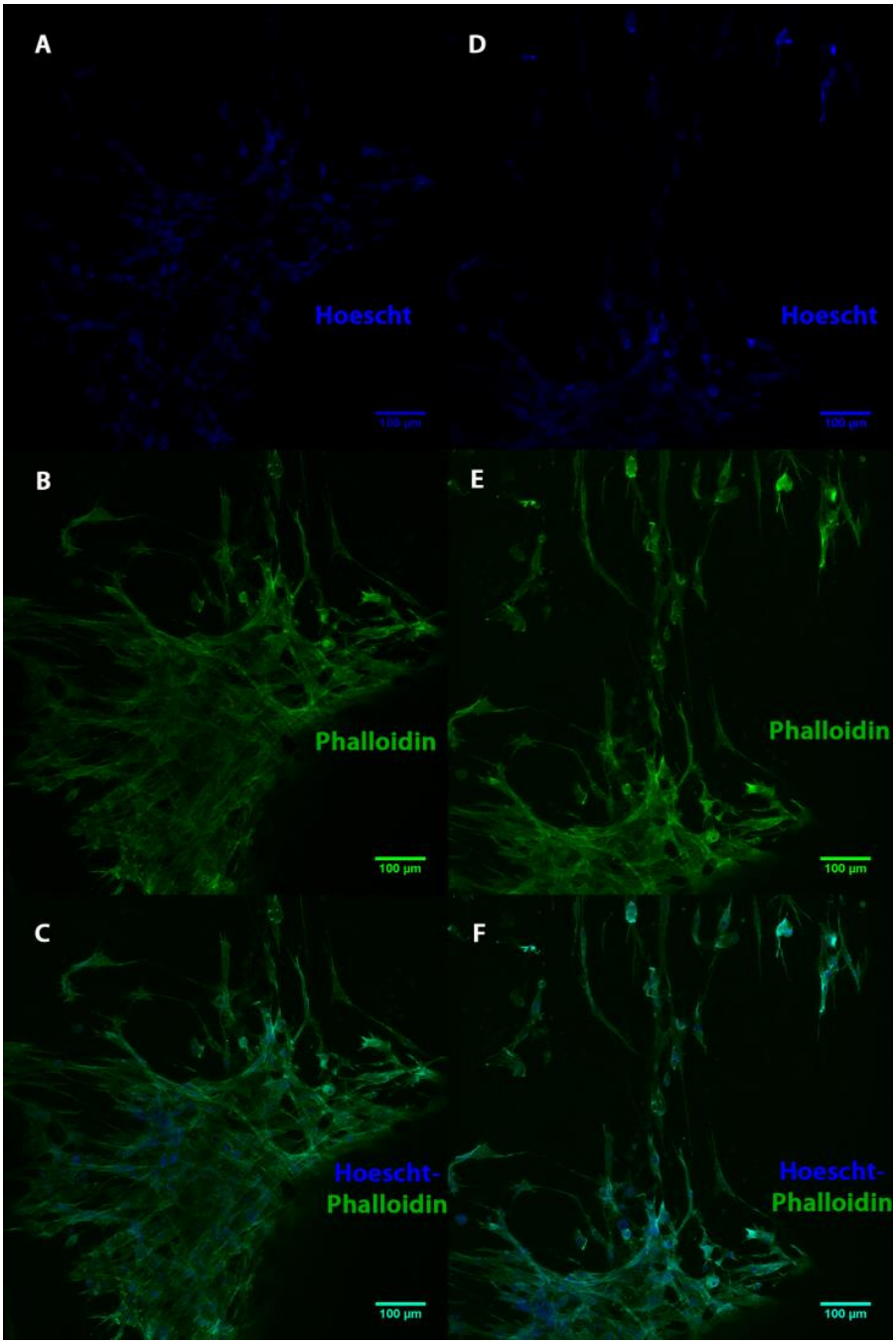

Figure 3.9. Confocal microscopy of the collagen fibers cultured with endothelial and fibroblast cells after 5 days of culture. A-C, a high density cluster of cells is shown. D-F, elongated projections at the top of the cluster of cells are shown that appears to represent sprouting between two dense cell bodies. (A and D – Hoechst [blue], B and E – Phalloidin [green], and C and F – merge image, 40× magnification, scale bar 100 µm)

CHAPTER 4:

DESIGNER OF COLLAGEN HYDROGEL TO REGULATE SATELLITE CELL PHENOTYPE[2]

[2] Rodriguez-Rivera, V; Goodwin, RL; Mohsen, N; Terracio, L; Weidner, JW; Yost, MJ. Submitted to *Plastic and Reconstructive Surgery*, 01/2012

4.1 ABSTRACT

The regenerative capabilities of muscle stem cells, satellite cells, are lost once they are culture in a rigid environment such as a polystyrene plastic that possess an elastic modulus of 3 GPa. In order for the satellite cells to remain undifferentiated and proliferative, it is imperative to recreate the biophysical properties of the stem cells niche, which includes the extracellular matrix and the basement membrane.

Our goal is to tune the extracellular matrix to the elastic modulus found in vivo for the skeletal muscle stem cells niche which is estimated to be 12 KPa. We used natural components of the ECM such as collagen and laminin and vary the concentrations of the collagen and crosslink them in order to achieve the desired Young's modulus. This approach has vast applications for tuning substrate to mimic in vivo mechanical properties of other tissues such as neuro tissues, cartilage, and heart. The "stemness" of the cells was maintained on the collagen hydrogel that closely replicated the *in vivo* Young's modulus of the skeletal muscle.

4.2 INTRODUCTION

Tissue engineering by employing the body cells to repair and replace damaged tissue is a rapidly growing and evolving field. Vast amount of research has been done on identifying the source of the differentiation of multiple tissues in the body, especially for skeletal muscle repair. Skeletal muscle is a convenient source of stem cells that can be implemented for cellular therapy and can be easily obtained via a minimally invasive skeletal muscle biopsy[1].

Satellite cells have unique properties such as self renewal, proliferation, and differentiation (stemness) into skeletal muscle cells for the repair of terminately differentiated skeletal muscle making their therapeutic potential significant. These cells accomplish these repairs while also retaining a population of unspecialized cells that become quiescent until recruited.

It has been shown that these muscle stem cells, grown on standard tissue culture plastic, lose their "stemness" characteristics and produce progenitors with a decrease in their regenerative potential. The matrix mechanical properties influence the proliferation and differentiation of these stem cells.

It is imperative to develop strategies to maintain the satellite population in a proliferative state *in vitro* to exploit their regenerative characteristics. Recent efforts have been made using tissue engineering with primary cells and matrixes such as collagen[2], collagen-poly(vinyl alchohol)[3], acellular matrices[4], PEG[5], and poly(glycolic acid)(PGA)/poly-L-lactic acid (PLLA)[6] for regenerative purpose but with some restrain[7]. To reinstate the muscle rigidity found in the in vivo niches, recently investigators have developed a tunable polyethylene glycol (PEG) hydrogel plataform. This was created by using precursors such as 4 arm 10KDa PEG-SH and 8-arm 10 KPa PEG-VS that were synthesized as previously described[8]. Through several steps, the end result was a hydrogel covalent crosslinked with laminin[5]. By altering their percentage of the PEG polymer precursor solution, they were able to change the mechanical properties of the niche by mimicking the *in vivo* elasticity. The muscle stem cells propagated in the PEG hydrogel retain their stemness by promoting their proliferation and preventing their differentiation and did not experience the

significantly cell death. They also demonstrated by *in vitro* studies that the substrate rigidity has no influence in the cell division rate in culture but inhibit differentiation.

Furthermore, it is potentially advantageous to use natural constitutes of the basement membrane for *in vitro* culture and recapitulate the biophysical and biochemical features of the environment found *in vivo* niches. The natural derived matrices are standards for biomaterial development for tissue regeneration and matrix 3D cell culture models [9]. Developing tunable 3D niches, the behavior of the cells can be control and study.

Using natural ECM components, Type I collagen and laminin, we created numerous collagen hydrogels and demonstrated that we can control the elastic modulus and create materials that closely mimic 12 KPa elastic modulus found in the stem cell niche. Satellite cells were grafted on the collagen hydrogels of varying collagen concentration and Young's modulus. Satellite cells retained expression integrin α7 on substrates that closely mimic their modulus *in vivo*. We further investigate the presence of Pax7 characteristic of quiescent satellite cells and myogenic factors such as MyoD. Their expression was reduced or lost as the stiffness increased.

4.3 MATERIALS AND METHODS

4.3.1 Collagen

Collagen was obtained as previous described in Yost et al., 2004[10]. The percentage of collagen solid was determined for each sample as described. Using

concentrated hydrochloric acid, the collagen was brought to a pH 3 while keep at 4˚C or ice. The samples were diluted to the desired concentration (10-20 mg/mL) using sterile water and sterilized using a UV source. Samples were centrifuged to 15000 rpm for 20 minutes at 4 ˚C to avoid air bubbles.

4.3.2 Mechanical Properties of the Collagen hydrogels

4.3.2.1 Collagen hydrogels

The collagen hydrogels were mixed with 10 ug/mL of laminin. To polymerize the collagen, MEM and HEPES were added in an 8:1:1 ratio at 4˚C. The gels were casted to cylindrical molds (six well plate, 29 mm). They were placed in 37 ˚C incubator for 1 hr.

4.3.2.2 Crosslinked collagen

After the incubation period, the hydrogels were UV crosslinked using energy of 630000 microjoules per centimeter squared.

4.3.2.3 Mechanical Properties

The mechanical properties of the hydrogels vary as a function of strain and frequency of oscillation. Since these hydrogels are designed to be used in cell culture and in vivo transplant, the measurements were conducted in isothermal conditions at 37˚C. These properties were measured using the Rheometrics Fluid Spectrometer RFS II. The rheometer consists of a parallel plate assembly of 25 mm diameter that was compressed until the hydrogel exerted a normal force opposite to the assembly. The

parallel plates were covered with a 120 grit sandpaper to avoid slipping of the sample. The shear modulus (G') was recorded at constant strain (0.5%) as a function of frequency (0.10 rad/s to 25 rad/s or 0.016 Hz to 4.0 Hz) with 25 data points recorded.

4.3.3 Cell-Collagen Hydrogel interactions

4.3.3.1 Tissue Explant Protocol

Skeletal muscle biopsies were obtained from the hind limb of adult male Sprague-Dawley rats that were approximately 300 grams in weight. The tissue was rinsed in 1 x Phosphate Buffer Solution (PBS) containing 200 U/ml penicillin G and 200ug/ml streptomycin (Sigma Chemical Co., St. Louis, MO). The tissue was then transferred to a 150mm tissue culture dish where the tissue was cut into 1-2mm pieces using a sharp sterile scalpel blade. To prevent the dehydration of the tissue, a small amount of Explant medium which consists of Dulbecco's modified eagle's medium, (DMEM; Sigma), 25% fetal bovine serum (FBS, Atlanta Biological, Atlanta, GA) 200U/ml penicillin G and 200 ug/ml streptomycin (Sigma), 0.1% gentamycin (Sigma) and 5ug/ml amphotericin B (Lonza, Inc.) was added to the dish. Using sterile forceps, the tissue was transferred to a sterile 100mm tissue culture dish and arranged in clusters of 5-6 pieces. The tissue clusters were then covered with sterile coverslips and 5-8mls of explant medium was then carefully added to the dish. The dishes were then incubated in a 37°C humidified incubator under 5% CO_2. They were refed with fresh explant media on the third day. After seven days, the coverslips and tissue pieces were removed and the dishes were refed with explant media. Once the cells were about 50 % confluent they were passed into 150mm tissue culture dishes with SAT medium(muscle

culture selective medium) that consists of Ham's F10 medium (Fisher, Sci.) containing 20% FBS, 2.5ng/ml bFGF human recombinant (Fisher, Sci.), 100 U/ml penicillin G/100ug/ml streptomycin(Sigma), 0.1% gentamycin(Sigma) and 2.5 ug/ml amphotericin B(Lonza, Inc).

4.3.3.2 Flow Cytometry and Cell Sorting

Cells that were harvested from muscle biopsies were detached from tissue culture dishes with accutase (eBiosciences, San Diego, CA) and resuspended in flow buffer (PBS-without Ca2+ and Mg and 1% Bovine Serum Albumin) at a concentration of $5x10^6$ cells/ml. Cell suspensions were then put into flow tubes at a concentration of $5x10^5$ cells/ml and blocked with 10% normal goat serum (Sigma) in flow buffer for 10 minutes. The cells were then stained with either Integrin Alpha 7-PE (MBL Int., Woburn, MA) or Mouse IgG1-PE (MBL, Int.) as a control. Cells were then centrifuged and resuspended in flow buffer before being sorted using a BD Biosciences FACS Aria II. Positive fractions were collected in SAT medium.

4.3.3.3 Grafting cells on the hydrogels

Sorted cells (satellite cells) were incubated in a 150 mm culture dish until confluency and feed every two days in SAT media. The media was extracted from the well plate and rinse with Mosconas, which was then replaced with 0.25% Trypsin solution. The contents were transferred to a 50 mL conical tuve in wich the same amount of SAT was added. It was centrifuge for 5 min at 8000 rpm. The supernatant was extracted and add a specific amount of media. The cells were counted and 100,000

cells were placed on the hydrogels. They were incubated for 3 days at 37˚C.

4.3.3.4 Confocal Microscopy

The hydrogels were fixed with 4% formaldehyde for 15 minutes and stored in sterile PBS solution. The hydrogel was cut into 4 pieces. One-half of the hydrogel was taken to process as control and transcription factor (one-fourth each).

The samples were placed in a 48 well plate and filled with 1X PBS. The PBS was replaced with 1 mL of a solution of 1X PBS and 0.01% TritonX-/0.01M Glycine for 30 minutes twice, which will permeabilize the gel to incorporate the antibodies. This solution was replaced with 1 mL of 5% BSA solution for 1 hr. We proceeded by aspirating the 5% BSA solution from the control samples and added 500 uL of 1% BSA solution. For the other set of samples, we aspirated the 5% BSA solution and added 500 uL of the primary antimouse antibody of integrin α-7 at 1:200 ratio. The Anti-Mouse Integrin α7 is an adhesion molecule that is expressed mainly on skeletal muscle cell precursors that contributes to differentiation and migration process during the myogenesis, or the formation of muscle tissue. The hydrogels were keep at 4˚C overnight.

To incorporate the secondary antibody which is an antimouse antibody 546 Texas red, we aspirated the primary antibody and wash the hydrogels with 1% BSA solution. After extracting this solution, 500 uL of the secondary antibody were added to both sets of samples. The well plate was covered and left for 2-3 hr. The hydrogels were washed with 1X PBS solution and they were maintained at 4˚C in the dark.

The hydrogels were stained for f actin and nuclei by adding 1:200 rhodamine-

labeled phalloidin 488 and 1:1000 of 4',6-diamidino-2-phenylinodole (Dapi 405). They were left for 2hr and then washed with 1X PBS.

The same procedure was used for another set of hydrogels to incorporate the primary antibody anti-mouse Pax7 and anti-rabbit MyoD. The secondary antibody used was anti mouse 546 Texas red and anti rabbit 488. These hydrogels were stained with Dapi 405 and phalloidin 655.

Hydrogels were mounted on glass slides to further analyze them using the Zeiss LSM 510 META Confocal Scanning Laser Microscope.

4.4 RESULTS

Several collagen concentrations were tested using the RFSII. The collagen hydrogels were seeded with satellite cells and incubated for period of three days. The behavior of the satellite cells related to the stiffness of the niche was studied.

4.4.1 Collagen hydrogel properties

Following the described procedure, the collagen hydrogels were casted in a 29 mm diameter well plate. Collagen hydrogels with concentration of 10, 12, 14, 16, and 20 mg/mL were placed on the parallel plates assembly of the Rheometrics Fluid Spectrometer RFS II and compressed until a normal force opposite to the compression was seen. After compression, the hydrogel gap varied from 2 – 4.3 mm depending on the properties of the hydrogels. Figure 4.1 A shows the RFSII used to obtain the shear modulus for each of the samples. The parallel plates assembly allows the compression

of the sample while the bottom plate is oscilating at a strain of 0.5%.

The shear modulus was measured for each of the concentrations over a wide range of frequencies (Figure 4.1 B). Using this raw data, we calculated the Young modulus at the different hydrogel concentrations and establish their relationship with the frequency (Figure 4.1C). The relationship between the collagen concentration and the elastic modulus was established (Figure 4.1 D).

The concentration where we obtained a Young's modulus of 12 KPa was at 14 mg/mL. The standard deviation for 10 samples was 0.81 KPa, which shows minimal fluctuations fluctuation in our fabrication method. The relationship between the concentration and the Young's modulus is linear.

4.4.2 Satellite cells in the collagen hydrogel niche

Using confocal microscopy, we obtained images of the satellite cells for the different concentrations and elastic modulus. The primary α7 integrin antibody was absent in the control samples.

By comparing the images of the 14 mg/mL to the 20 mg/mL, we can see that there a decrease in the expression of satellite cells shown by the integrin α-7 in figure 4.1. The stiffness of the 20 mg/mL contributes to the reduction in the stemness of the satellite cells in the hydrogel.

A small cell population of cells was sorted and placed directly on the collagen hydrogels. Cells did not proliferated and their morphologies changed as a result of their modulus as seen in figure 4.3.

We furthermore investigated these hydrogels for the expression in the cells of Pax7 as well as the expression of a myogenic regulator factor MyoD. Pax7 is a transcription factor expressed in quiescent satellite cells, which is expressed beneath the basal lamina in a specific position that is characteristic of the quiescent satellite cells[11]. When they are activated, they coexpress Pax7 and MyoD which is a transcription factor for myogenic differentiation. The presence of quiescent satellite cells is determined by the expression of Pax7 and MyoD [11-13]. The data showed a decrease expression of Pax7 as the collagen hydrogel's stiffness increased (figure 4.4). Morphological changes were observed which was directly related to the increase of the collagen hydrogel's modulus.

A separate experiment, we placed satellite cells on collagen hydrogels that closely mimic the satellite cell niche modulus. They were cultured for 3 hr, 24 hr, 48 hr, and 72 hr as shown in figure 4.5. Our initial time point, indicates that the heterogeneous population consist of Pax7/+ve/MyoD/+ve. After 24 hr, the majority of the cells have been activated as seen by the expression of the MyoD. At 48 hr, they were coexpressing Pax7 and MyoD. However, after the 72 hr there was an increased expression of Pax 7, resulting in two population one that coexpress Pax 7 and MyoD and another that did not express Pax7. Similar findings were obtained by Zammit et al 2006[14]. At the same time point, we saw morphological changes that closely emulate the cell morphology seen in the first data point.

4.5 DISCUSSION

Collagen hydrogels with a concentration of 10, 12, 14, 16, and 20 mg/mL, were placed on the parallel plates assembly of the Rheometrics Fluid Spectrometer RFS II. The storage or shear modulus G' was measured for the different concentrations. Collagen behaves as a viscoelastic material. The data points obtain at 1Hz were reported in which constitutes the linear region of the elastic material. The material obeys Hooke's law in that the strain is directly proportional to the stress. As the frequencies increases, the shear modulus increases until it reaches a plateau. The collagen fibers by themselves have anisotropic behavior but as a whole we assume that the collagen in the hydrogel were randomly oriented behaving as an isotropic material. These assumption was correlated using a cross polarized light microscope were we saw some birefringence of the collagen. However, birefringence did not change as the sample's orientation changed with respect to the polarized light. We converted this data to Young's modulus using the following equation: $E' = 2(1+v)G'$ where E' is the Young's modulus or elastic modulus, G' is the storage or shear modulus, and v is the Poisson's ratio. We assumed a Poisson's ratio of 0.5 because the collagen hydrogel is a perfectly incompressible material deformed elastically at very small strains.

While having stiffness or an elasticity that modulates the *in-vivo* niche of these cells preserves the undifferentiated stage of the muscle fiber precursors. They were identified by the α7 integrin marker. The α7 integrin is a useful surface marker which has been used as a method of isolating multipotent myoblast and satellite cells. It has been used as a purification method for sorting primary myoblasts that remains quiescent satellite cells[15-17]. The α7 positive myoblasts expressed multiple muscle

specific markers with the ability to undergo myogenesis and follow other lineages under the influence of certain growth factors. Their expression aids to identify these skeletal muscle cell precursors[17]. From this data, we can determine that the cells that were sorted and further expanded were able to blend with the collagen fibers of the hydrogels, which provided cues for their development.

Furthermore, we determine the specific stage of the satellite cells in the myogenesis pathway. There was an indication of morphological changes in the cytoskeleton of the cells represented by the phalloidin that corresponds to cell differentiation, as well as lost or reduced Pax7 and MyoD expression at concentrations of 14 and 20 mg/mL. The data suggests that there may be changes in the stiffness of the collagen matrix as the cells interact with the hydrogel. Further testing on the collagen hydrogels after culture will clarify this aspect.

Heterogeneous muscle cell population was cultured on the collagen hydrogel that closely mimic the *in vivo* niche of the muscle precursor cells. The results showed an interesting satellite cell pathway. The Pax7/+ve/MyoD/+ve cells have two fates: one they fully differentiate, by expressing MyoD or continue to express both. Previous investigators reported this behavior as well as another fate in which Pax 7 expression is maintain while MyoD is lost as cells withdraw from myogenesis pathway[18]. This opens an interesting aspect, in which we can stipulate that using heterogeneous muscle cell population, we may replenish the satellite cells population as seen *in vivo* by providing the proper conditions.

The satellite cells cultured in an environment that mimics the muscle tissue exhibit proliferative behavior that is similar to cells that are freshly isolated. Their behavior in these niches enables the cell to maintain undifferentiated and quiescent such as the *in vivo* tissue and allows them to migrate to injured tissue and repair it by fusing with the available muscle fibers or undergoing myogenesis[7]. Preliminary *in vitro* data suggest that the mechanical behavior over time causes modifications in the cells by replenishing the quiescent satellite cell pool.

Consequently, previous studies and our new data using natural ECM components suggest that the mechanical properties for the muscle cell precursor niche are determined by the basal membrane. Additionally, the 3D dimensionality influences integrin ligation, cell contraction, signaling of the cells and their determined behavior[19]. The satellite cells are capable of self- renewal their pool and can follow myogenic pathways on demand[20]. These cells are self-sufficient source of regeneration in injury or diseased skeletal muscle. By maintaining the satellite cell population using the appropriate niche, we are able to maintain their abilities and employ them for regenerative therapy.

4.6 REFERENCES

1. Usas, A. and J. Huard, *Muscle-derived stem cells for tissue engineering and regenerative therapy.* Biomaterials, 2007. **28**(36): p. 5401-5406.

2. Grefte, S., et al., *Model for Muscle Regeneration around Fibrotic Lesions in Recurrent Strain Injuries.* Medicine and Science in Sports and Exercise, 2010. **42**(4): p. 813-819.

3. Abedi, G., et al., *A Collagen-Poly(vinyl alcohol) Nanofiber Scaffold for Cartilage Repair.* 2010: p. 1-11.

4. De Coppi, P., et al., *Myoblast-acellular skeletal muscle matrix constructs guarantee a long-term repair of experimental full-thickness abdominal wall defects.* Tissue Engineering, 2006. **12**(7): p. 1929-1936.

5. Gilbert, P.M., et al., *Substrate Elasticity Regulates Skeletal Muscle Stem Cell Self-Renewal in Culture.* Science, 2010. **329**(5995): p. 1078-1081.

6. Levenberg, S., et al., *Engineering vascularized skeletal muscle tissue.* Nature Biotechnology, 2005. **23**(7): p. 879-884.

7. Boonen, K.J.M. and M.J. Post, *The Muscle Stem Cell Niche: Regulation of Satellite Cells During Regeneration.* Tissue Engineering Part B-Reviews, 2008. **14**(4): p. 419-431.

8. Lutolf, M.P. and J.A. Hubbell, *Synthesis and Physicochemical Characterization of End-Linked Poly(ethylene glycol)-co-peptide Hydrogels Formed by Michael-Type Addition.* Biomacromolecules, 2003. **4**(3): p. 713-722.

9. Bott, K., et al., *The effect of matrix characteristics on fibroblast proliferation in 3D gels.* Biomaterials, 2010. **31**(32): p. 8454-8464.

10. Yost, M.J.B.C.F.S., Charles E.; Goodwin, Richard L.; Price, Robert L.; Davis, Jeffrey M.; Evans, Heather; Watson, Phillip D.; Gore, Michael; Sweet, Janet; Creech, Laura; Zile, Michael R.; Terracio, Louis, *A Novel Tubular Scaffold for*

Cardiovascular Tissue Engineering. Tissue Engineering, 2004. **10**(1/2): p. 273-284.

11. Seale, P., et al., *Pax7 Is Required for the Specification of Myogenic Satellite Cells.* Cell, 2000. **102**(6): p. 777-786.
12. Megeney, L.A., et al., *MyoD is required for myogenic stem cell function in adult skeletal muscle.* Genes & Development, 1996. **10**: p. 1173-1183.
13. Zammit, P.S., et al., *Kinetics of Myoblast Proliferation Show That Resident Satellite Cells Are Competent to Fully Regenerate Skeletal Muscle Fibers.* Experimental Cell Research, 2002. **281**(1): p. 39-49.
14. Zammit, P.S., et al., *Pax7 and myogenic progression in skeletal muscle satellite cells.* Journal of Cell Science, 2006. **119**(9): p. 1824-1832.
15. Blanco-Bose, W.E., et al., *Purification of Mouse Primary Myoblasts Based on α7 Integrin Expression.* Experimental Cell Research, 2001. **265**(2): p. 212-220.
16. Cachaço, A.S., et al., *Integrin Repertoire on Myogenic Cells Changes During the Course of Primary Myogenesis in the Mouse.* Developmental Dynamics, 2005. **232**: p. 1069-1078.
17. Ozeki, N., et al., *α7 integrin expressing human fetal myogenic progenitors have stem cell-like properties and are capable of osteogenic differentiation.* Experimental Cell Research, 2006. **312**(20): p. 4162-4180.
18. Zammit, P.S., et al., *Pax7 and myogenic progression in skeletal muscle satellite cells.* Journal of Cell Science, 2006. **119**: p. 1824-1832.
19. Bott, K., et al., *The effect of matrix characteristics on fibroblast proliferation in 3D gels.* Biomaterials, 2010. **31**: p. 8454-8464.

20. Collins, C.A., et al., *Stem Cell Function, Self-Renewal, and Behavioral Heterogeneity of Cells from the Adult Muscle Satellite Cell Niche.* Cell, 2005. **122**: p. 289-301.

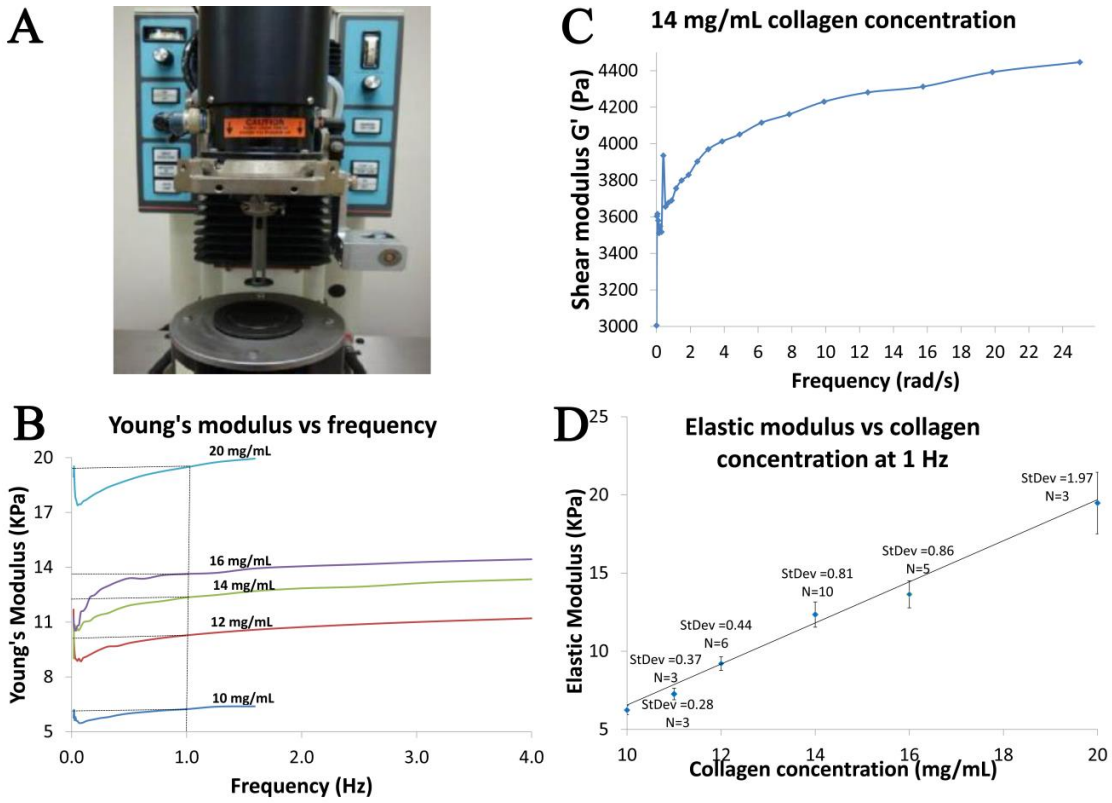

Figure 4.1. Collagen hydrogels modulus. The RFSII was used to measure the hydrogel's shear modulus. The sample was loaded between the parallel plates (a). Panel b shows the shear modulus response on a frequency range of 0-25 rad/s. Panel c shows the elastic modulus response to frequency at different concentrations of collagen. Panel d is a linear regression fit of the elastic modulus versus collagen concentration collected at 1 Hz; the error bars represent +/- standard deviation.

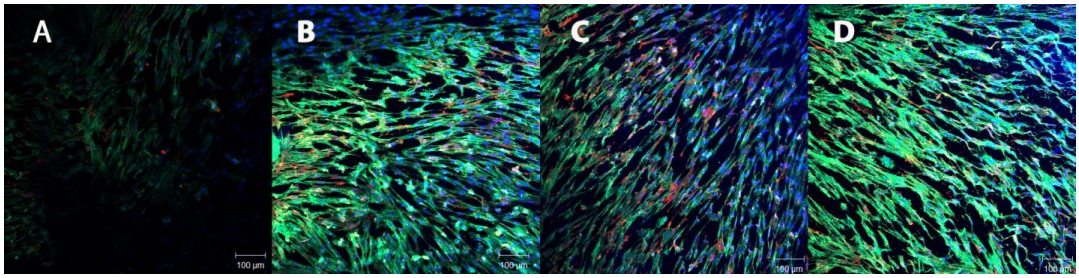

Figure 4.2. Immunohistochemical Analysis using α7 of expanded sorted satellite cells on different elastic modulus. Confocal Microscopy images using a 10X objective shows the sorted satellite cells after further expansion were cultured on collagen hydrogels at a concentration of 10 (A), 12 (B), 14(C) and 20 mg/mL (D) . The blue corresponds to DAPI stain which indicates the cell's nucleus. The green color corresponds to phalloidin that binds to the f actin composing the cytoskeleton of the cells. The red color is immunohistochemical labeling of integrin α7. There is a significant difference in the expression of the integrin α7 in the 14 and 20 mg/mL hydrogels that corresponds to the elasticity seen in vivo compared to a stiffer niche.

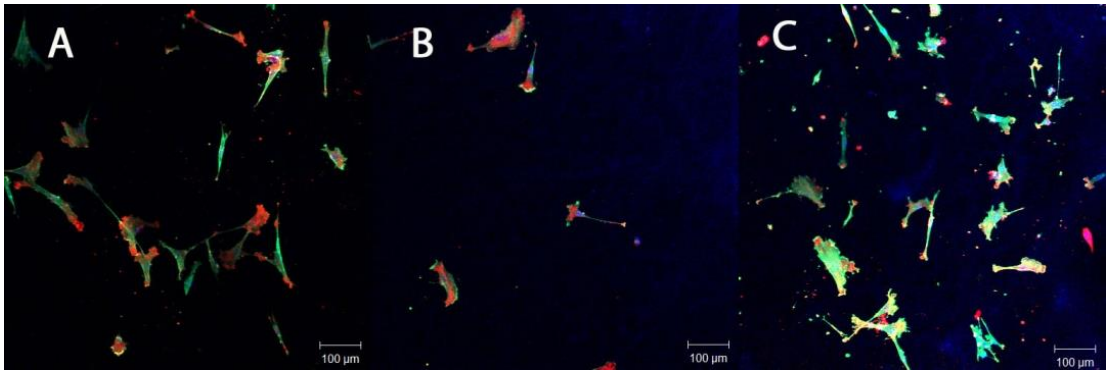

Figure 4.3. Immunohistochemical Analysis using α7 of sorted satellite cells on different elastic modulus Confocal Microscopy images using a 10X objective shows cultured sorted satellite cells cultured directly on hydrogels directly on collagen at a concentration of 10 (A), 14 (B), and 20 mg/mL (C). The blue corresponds to DAPI stain which indicates the cell's nucleus. The green color corresponds to phalloidin that binds to the f actin composing the cytoskeleton of the cells. The red color is immunohistochemical labeling of integrin α7. Satellite cells remained quiescent in the niche, but we can observe difference in the morphologies according to the stiffness of the niche.

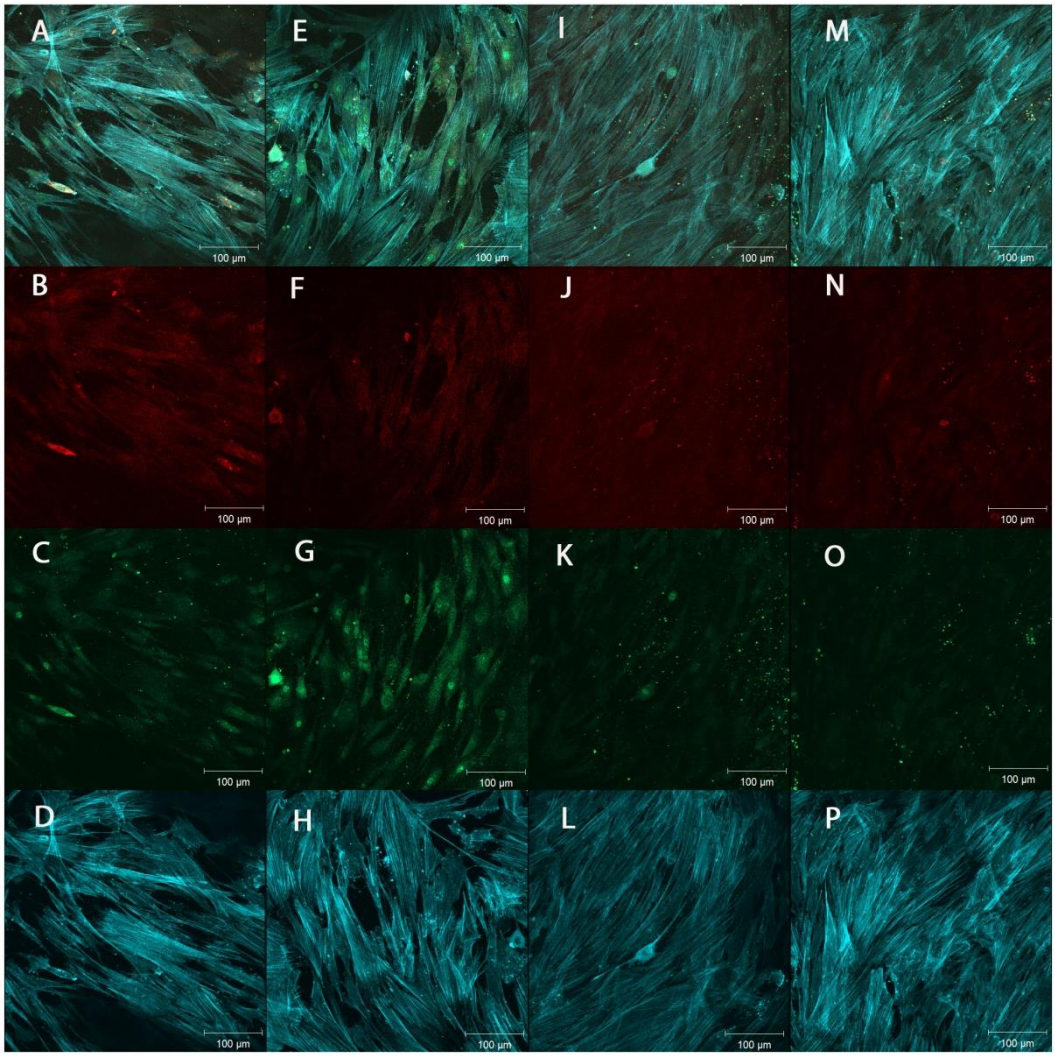

Figure 4.4. Immunohistochemical Analysis using Pax 7 and MyoD of expanded sorted satellite cells on different elastic modulus. Images obtained using 20X Zeiss LSM 510 META Confocal Scanning Laser Microscope showing cultured sorted satellite cells cultured after further expansion on collagen hydrogels at a concentration of 10(A-D), 12 (E-H), 14 (I-L), and 20 mg/mL (M-P) . The blue color corresponds to phalloidin that binds to the f actin composing the cytoskeleton of the cells. The red color is immunohistochemical labeling of Pax 7. The green color is immunohistochemical labeling of MyoD. There is a significant lost in the expression of the Pax7 and MyoD from 14 to 20 mg/mL hydrogels. This may be due to the differentiation of satellite cells into muscle fibers.

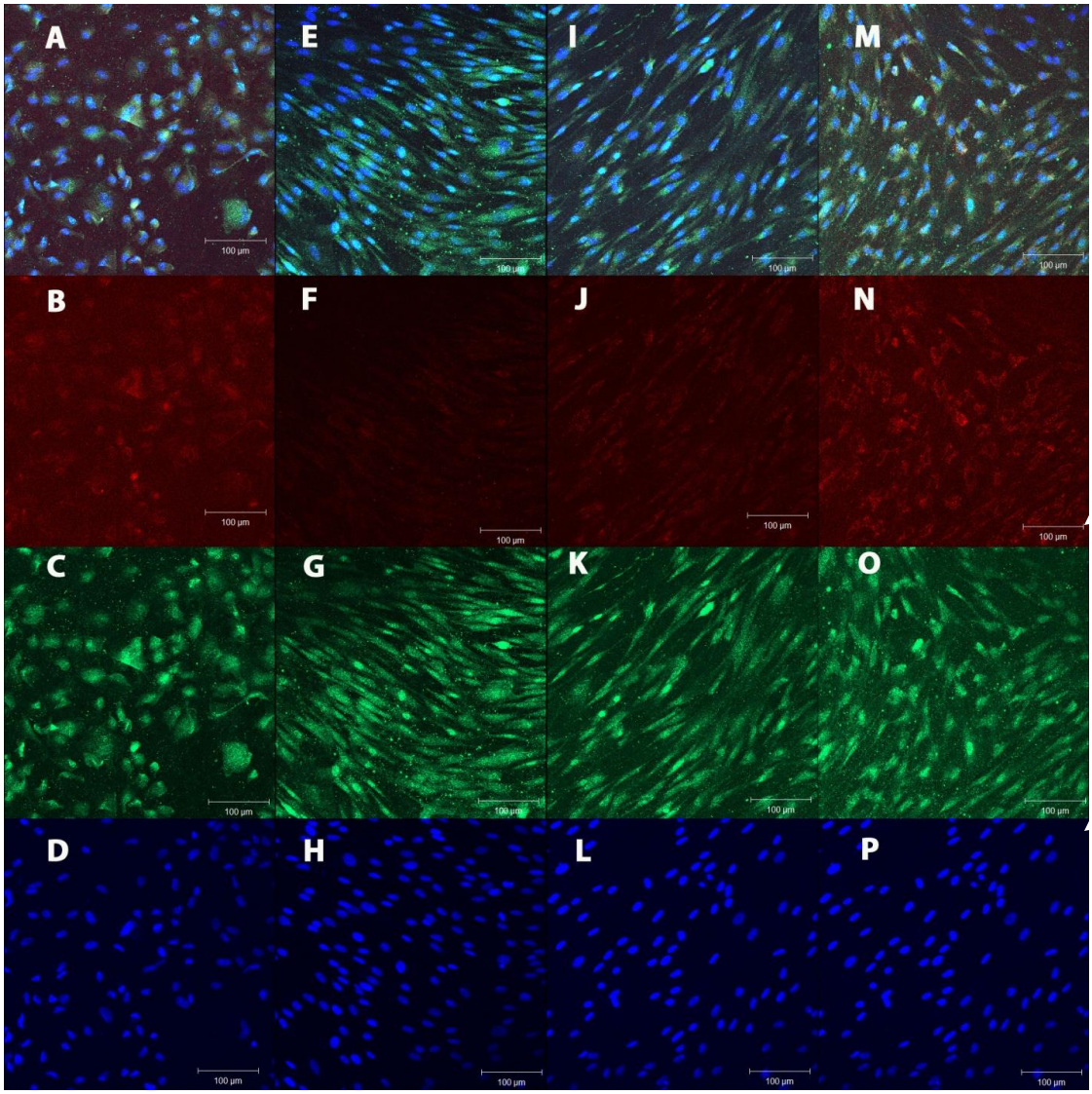

Figure 4.5. Immunohistochemical Analysis using Pax7 and MyoD of heterogeneous muscle cell population in a 12 KPa hydrogel. Images obtained using 20X Zeiss LSM 510 META Confocal Scanning Laser Microscope showing cells cultured after further expansion on 14 mg/mL collagen hydrogels for 3 (A-D), 24 (E-H), 48 (I-L), and 72 hr (M-P) . The blue color corresponds to dapi staining that binds to the cell nuclei. The red color is immunohistochemical labeling of Pax 7. The green color is immunohistochemical labeling of MyoD. We can see that there are cells in the 72 hr period that coexpress Pax 7 and MyoD as well as others that only express MyoD as indicated by the arrows. There is an increased expression of Pax 7 in the 72 hr period as well as changes in the cell morphology.

CHAPTER 5:

THREE-DIMENSIONAL BIOMIMETIC TECHNOLOGY: NOVEL BIOMATERIALS TO CREATE DEFINED ARCHITECTURES IN COLLAGEN HYDROGELS

5.1 ABSTRACT

Tissue scaffolds play a crucial role in the tissue regeneration process. The ideal scaffold must fulfill several requirements such as having adequate composition, a specific cell population, and well-defined architectural features. We have developed a novel biofabrication technique that combines state of the art imaging, three-dimensional (3D) printing, and selective enzymatic activity to create a new generation of biomaterials for research and clinical application. The purpose of this study was to characterize our developed mold system called "BSA rubber." This material allows the adequate transfer of specific architectural features to a natural scaffold material. Our prototype consists of a 3D collagen scaffold with 4- and 3-mm channels that represent a branched architecture. Biomaterials that recapitulate the intrinsic architecture of *in vivo* tissue are vital for studying diseases as well as to facilitate the regeneration of lost and malformed soft tissue.

5.2 INTRODUCTION

In the tissue engineering field, the ability to fabricate tissue scaffolds is integral. A suitable tissue scaffold has a 3D structure, is composed of biocompatible materials, and mimics *in vivo* tissue architecture to facilitate cell and tissue growth and remodeling, as well as the ability to transport nutrients and remove wastes [1-4]. One of the main obstacles in the production of these scaffolds is the ability to recapitulate specific geometrical features into a biocompatible material. Several biofabrication techniques have been reported to control the geometrical features of these scaffolds, such as

electrospinning[5-8], solvent-casting[9], stereolitography[10], and 3D printing[11], among others. However, these techniques fall short in providing a relatively easy transfer of controllable architectural features, are expensive, or require long a period of time to produce viable scaffolds.

In many commercial fabrication systems, the creation of internal voids, channels, and features is achieved using sand or other suitable removable or sacrificial materials. The metal or plastic part is formed around the sand mold, and once it is solidified, the sand is removed. In much the same manner, the next generation of biomaterials needs the "biosand" equivalent. Therefore, we developed the BSA rubber as a substitute for biosand. The BSA rubber is a newly formulated material that consists of bovine serum albumin crosslinked with glutaraldehyde. The ultimate goal is to recreate specific architectural features into a biodegradable collagen scaffold. We also describe the characteristics of the sacrificial biorubber that maintains dimensional fidelity with the mold of the original tissue.

We tested different combinations of BSA and glutaraldehyde concentrations in different solvents. BSA rubber can be reaction injection molded into the intricate geometries of our tissue molds. Crosslinked BSA is trypsin labile and readily digested by the enzyme at mild pH and temperature conditions. Conversely, intact type I collagen is very resistant to trypsin digestion. We capitalized on these features to selectively remove the BSA rubber leaving the collagen behind. The present work consisted of determining the ideal parameters needed to obtain a labile mold that can deliver specific architectural features to a biocompatible scaffold. The specific features that we evaluated included mixability, enzyme digestion, load bearing, and ability to be reaction injected into a

negative mold. We determined that the combination of 30% BSA and 3% glutaraldehyde fulfills these requirements. Our prototype consists of a collagen scaffold that consists of a branched architecture. This technology provides a viable technique to deliver a specific geometrical instructive to a biodegradable material which can be tuned to mimic the *in vivo* tissue elasticity and other characteristics of the tissue of interest.

5.3 MATERIALS AND METHODS

5.3.1 BSA rubber

BSA (lyophilized and deionized powder, purity grade >98%, Sigma) and glutaraldehyde (25%, Sigma) were used. We used three solvents: 2× PBS, 1× PBS, and DI (deionized) water. We used pure water for making all solutions (Milli-Q, Millipore). The BSA concentrations used were 20%, 30%, and 40% wt. The glutaradehydye concentrations used were 2%, 3%, and 6% v/v. Table 5.1 lists the combinations of BSA and glutaraldehyde tested. Using a 24-well plate (Corning), we added 1 mL of BSA mixture at the appropriate concentration and crosslinked it with 250 µL of the appropriate concentration of glutaraldehyde (Figure 5.1B). These solutions were left to react overnight at 4°C in the molds. The next day, we obtained an 8-mm punch of each sample. For each concentration, we made four samples, and conducted testing in triplicates.

5.3.2 Compression testing of the BSA rubber

To characterize the fabricated rubbers, we conducted compressive testing. Four samples were tested: 30% BSA and 3% glutaraldehyde in 2× PBS, 30% BSA and 3%

glutaraldehyde in 1× PBS, 20% BSA and 3% glutaraldehyde in 2× PBS, and 20% BSA and 2% glutaraldehyde in 1× PBS. Using the Bose Electroforce 3100 (Bose Corporation), we tested three samples of each set using a 5-lb_f load cell. Displacement and load measurements were obtained having the load as the feedback. Five load cycles were performed using sine wave compression (experimental parameters are found in Table B.1). The stress and strain at each point was determined. We obtained the elastic modulus from the slope of the stress and strain curve in the elastic region.

5.3.3 Solids content of the BSA rubber

A separate set of samples was used to quantify the percentage of dry solids in each of the BSA rubber samples shown in Table 5.1. Using a 24-well plate (Corning), we added 1 mL of BSA mixture at the appropriate concentration and crosslinked it with 250 μL of glutaraldehyde at the appropriate concentration (Table 5.1). They were left to react overnight at 4°C in the molds. The next day, we obtained an 8-mm punch of each sample. We determined the initial wet weight of the rubbers and then placed then on the lyophilizer overnight. Then, we determine the dry weight of the rubbers. These tests were performed in triplicate.

5.3.4 Enzyme digestion

BSA rubbers were enzyme digested using trypsin (pH 7.8) at 30°C. We placed an 8-mm BSA rubber punch on a 15 mL conical tube and determined the initial rubber weight. We added 1 mL of 0.25% Trypsin in DI at pH 7.8 and 30°C. Samples were taken

at 15, 24, 48, and 72 hr. At each time point, we extracted the supernatant and lyophilized the remaining rubber. To determine the total protein dissolved by trypsin, we performed a total protein assay (Bicinchoninic Acid Assay, BCA, Pierce). The absorbance was obtained at 562 nm using a multi mode microplate reader (Biotel). BSA rubbers were exposed to a 0.25% trypsin solution (pH 7.8) at 30°C. The weight of the rubber was determined prior and after the enzyme treatment by lyophilizing the sample.

5.3.5 3D mold

To create a customized biodegradable rubber mold, we made 3D solid mold pieces that would hold the model dimensions. Using MasterCAM® we designed a solid model. We converted the solid model into machine G-code language. Once in G-Code we transfer the program to our Microlution 363-S micro milling machine to create the mold in stainless steel and brass. We fabricated what we called a "Y Mold." We also created another mold called the "Loop Mold" using a MakerBot Replicator2 3D printer. Using Replicator software, we were able to import the program into the 3D Printer. This printer has a 100-micron layer resolution and allows the fabrication of polylactic acid (PLA) molds by depositing layer after layer of this material to build the piece. We also made a "stability piece," in which we tested the fidelity of the smallest features that we can replicate with a BSA rubber. This piece contains channels with diameters from 0.3- to 4-mm.

5.3.6 BSA rubber molds

The BSA rubber is a reaction injection molded into the intricate geometries of our tissue molds. Using an air brush sprayer (Air Brush Kit, Central Pneumatic), a release agent (Lard, Fields) was distributed on the surface of the mold. The sprayed mold was left to cool down for approximately 2 hr. The 30% BSA and 3% glutaraldehyde in 2× PBS solution were added to the dispenser (Medmix) in order to deliver a 4:1 ratio, respectively. The solution was reaction injected into the flowpaths to create a biodegradable rubber. The molds were left to react overnight at 4°C.

5.3.7 3D collagen scaffold

We extracted collagen by a procedure we previously published [12]. After determining the solid percentage, collagen was acidified and mixed to obtain the desired concentration. We produced 4 mL of a 1.75% collagen hydrogel. The collagen hydrogel was mixed with 10 µg/mL of laminin [13]. To polymerize the collagen, 10× Minimum Essential Medium (MEM-Gibco) and 0.2 N HEPES (Sigma) at pH 9 were added in an 8:1:1 ratio at 4°C. About half of the hydrogel was casted on a 12-well plate. We proceeded with placing the BSA rubber on top and covered it with the rest of the collagen. The plate was placed in 37°C incubator for 1 hr. After the incubation period, the hydrogels were UV cross-linked using energy of 630,000 microjoules per centimeter squared. The BSA rubber was enzyme digested with a 0.25% Trypsin solution. We digested the BSA rubber using this 0.25% trypsin solution at a pH of 7.8 and at 30˚C for 15 hr. After the 15-hr period, two sterile Mosconas washes (136.8mM NaCl, 28.6 mM

KCl, 11.9mM $NaHCO_3$, 9.4 mM glucose, and 0.08mM NaH_2PO_4 , pH 7.4) (Sigma-Aldrich) were performed for 30 min each.

5.3.8 Statistical Analysis

Data presented are expressed as mean±standard deviation (SD). One way analysis of variance (ANOVA) for multiple comparisons was employed to determine the variance of the population of the samples. Statistical significance was accepted at $p<0.05$. When comparing the effects of the solvent concentration, we used the NaH_2PO_4 concentration in the buffer solution, which is present in the 1x PBS and 2x PBS at concentration of 0.01 M and 0.02 M, respectively.

5.4 RESULTS

5.4.1 Consistency and mixability of the BSA rubber

The solubility of proteins is determined by intermolecular effects, such as the protein–protein interaction, and the interaction with the solvent induces changes on the overall protein behavior. Since the proteins are polyelectrolytes, solubility was determined by electrostatic interactions [14-16]. It has been shown that at low salt concentrations, there is a salting-in effect on the a protein facilitating its own solubility[17]. We measured the conductivity of the BSA solution, which is a way of determining the ionic strength. As expected, we saw that in samples with higher conductivity, the solubility of the BSA was facilitated. The DI samples, which showed

the least conductivity, took more time to obtain a homogeneous solution at higher concentrations (30-40% BSA).

The reaction time of the BSA decreased as the concentration of glutaraldehyde increased, as expected. The fixative reacts with the α-amino groups of the amino acids, the N terminal amino group of peptides, and the sulfhydryl group of cysteine. The glutaraldehyde reacts predominantly with the BSA through the amino groups of lysine to form the intermolecular covalent bonds (Figure 5.1A) [18]. It is the crosslinks that give the protein a rubbery consistency. After an incubation period, the samples showed a color change from pale yellow to dark yellow and brown, increasing in intensity with increased glutaraldehyde concentration (Figure 5.1B). This color change is attributed to the formation of the aldimine linkages [19-21]. The 20%, 30%, and 40% BSA with 2% glutaraldehyde in DI did not form a rubber. A previous study has described a rapid reaction of the glutaraldehyde when placed in contact with the protein [22]. The 40% BSA solution, due to its high viscosity and the highly reactive fixative, resulted in varying strength along the rubber. This behavior can be caused by the difficulty in the ability of glutaraldehyde to penetrate the protein chains homogeneously. The solvent greatly influenced the solubility of the protein as well as its reaction with the fixative. The 2× PBS solutions were easily mixable. The BSA solution with DI was difficult to mix. BSA solubility is greatly affected by the ionic strength of the solvent (Table 5.2), causing conformational changes in the protein. The most promising samples were the 30% BSA with 3% glutaraldehyde in 1× PBS and 2× PBS. Table 1 contains a brief visual description of the BSA rubber formation.

5.4.2 Compression test on the BSA rubber

We measured the mechanical properties of four samples of BSA rubber: 30% BSA 3% glutaraldehyde in 2× PBS, 30% BSA 3% glutaraldehyde in 1× PBS, 20% BSA 3% glutaraldehyde in 2× PBS, and 20% BSA 2% glutaraldehyde in 1× PBS. The sine waves showed a very small phase change between the load and displacement curves (Figure B.2) that are transferred to the stress and strain curves (Figure B.3). Based on the stress and strain curves, the first three samples showed hysteris in between loading and unloading (Figure 5.2:1:A-1C). These three specimens behaved as a viscoelastic material that contains elastic and viscous properties when forces were applied to it. The 20% BSA 2% glutaraldehyde showed signs of permanent deformation (Figure 5.2:1D). The 30% BSA 3% glutaraldehyde in 1× PBS and 2× PBS showed a similar behavior (Figure 2:2– one loading and unloading cycle). We determined the elastic modulus in the linear portion of these four samples (Figure 5.2:3). The concentration of the phosphate solvent significantly increased the elastic modulus in our range ($p=0.03$). The BSA and glutaraldehyde concentration did not contribute to the elastic modulus ($p>0.05$). The 20% BSA 2% glutaraldehyde in 1× PBS deformed easily, showing a lower elastic modulus.

5.4.3 Determination of Reaction Rate of the BSA rubber digestion

We determined the reaction rate based on the disappearance of the BSA rubber caused by the enzyme digestion at each time point. The enzymatic digestion process was treated as a batch reactor. A comparison between the starting rubber concentration prior to treatment and the rubber left after being lyophilized was made to obtain the kinetics of

the digestion. Figure 5.3 shows the rate of reaction for each sample in relation to the concentration of glutaraldehyde, BSA concentration, solvent, and the residence time. A clear trend was observed between the crosslinker concentrations and the reaction rate of dissociation of the entity. Statistical analysis was performed at each time point, and correlated the initial observation. For the 15-hr time point, the glutaraldehyde concentration significantly affected the reaction rate resulting in a p value of 0.02 (Table B.4). After that time point, both the glutaraldehyde and the BSA concentration significantly affected the rate (Table B.5-B.7). We determined that the most influential factor overall was the glutaraldehyde concentration, indicated by a more significant p value. The increase in glutaraldehyde concentration decreased the reaction rate of the digestion of the rubber entity.

5.4.4 Quantification of Soluble Protein

The amount of protein dissolved by trypsin was determined using a BCA assay (Figure 5.4). A common trend was observed: the lower the concentration of the fixative, the more protein was digested from the BSA rubber. Trypsin interacted with the rubber sample by cleaving the BSA and the newly created covalent bonds formed by the glutaraldehyde, thus dissolving the overall structure over time. It seems that with the 1× PBS there is more solubilized protein at an earlier time point compared to the 2× PBS. Over time, we saw it increased on proteins in solution at 15 hr, which continued to increase until 48 hr and then it decreased. This might be due to the trypsin constantly cleaving the proteins and, thus, creating smaller peptides and amino acids. The BCA assay has some limitations in that it can only read peptides that are composed of three or more amino acids. Statistical analysis showed that the BSA and glutaraldehyde

concentration significantly affected the release of the protein from the BSA rubber ($p<0.05$). An increase in BSA concentration caused an increase of protein in solution, while an increase in glutaraldehyde caused a decrease in dissolved protein.

5.4.5 Dissociation of the BSA rubber

The rubber was weighted (wet basis) before placing it in contact with the trypsin. We determined the equivalent of dry weight of the rubber placed in the enzyme digestion solution using the values shown in Figure B.1. The enzyme solution reacted with the BSA rubber, and thus, solubilized the protein. The rubber remaining after the treatment was lyophilized overnight and weighed. Figure 5.5 shows that the solvent influenced the dissociation of the rubber. At the same concentration of BSA and glutaraldehyde, the 2× PBS solvent rubbers retained more of their material compared to the 1× PBS.

5.4.6 3D collagen scaffold

We fabricated three solid mold pieces: "Loop Mold" (Figure B.4A), "Stability Piece" (Figure B.4B), and "Y Mold" (Figure 5.6A, left). We obtained the stainless steel Y mold piece using the Microlution machine (Figure 5.6A, right). This mold was reaction injected with 30% BSA and 3% glutaraldehyde in 2× PBS (Figure 5.6B, left). The rubber was allowed to react overnight at 4°C. The rubber was casted with collagen (Figure 5.6B, center) and then enzyme digested. Our preliminary data suggest that at pH 7.8 and a temperature of 30°C for 15 hr, we can digest the BSA rubber with minimal impact on the collagen scaffold. After 15 hr, the rubber is loose enough and weakened by the enzyme that it leaves the channels without affecting the geometrical features of the collagen. We obtained a 3D collagen scaffold that had specific geometrical features. Figure 5.6B (right)

shows a 4-mm diameter channel inside a collagen hydrogel after enzyme digestion of the BSA rubber. We determined that we can create BSA rubber molds that have diameters as small as 300 μm using the stability mold.

5.5 DISCUSSSION

Biofabrication is a highly multidisciplinary field in which biology and engineering principles need to be merged to generate complex materials that mimic the native tissue. In order to achieve this, we need to develop techniques that involve the implementation of the information gathered from *in vivo* tissue and translate it into an *in vitro* scaffold. This way, we can engineer a platform that closely resembles the architectural, functional, and mechanical properties of the *in vivo* tissue. The optimal scaffolding material should posses certain properties, such as being biocompatible, immunogenic, non-toxic, capable of controlled degradation, able to support cell viability, and capable of allowing tissue remodeling.

Various fabrication techniques have been developed. Each technique has its pros and cons in advancing the new generation of tissue scaffolds. Each technique needs to provide the material, geometrical features, and specific instructive characteristics of the tissue of interest. Most fabrication techniques based on creating specific geometries fall under two categories: conventional and advanced. The conventional techniques include the use of synthetic and natural traditional materials to make porous structures. Some examples are solvent-casting, freeze drying, and melt molding. Disadvantages of these techniques include poor control of porosity within the structure (pore size and pore

interconnectivity) and difficulty making internal channels within the scaffolds. Advanced techniques include sterolitography, molding, 3D printing, and electrospinning, among others[1]. Our technology incorporates both conventional and advanced fabrication techniques. With the convergence of the computer-aided manufacturing, where we create or import the desired architectural features, and the development of an enzyme-labile rubber, we take advantage of the best of both worlds. The negative molds milled using architectural directives designed by the CAD program provide solid molds that after being reaction injected with the BSA rubber components create an easy and reliable transfer of features to any material. This allows not only the control of external tissue composition, but also of internal highly complex structures. The work presented here focuses primarily on characterizing the BSA rubber. Our goal was to obtain a material that mixed homogeneously, digested in a reasonable amount of time, was resistant to alterations in its structure, and was able to mimic the smallest of features while holding its stability during the casting process.

Serum albumin is the most abundant protein in the circulating system. Albumin is one of the longest known and most studied of all proteins, with research dating to the 1940s, where it became important in World War II as a stable blood substitute [23]. This protein is used in biochemical and food industries [24]. Glutaraldehyde is a crosslinking agent that causes changes in the solubility of albumin. It is a compound that binds covalently to the amine group of lysine or hydroxylysine of protein molecules and, thus, stabilizes the protein structure. Silva, *et al*. indicated that the number of free lysine groups is important for the formation of aggregates when using glutaraldehyde as the crosslinking reagent [22, 25]. Based on our data, the increase of salts improved the

elasticity of the rubber (from 1xPBS to 2xPBS). The behavior of the ideal rubber (30% BSA 3% glutaraldehyde in 2× PBS or 1× PBS) behaves as a viscoelastic material that can withstand loading without permanently deforming. This becomes very important when handling and casting material around this structure.

In our study, trypsin readily digested the BSA rubber while leaving the collagen untouched. Trypsin is a serine protease that hydrolyzes proteins. Trypsin is a widely used enzyme that has high cleavage specificity. It cleaves the peptide chains mainly at the carboxyl side of the amino acids lysine and arginine. It has been reported in the literature that long incubation periods produce non-specific cleavage, deamination and oxidation, and trypsin autlolysis products [26]. In our studies, the trypsin readily digested the BSA rubber leaving the collagen intact and relatively untouched. This demonstrates the efficacy of the BSA rubber as a sacrificial material for biofabrication.

Currently, a similar system called BioGlue is being used as a surgical adhesive. This sealant is composed of 10% glutaraldehyde and 45% bovine serum albumin. This material has been used for the treatment of aortic dissections, ventricular septal defects, pulmonary air leaks, hemorrhage, and reinforcement of synthetic grafts. One of the main concerns of using this glue is the release of free glutaraldehyde that may be delivered to the tissue. There is evidence supporting that the direct contact between the BioGlue and the phrenic nerve causes nerve injury and even paralysis of the nerve [27]. Furst, *et al.* showed that after the glue polymerizes and is placed in contact with fluid, free glutaraldehyde is released, enough to become cytotoxic to cells [28]. In our studies, we use the BSA rubber as a sacrificial material to transfer the geometrical features to a scaffold material and release it as soon as possible. The material will not have any contact

with cells. The construct will be thoroughly free of any BSA and glutaraldehyde material that can affect the *in vivo* behavior of cells.

5.6 CONCLUSIONS

This biofabrication technique is a step forward in the generation of *in vitro* scaffolds that can recapitulate intrinsic geometrical features quickly and reliably. We selected a natural material such as collagen because natural materials offer superior chemical and physical cues to cells. These materials can be used for therapeutic research, as *in vitro* models of development, malformation, and disease tissue, as well as for replacement of damaged tissue.

5.7 REFERENCES

1. Kundu, J., et al., *Chapter 2 - Biomaterials for Biofabrication of 3D Tissue Scaffolds*, in *Biofabrication*, G. Forgacs and W. Sun, Editors. 2013, William Andrew Publishing: Boston. p. 23-46.
2. Vats, A., et al., *Scaffolds and biomaterials for tissue engineering: a review of clinical applications.* Clinical Otolaryngology, 2003. **28**(3): p. 165-172.
3. Chan, B.P. and K.W. Leong, *Scaffolding in tissue engineering: general approaches and tissue-specific considerations.* Eur Spine J, 2008. **17 Suppl 4**: p. 467-79.

4. Salerno, A., et al., *Tailoring the pore structure of PCL scaffolds for tissue engineering prepared via gas foaming of multi-phase blends.* Journal of Porous Materials, 2011. **19**(2): p. 181-188.

5. Hasan, A., et al., *Electrospun scaffolds for tissue engineering of vascular grafts.* Acta Biomater, 2014. **10**(1): p. 11-25.

6. Huang, Z.-M., et al., *A review on polymer nanofibers by electrospinning and their applications in nanocomposites.* Composites Science and Technology, 2003. **63**(15): p. 2223-2253.

7. Sell, S.A., et al., *Electrospinning of collagen/biopolymers for regenerative medicine and cardiovascular tissue engineering.* Advanced Drug Delivery Reviews, 2009. **61**(12): p. 1007-1019.

8. Zheng, W., W. Zhang, and X. Jiang, *Biomimetic Collagen Nanofibrous Materials for Bone Tissue Engineering.* Advanced Engineering Materials, 2010. **12**(9): p. B451-B466.

9. Cao, H. and N. Kuboyama, *A biodegradable porous composite scaffold of PGA/beta-TCP for bone tissue engineering.* Bone, 2010. **46**(2): p. 386-95.

10. Ankam, S., et al., *Substrate topography and size determine the fate of human embryonic stem cells to neuronal or glial lineage.* Acta Biomater, 2013. **9**(1): p. 4535-45.

11. Bose, S., S. Vahabzadeh, and A. Bandyopadhyay, *Bone tissue engineering using 3D printing.* Materials Today, 2013. **16**(12): p. 496-504.

12. Yost, M.J., et al., *A novel tubular scaffold for cardiovascular tissue engineering.* Tissue Eng, 2004. **10**(1-2): p. 273-84.

13. Lundgren, E., et al., *Extracellular matrix components influence the survival of adult cardiac myocytes in vitro.* Exp Cell Res, 1985. **158**(2): p. 371-81.

14. Tanford, C. and J.G. Buzzell, *The Viscosity of Aqueous Solutions of Bovine Serum Albumin between pH 4.3 and 10.5.* The Journal of Physical Chemistry, 1956. **60**(2): p. 225-231.

15. Yadav, S., S.J. Shire, and D.S. Kalonia, *Viscosity analysis of high concentration bovine serum albumin aqueous solutions.* Pharm Res, 2011. **28**(8): p. 1973-83.

16. Tobitani, A. and S.B. Ross-Murphy, *The intrinsic viscosity of polyelectrolytes revisited.* Polymer International, 1997. **44**(3): p. 338-347.

17. Arakawa, T. and S.N. Timasheff, *Theory of protein solubility.* Methods in Enzymology, 1985. **114**: p. 49-77.

18. Habeeb, A.F.S.A. and R. Hiramoto, *Reaction of proteins with glutaraldehyde.* Archives of Biochemistry and Biophysics, 1968. **126**(1): p. 16-26.

19. Migneault, I., et al., *Glutaraldehyde: behavior in aqueous solution, reaction with proteins, and application to enzyme crosslinking.* Biotechniques, 2004. **37**(5): p. 790-6, 798-802.

20. Burmeister, J.J., et al., *Glutaraldehyde cross-linked glutamate oxidase coated microelectrode arrays: selectivity and resting levels of glutamate in the CNS.* ACS Chem Neurosci, 2013. **4**(5): p. 721-8.

21. Chatterji, P.R., *Gelatin with hydrophilic/hydrophobic grafts and glutaraldehyde crosslinks.* Journal of Applied Polymer Science, 1989. **37**(8): p. 2203-2212.

22. Silva, C., et al., *Chemical modifications on proteins using glutaraldehyde.* Food Technology and Biotechnology, 2004. **42**(1): p. 51-56.

23. Peters, T., Jr. and A.J. Stewart, *Albumin research in the 21st century.* Biochim Biophys Acta, 2013. **1830**(12): p. 5351-3.

24. Masuelli, M.A., *Study of Bovine Serum Albumin Solubility in Aqueous Solutions by Intrinsic Viscosity Measurements.* Advances in Physical Chemistry, 2013. **2013**: p. 1-8.

25. Habeeb, A.J. and R. Hiramoto, *Reaction of proteins with glutaraldehyde.* Arch Biochem Biophys, 1968. **126**(1): p. 16-26.

26. Freije, J.R., et al., *Chemically modified, immobilized trypsin reactor with improved digestion efficiency.* J Proteome Res, 2005. **4**(5): p. 1805-13.

27. Lemaire, S.A., et al., *Nerve and conduction tissue injury caused by contact with BioGlue.* J Surg Res, 2007. **143**(2): p. 286-93.

28. Furst, W. and A. Banerjee, *Release of glutaraldehyde from an albumin-glutaraldehyde tissue adhesive causes significant in vitro and in vivo toxicity.* Ann Thorac Surg, 2005. **79**(5): p. 1522-8; discussion 1529.

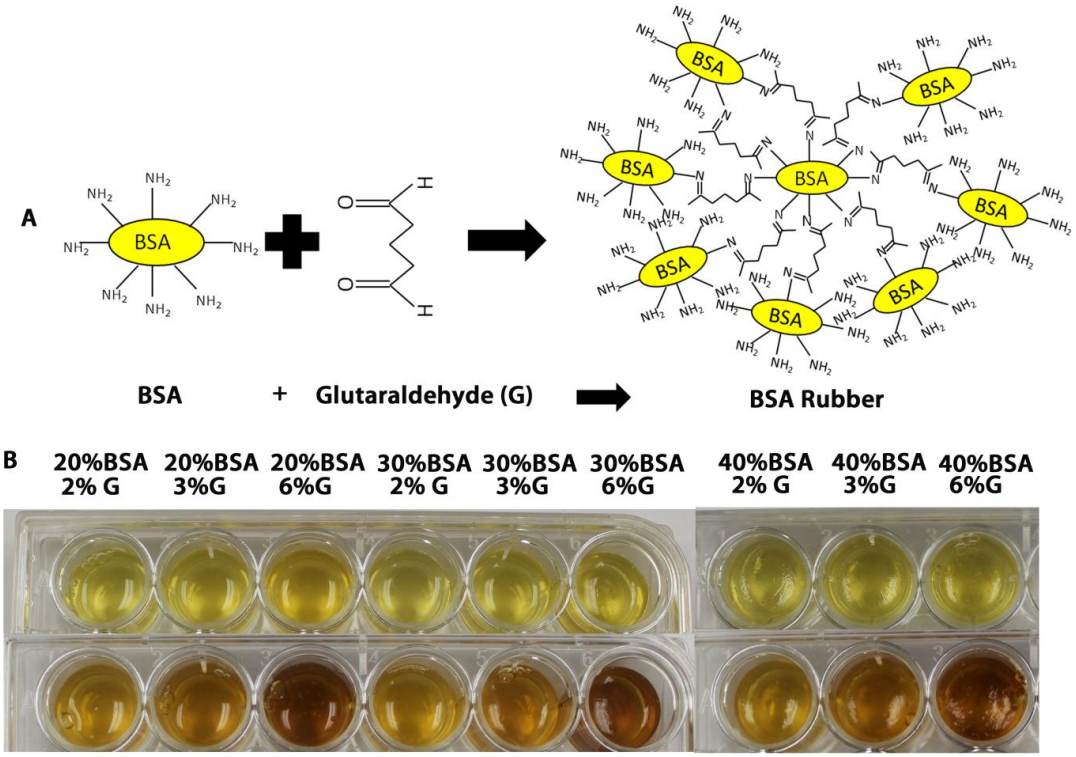

Figure 5.1: BSA rubber. A. BSA rubber reaction. The glutaraldehyde crosslinks the BSA by creating covalent bonds. B. BSA Rubber. Different concentrations of BSA, concentrations of glutaraldehyde, and type of solvent were casted on 24-well plates and reacted overnight at 4°C.

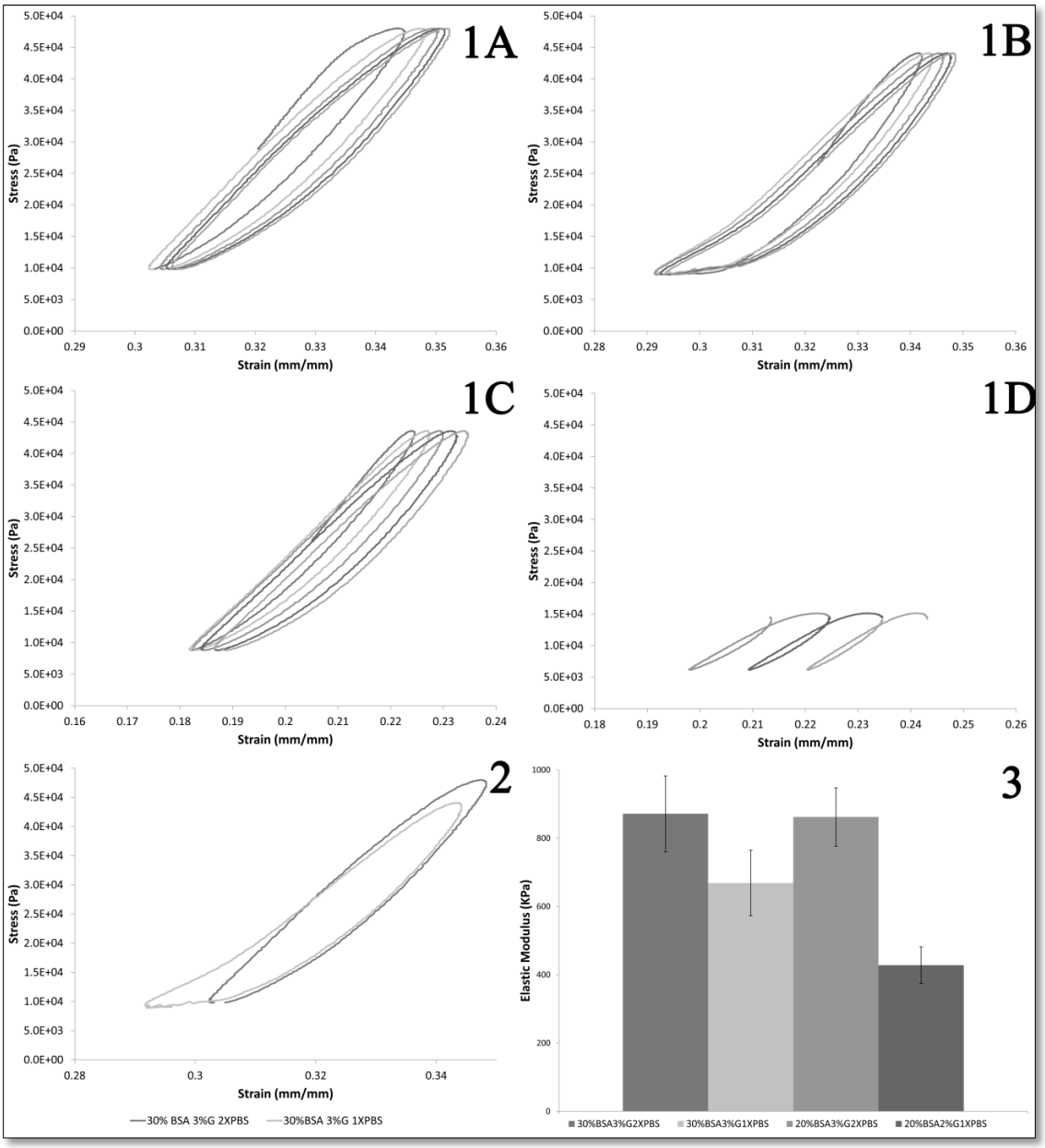

Figure 5.2: Stress-Strain curves of BSA rubbers. (1A) 30% BSA 3% glutaraldehyde in 2× PBS (1B) 30% BSA 3% glutaraldehyde in 1× PBS (1C) 20% BSA 3% glutaraldehyde in 2× PBS and (1D) 20% BSA 2% glutaraldehyde in 1× PBS (3 cycles). The curves 1A-1C show rubbers that have some hysteris, but return to their original shape. Sample 1D shows a rubber with a very low elastic modulus that easily deforms permanently during the loading and unloading processes. Sample 1A and 1B showed a very similar behavior as seen in one loading and unloading cycle on graph 2. The elasticity was influenced by the solvent used (graph 3). The samples displayed a significant increased in modulus with an increase of salts ($p<0.05$).

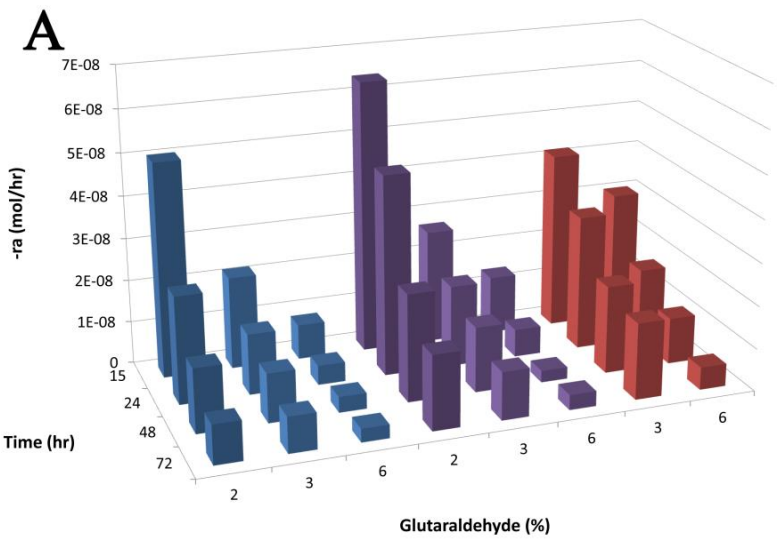
A
7E-08
6E-08
5E-08
4E-08
3E-08
2E-08
1E-08
0
-ra (mol/hr)
15
24
48
72
Time (hr)
2
3
6
2
3
6
3
6
Glutaraldehyde (%)

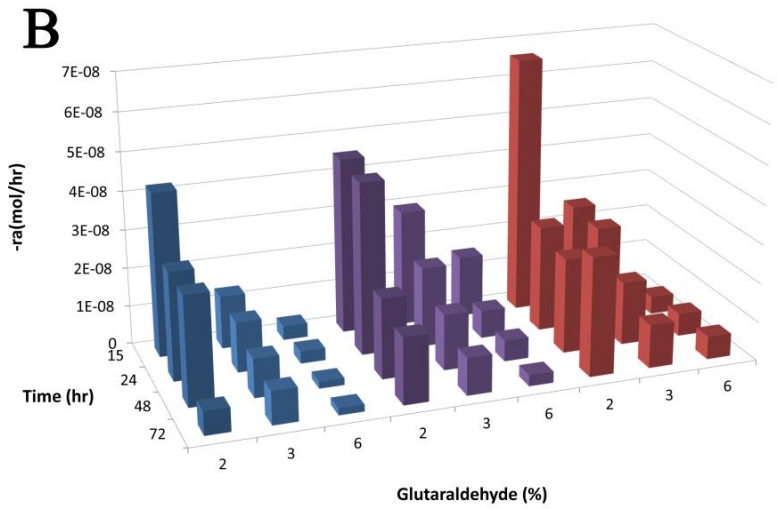
B
7E-08
6E-08
5E-08
4E-08
3E-08
2E-08
1E-08
0
-ra(mol/hr)
15
24
48
72
Time (hr)
2
3
6
2
3
6
2
3
6
Glutaraldehyde (%)

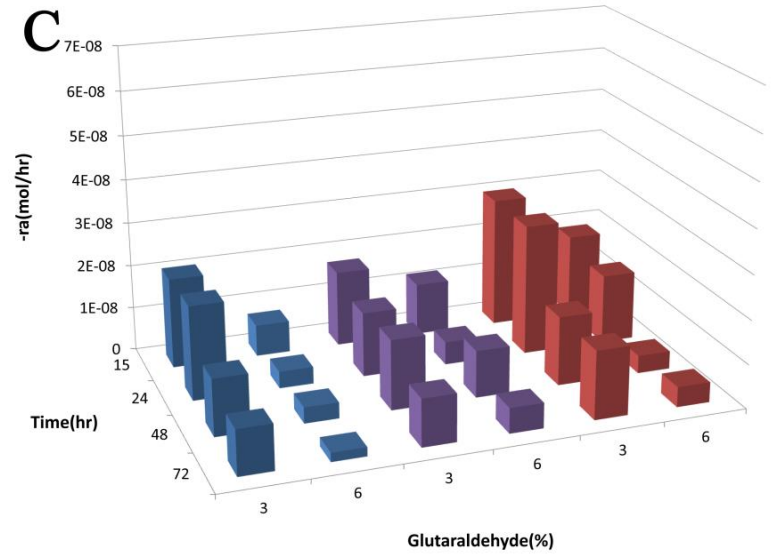
C
7E-08
6E-08
5E-08
4E-08
3E-08
2E-08
1E-08
0
-ra(mol/hr)
15
24
48
72
Time(hr)
3
6
3
6
3
6
Glutaraldehyde(%)

Figure 5.3: Reaction rate of the disintegration of the BSA rubber. As the fixative increases, the reaction rate decreases for all samples in 1× PBS (A), 2× PBS (B), and DI (C). The 40% BSA 2%G 2× PBS shows one of the highest rates of reaction. This is due to the difficulty encountered in making the BSA protein homogeneous. (blue-20% BSA, purple-30% BSA, and red–40% BSA)

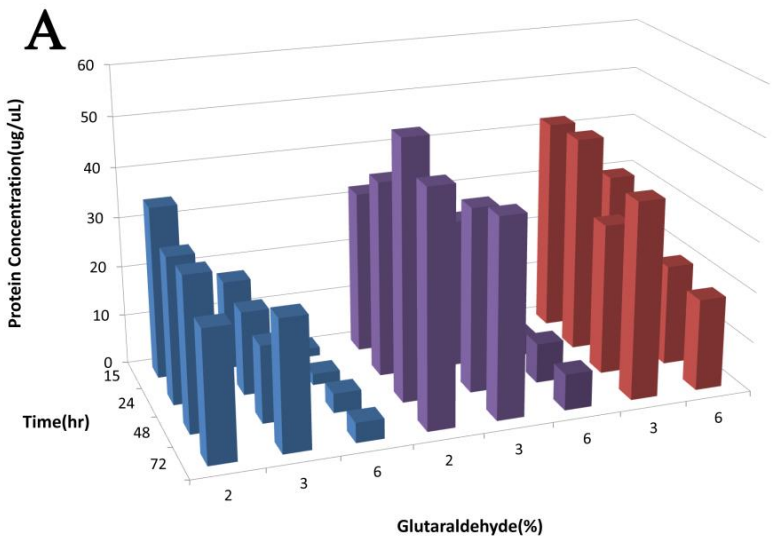
A
Protein Concentration(ug/uL)
60
50
40
30
20
10
0
Time(hr)
15
24
48
72
2
3
6
2
3
6
3
6
Glutaraldehyde(%)

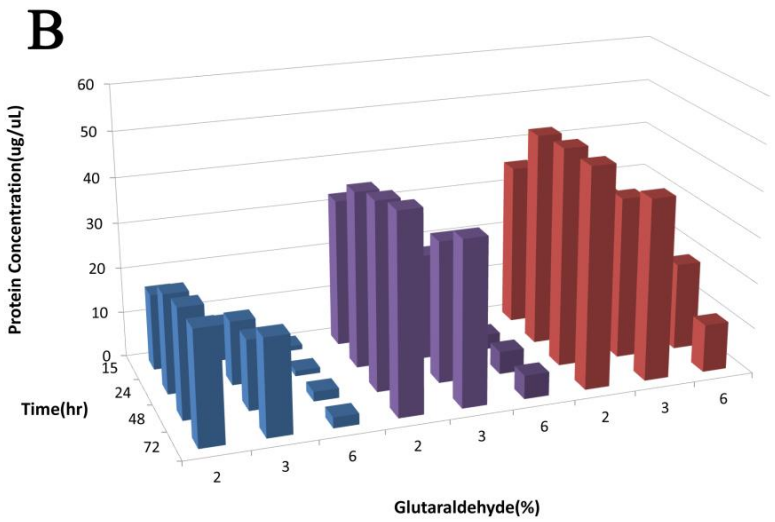
B
Protein Concentration(ug/uL)
60
50
40
30
20
10
0
Time(hr)
15
24
48
72
2
3
6
2
3
6
2
3
6
Glutaraldehyde(%)

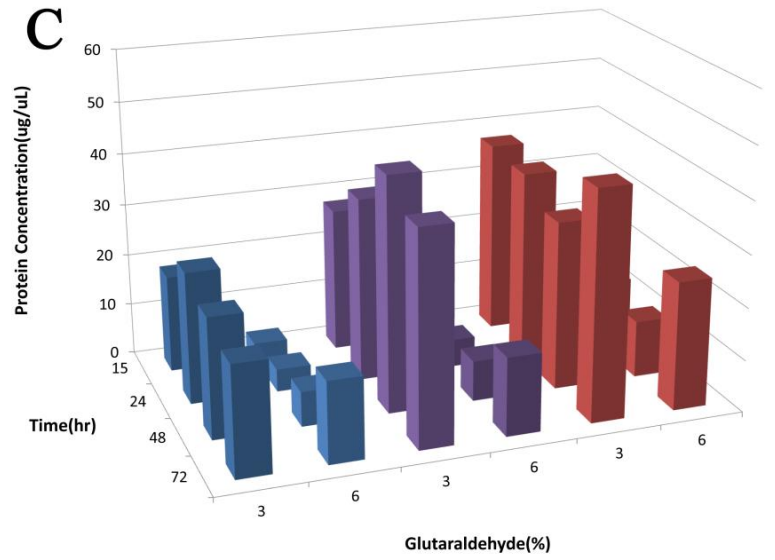
C
Protein Concentration(ug/uL)
60
50
40
30
20
10
0
Time(hr)
15
24
48
72
3
6
3
6
3
6
Glutaraldehyde(%)

Figure 5.4: Protein quantification after enzyme digestion. As the fixative increases, the protein dissolved from the rubbers decreases for all samples in 1× PBS (A), 2× PBS (B), and DI water (C). This relationship can also be seen in Figure 3. (blue-20% BSA, purple-30% BSA, and red-40% BSA)

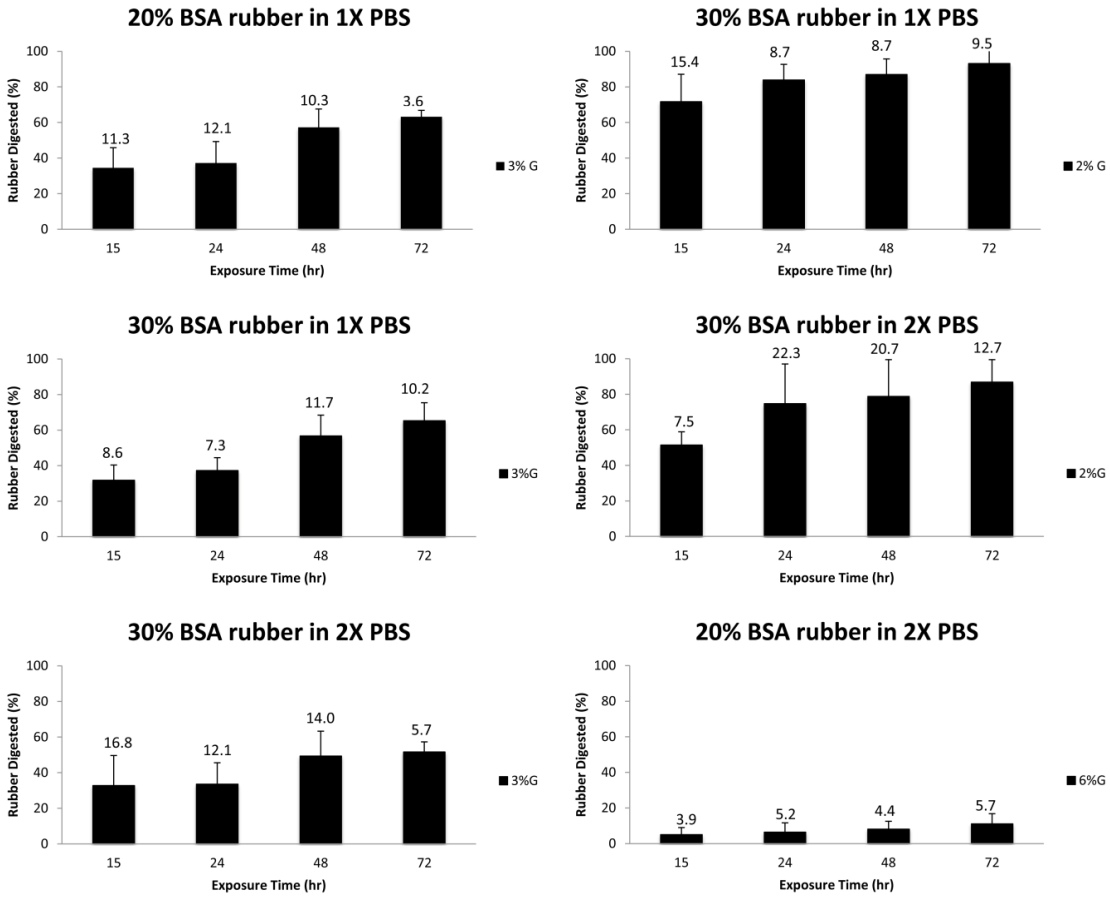

Figure 5.5: Rubber digestion. We determined the amount of rubber digested by comparing the starting and end dry basis products. We obtained the least amount of digestion on the 6% glutaraldehyde sample and the most (earlier) at 30% BSA 2% glutaraldehyde in 1× PBS.

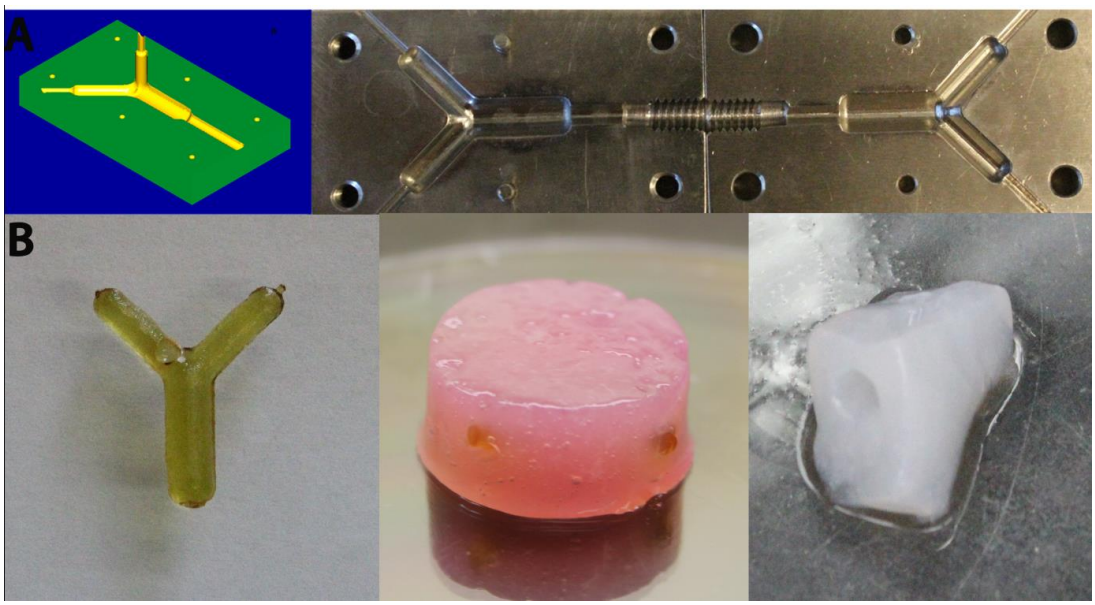

Figure 5.6: Branched prototype (A) Representation of branch vasculature. Shown on the left is the solid created in Mastercam which was converted to G Code and fabricated using the Microlution®363-S as seen on the right. (B) 3D collagen scaffold. Shown on the left is the BSA rubber made using the mold shown above (Figure 5.6A). The center shows the rubber embedded in the collagen hydrogel. Shown on the right are the channels left within the collagen scaffold after the rubber was enzyme digested.

Table 5.1: BSA rubber parameters. BSA and fixative were mixed at a 4:1 ratio using three different solvents.

BSA Rubber	
BSA (%)	***Glutaraldehyde (%)***
20	2
20	3
20	6
30	2
30	3
30	6
40	2
40	3
40	6

Table 5.2: Conductivity and pH of BSA samples. We determined the conductivities and pH of the BSA solutions using different solvents. An increase in conductivity is shown between 2× and 1× PBS.

Sample		Conductivity (mS/cm)	pH
BSA (%)w/w	***Solvent***		
30	2×PBS	11.43	7.06
30	1×PBS	6.35	7.05
30	DI	2.39	6.76
20	2×PBS	13.00	6.92
20	1×PBS	8.67	7.09
20	DI	2.08	6.90

Table 5.3: BSA rubber. After the BSA rubber reacted overnight, we proceeded to take an 8-mm punch hole of the sample. This table contains some visual observations of the consistency and appearance of the samples.

BSA (%)	G (%)	Solvent	Observations
20	**2**	**1× PBS**	Soft, easy deformable material
20	**3**	**1× PBS**	Soft but more sturdy than the 2% glutaraldehyde
20	**6**	**1× PBS**	Stiff, a little brittle
30	**2**	**1× PBS**	Good consistency
30	**3**	**1× PBS**	Good consistency
30	**6**	**1× PBS**	Brittle
40	**2**	**1× PBS**	Very inconsistent in creating a gel/rubber consistency
40	**3**	**1× PBS**	The consistency vary along the sample
40	**6**	**1× PBS**	Brittle
20	**2**	**2× PBS**	Soft, easy deformable material but more sturdy than the 1× PBS sample
20	**3**	**2× PBS**	Soft but stiffer than the 2%
20	**6**	**2× PBS**	Good consistency
30	**2**	**2× PBS**	Good consistency, more sturdy than with 1× PBS
30	**3**	**2× PBS**	Good consistency, more sturdy than with 1× PBS
30	**6**	**2× PBS**	Good mixability but brittle
40	**2**	**2× PBS**	The consistency vary along the sample
40	**3**	**2× PBS**	The consistency vary along the sample
40	**6**	**2× PBS**	The consistency vary along the sample and it was brittle
20	**2**	**DI**	Did not form a gel/rubber material
20	**3**	**DI**	Formed a gel but seem stiffer than the 1× PBS and 2× PBS, inconsistent
20	**6**	**DI**	Formed a gel but seem stiffer than the 1× PBS and 2× PBS, inconsistent
30	**2**	**DI**	Did not form a gel/rubber material
30	**3**	**DI**	Formed a gel but seem stiffer than the 1× PBS and 2× PBS, inconsistent
30	**6**	**DI**	Formed a gel but seem stiffer than the 1× PBS and 2× PBS, inconsistent
40	**2**	**DI**	Did not form a gel/rubber material
40	**3**	**DI**	The consistency vary along the sample-stiffer on top
40	**6**	**DI**	The consistency vary along the sample-stiffer on top

CHAPTER 6:

THREE-DIMENSIONAL PRINTING: MIMICKING *IN VIVO* ENVIRONMENTS

6.1 ABSTRACT

Biomaterials that recapitulate the intrinsic architecture of *in vivo* tissue are vital for study diseases, as well as to facilitate the regeneration of lost and malformed soft tissue. We have developed a novel biofabrication technique that combines state of the art imaging, micromachining and selective enzymatic activity to create the new generation of biomaterials for research and clinical application.

The purpose of this work is to transfer the in vivo tissue architectures by creating a negative mold in a solid piece. The mold piece contains the true three dimensional architecture which contains flow channels or tissue voids that represent the *in vivo* niches. Using human renal CT angiograms, we created a 3D model with the specific in vivo architectural features. These models was translated to a mold, where we can later on transfer its features into a enzyme labile material, BSA rubber, and obtain a 3D biodegradable scaffold that resembles the original architecture.

6.2 INTRODUCTION

Tissue engineering has emerged as a multidisciplinary field combining science, engineering and manufacture to engineer biomimetric scaffolds. The success of tissue engineering relies on the capability of designing biological scaffolds that closely resemble native tissue to regenerate defective, diseased or malformed tissue. Native tissue is a complex three-dimensional environment composed of cells and extracellular matrix with a specific structural order that can be found at different length scales. In order to engineer such a construct, there are certain requirements: it must provide the

proper architectural features, must be composed of the appropriate cell population, become functional, nonthrombogenic, provide the appropriate extracellular matrix composition, and allow proper mechanical and humoral signaling to regulate the remodel and maintenance of the scaffold[1, 2]. The scaffold materials must incorporate geometric features seen on the microenvironments on the same length scale as native tissues.

The niche provides the necessary cues such as structural, biochemical, and mechanical signaling for the stem cells to respond to physiological change and induce in vivo behavior. It has been seen that these features influence the cell behavior in a variety of tissue such as neuronal[3, 4], cardiac[5], and skeletal muscle[6]. The geometrical and architectural cues are critical and provide guidance for cells to align and orientate according to the tissue. Different biofabrication approaches have been used to mimic key features of these microenviroments. The architectural features of this complex environments aid in providing functionality to the tissue. In order to restore function or replace end-stage organs, new approaches have been made involving the production of three-dimensional decellularized matrix [7]. These tissue templates can be reseeded with autologous stem cells and produce at some degree functional tissue [8]. However, there are risks of immune response [9], availability, and that in fact restores the functionality of the tissue. Other technique that has been used is 3D printing in which cells and extracellular matrix can be placed in a particular spatial arrangement to mimic vasculature.

The goal of this biofabrication technique is to engineer a custom made collagen scaffolds that mimic the native tissue architecture (figure 6.1). The first step is the selection of the tissue of interest and imaging it. After imaging the tissue, we can obtain

the specific architecture and transfer it to a PLA, brass, or stainless steel mold. These molds can then be reaction injected with a customized biodegradable rubber, BSA rubber, which allows the transfer of the specific dimensions to the collagen hydrogel. Then, seeded with autologous cells, this scaffold can be incubated in a bioreactor and transplanted to the patient. In this work, we used two tissues: heart and renal artery. We created 3D models showing the specific architectural features. Then, using a 3D printer, we created a negative mold of the renal artery 3D model. This mold upholds the specific intrinsic architectural features, allowing the previously developed BSA rubber to be reaction injected and deliver the specific features into a scaffold material. These next generations of materials that mimic tissue architectural features not only further provide information about the cellular interaction with geometrical and topographical cues in their three-dimensional environment, but also allow the fabrication of functional tissue constructs ideal for the regeneration field.

6.3 MATERIALS AND METHODS

6.3.1 Imaging of the tissue architecture

We selected two tissues to image: an embryonic chick heart and a human renal artery.

Heart. Embryonic Hamburger-Hamilton (HH) stage 40 (day 14) chick heart was selected. This stage represents the postcardiac morphogenesis period, which allowing us to study the architectural feature of the fully developed heart[10]. Different stages of the embryonic chick heart are used as models for the study of heart diseases such as tetralogy

of fallot (TOF). This stage in particular is used as comparison of a healthy developed heart versus a disease one.

Embryonic chick heart was isolated and fixed in 4% paraformaldehyde. The fixed tissues was embedded in parafilm and sectioned at 8 μm using a Vibratome. Each section was collected in a water bath and placed on slides, carefully maintaining the order from which they were sectioned. The sections were stained with hematoxylin (nuclei) and eosin (cytoplasm, collagen, and muscle fiber). Light microscopy was used to obtain detail images of the intrinsic geometrical features.

Renal Artery. Human renal CT angiogram was used to obtain detail geometries of the renal artery. Renal artery stenosis is a major cause of renovascular hypertension that can result in the long run in organ damage, ischemic nephropathy, cardiac destabilization syndromes and end-stage renal disease. Despite numerous research based on understanding this disease, is still not fully understand the mechanisms responsible for the development of it[11]. Having an in vitro model that contains the complex architectural features of the renal artery can be useful to isolate specific parameters of interest and mimic in vivo conditions.

We obtained deidentify formatted DICOM data from healthy patients. This data was already on the database. Approximately 250 z stack images were obtain from each CT angiogram patient. Briefly, a 29 gauge IV access was obtained in the anticubital fossa. A dose of contrast agent at 100 cc of Omni 350 was injected through the IV at a rate of 4 cc/sec. Images were assessed until 100 houndsfield units were obtained at level

of abdominal aorta. Multiple slices were obtained of arterial, venous, ad delayed phases of the renal artery and kidneys.

6.3.2 3D model reconstructions

Because of the importance of mimicking the microenvironment of the tissue of interest, we created a model of the renal artery and chick heart. Amira® (FEI Visualization Science Group) software is a powerful tool that has been used to recreate specific 3D architecture from 2D images.

The H&E images from the embryonic heart were imported into Amira. We selected the area of interested using the magnetic lasso tool. We selected the right ventricle and pulmonary truck with its ramifications. 3D models were created for the chick heart and we were able to determine the precise dimensions of the pulmonary trunk and the right ventricle of a chick heart (figure 6.2).

For the renal artery reconstruction, we used CT angiography (CTA) images. De-identified DICOM format data was obtained from healthy donors. The images were loaded to Amira and compiled to create a model with specific interest in the renal artery ramifications. Approximately 250 z stack images were used to reconstruct the vasculature model. In order to focus in our area of interest, several filters were applied which will help visualizes the abdominal aorta and how it ramifies to each of the kidneys. We proceeded to identifying the three areas of interest: the abdominal aorta, right and left renal artery. Each structure was outlined in each 2D section with a magnetic lasso tool. Then each structure was established as a different material and filled with a different

color. Each material was assigned an anatomical name and saved. After the segmentation, all the segmented structures were surface rendering reconstructed as a 3D model. Having the three area of interest, we obtained the 3D model which showed the intrinsic geometrical features (figure 6.3).

6.3.3 Molds

To create a customized biodegradable rubber mold, we needed to make a negative mold that contained the architecture and features of the tissue of interest.

Using Amira® model, we imported into MasterCAM® or trueSpace(Caligari Corporation), where it can be manipulated. With Master Art®, we converted the model into machine G-code language. We also designed a solid on MasterCAM and converted in G code. Once in G-Code we can then transfer the program to our Microlution 363-S micro milling machine to create the mold in stainless steel and brass. We fabricated three pieces: a branched ramified construct or Y mold, pulmonary trunk, and a test blank mold. We also created the models using MakerBot Replicator2 3D Printer. Using the Replicator software, we are able to import the program into the 3D Printer. This printer has a 100 micron layer resolution and allows the fabrication of polylactic acid (PLA) molds by depositing layer by layer of this material to build the piece. We fabricated two pieces: a loop and a renal artery mold.

6.4 RESULTS

6.4.1 3D Reconstructions

We selected an embryonic stage 40 chick heat. At this stage, the heart is fully developed, allowing us to study its architectural features. Each stained section was imported into Amira, where they were carefully stacked one over the other one to reconstruct the architecture seen in figure 6.2. The green area represents the right atrium and right ventricle. The yellow area corresponds to the pulmonary artery and branches to each bronchus. Using this model, we were able to obtain specific dimensions of the pulmonary trunk such as length, width, and height which are 1304, 189, and 409 μm respectively.

Using CT renal artery angiograms, we were able to reconstruct the architectural features of the abdominal aorta and renal arteries. We obtained deidentify formatted DICOM data from healthy patients. This data was already on the data base. After obtaining this data, we imported to the Amira software in order to reconstruct the 3D vasculature using approximately 250 z- stack images (figure 3). In order to focus in our area of interest, several filters were applied which will help visualizes the abdominal aorta and how it ramifies to each of the kidneys. We proceeded to identifying the three areas of interest: the abdominal aorta, right and left renal artery. Before reaching the hilus of the kidneys, each artery divides into several branches. These branches lie between the renal veins and the ureter. Each vessel branches to the suprarenal glands, the ureter and surrounding tissues. For our purposes, we did not include these branches: we only focus on the connection between the aorta and the kidney. Using our 3D model, we were able

to measure several areas of interest. The segment of the aorta prior to reaching the ramification of the renal artery was 11.18 mm diameter. This dimension increased to 16.69 mm below the right renal artery. The right and left renal artery diameters were 5.84 mm and 5.95 mm respectively

Figure 6.4 and 6.5 show the 3D model overlapping the raw ortho slices images. This shows good agreement between the raw data and our model. The model shows some areas of discontinuity. This was due to the difficulty in some areas, especially on the ramifications of the left renal artery, to distinguish the area of interest from all the surrounding data.

6.4.2 Molds

Using Mastercam, we created our prototype that represents a branched vasculature. Several toolpaths operations were used on order to create a hollow structure in the Mastercam solid. Two pieces per mold were build, each one holds half of the diameter of the channel structure. This makes it easy to release the rubber mold from the piece. All molds were created using the same principle.

We isolated the pulmonary trunk and the branches to the lungs from the heart 3D reconstruction model. We generated a G code for it and made an acrylic piece of it using the Microlution machine (not shown).

We also made a 3D representation of the vessel which contains the special architectural features of the aorta and how it branches out to form the renal artery. The renal artery 3D model was visualized in Mastercam program (figure 6.7), and then imported to true space program. The model was embedded into a solid and common areas

were removed, leaving the hollow structure (figure 6.8). The solid program was broken into 4 pieces and loaded to the 3D Makerbot Replicator to create a mold made of PLA (figure 6.9)**.** The Makerbot deposits material to create a piece, compared to the Microlution machine which mills a solid block, removing materials to replicate the model. The resulting surface is rougher piece compared to the one made using the Microlution, which produced a polished stainless steel mold. Nevertheless, both machines can create a structure that upholds the specific architectural features of the tissue of interest.

6.5 DISCUSSION

In the present study, it's the first time to our knowledge, that in vivo vasculature architecture is transferred to a biocompatible material to re create the true dimensionality of the native tissue. Previous studies have been based on relating the phenotypical expression of the cells and its relationship with the specific nanotopographical features. Topography can up regulate markers of neuronal[3], muscular[5], or vascular lineages. Ankam showed that the hESCs cultured in anisotropic patters promoted neuronal differentiation while the isotropic patterns promoted glial differentiation[3]. It has been showed that only architectural features induce certain phenotypical expression even without biochemical cues such as growth factors [4]. By creating 3D architectures in biomaterials, we can begin to engineer more full thickness tissues with more *in vivo* like characteristics.

The research presented is part of the overall biofabrication scheme to create biomaterials that mimic the native tissue architecture. This technique incorporates the architectural features seen *in vivo* to an *in vitro* collagen gel. Our biomaterial is a collagen scaffold molded around enzyme labile core that upholds the 3D architectural features serving as a mold. We previously showed our prototype that represents a branched architecture tissue. This collagen construct, can be used as a model to study several diseases as well as replace damaged tissue. Collagen was the selected backbone of our construct because it has excellent mechanical properties and it provides the required instructions for cells to modulate its behavior [5, 12]. This simple and economical technique will recapitulate the true three dimensional architecture-recreating the flow channels or tissue voids that truly represent the *in vivo* niche.

Because of the importance of mimicking the microenvironment of the vasculature of interest, we created a model of the renal artery. Kidney transplantation is now a routine surgical procedure with a success rate of 90–95% one year after implantation[13]. However, shortage of organ donors creates a waiting list of 60,000 patients, many of whom die before a suitable donor kidney is found[14]. Although modern dialysis saves human lives, it is not a radical but rather a palliative, temporary and very expensive solution that costs an average of $250,000 to maintain the life of one patient with end stage kidney disease. One of the critical features of creating an engineered tissue such as the kidney is the multiple branching architecture of the renal artery. Every patient shows variation in the architectural features of tissue based on age, health and hereditary conditions. Several approaches have been attempted including the use of decellularized kidney matrix. Using this platform and reconstituting the endothelium of the hollow

structure, researchers were able to show some function [15]. We created a model using *in vivo* data provided by human renal CT angiograms. We will be able to fabricate a custom made scaffold, which when seeded with autologous cells, will create a viable graft. The purpose of this work is not to generate an organ replacement, but to fabricate biocompatible constructs that can repair or improve the function of the damage kidney and prevent and/or remove patients for the need of dialysis. The next step of this project will focus on delivering the geometrical instructive to collagen scaffolds using the BSA rubber, and reconstitute the endothelium. This model will be useful to study the mechanotransduction of the topographical cues and how they influence the cell behavior.

This new generation of biomaterials is ideal for research and clinical application. Currently our technology has been applied mimicking renal arteries but it is suitable for many applications such as spinal injury, congenital heart diseases, fabrication of coronary mitral valve, hip replacement, custom graph for aneurysm, and many others. This is a versatile fabrication technique that provides the necessary elasticity, extracellular components, and architectural features to engineer a viable and functional graft.

6.6 REFERENCES

1. Cleary, M.A., et al., *Vascular tissue engineering: the next generation.* Trends Mol Med, 2012. **18**(7): p. 394-404.
2. Ott, H.C., et al., *Perfusion-decellularized matrix: using nature's platform to engineer a bioartificial heart.* Nat Med, 2008. **14**(2): p. 213-21.

3. Ankam, S., et al., *Substrate topography and size determine the fate of human embryonic stem cells to neuronal or glial lineage.* Acta Biomater, 2013. **9**(1): p. 4535-45.

4. Yim, E.K., S.W. Pang, and K.W. Leong, *Synthetic nanostructures inducing differentiation of human mesenchymal stem cells into neuronal lineage.* Exp Cell Res, 2007. **313**(9): p. 1820-9.

5. Zhao, Y., et al., *Fabrication of skeletal muscle constructs by topographic activation of cell alignment.* Biotechnol Bioeng, 2009. **102**(2): p. 624-31.

6. Yost, M.J., et al., *A novel tubular scaffold for cardiovascular tissue engineering.* Tissue engineering, 2004. **10**(1-2): p. 273-84.

7. Badylak, S.F., et al., *Engineered whole organs and complex tissues.* Lancet, 2012. **379**(9819): p. 943-952.

8. Song, J.J., et al., *Regeneration and experimental orthotopic transplantation of a bioengineered kidney.* Nature Medicine, 2013. **19**(5): p. 646-651.

9. Badylak, S.F. and T.W. Gilbert, *Immune response to biologic scaffold materials.* Semin Immunol, 2008. **20**(2): p. 109-16.

10. Tobita, K., et al., *Engineered early embryonic cardiac tissue retains proliferative and contractile properties of developing embryonic myocardium.* American Journal of Physiology - Heart and Circulatory Physiology, 2006. **291**(4): p. H1829-H1837.

11. LERMAN, L.O., et al., *Noninvasive Evaluation of a Novel Swine Model of Renal Artery Stenosis.* Journal of the American Society of Nephrology, 1999. **10**(7): p. 1455-1465.

12. Clyman, R.I., K.A. McDonald, and R.H. Kramer, *Integrin receptors on aortic smooth muscle cells mediate adhesion to fibronectin, laminin, and collagen.* Circulation Research, 1990. **67**(1): p. 175-186.

13. Briggs, J.D., *Causes of death after renal transplantation.* Nephrology Dialysis Transplantation, 2001. **16**(8): p. 1545-1549.

14. O'Connor, K.J. and F.L. Delmonico, *Increasing the supply of kidneys for transplantation.* Seminars in Dialysis, 2005. **18**(6): p. 460-462.

15. Peloso, A., et al., *Considerations on the development of a model of kidney bioengineering and regeneration in rats.* Expert Review of Medical Devices, 2013. **10**(5): p. 597-601.

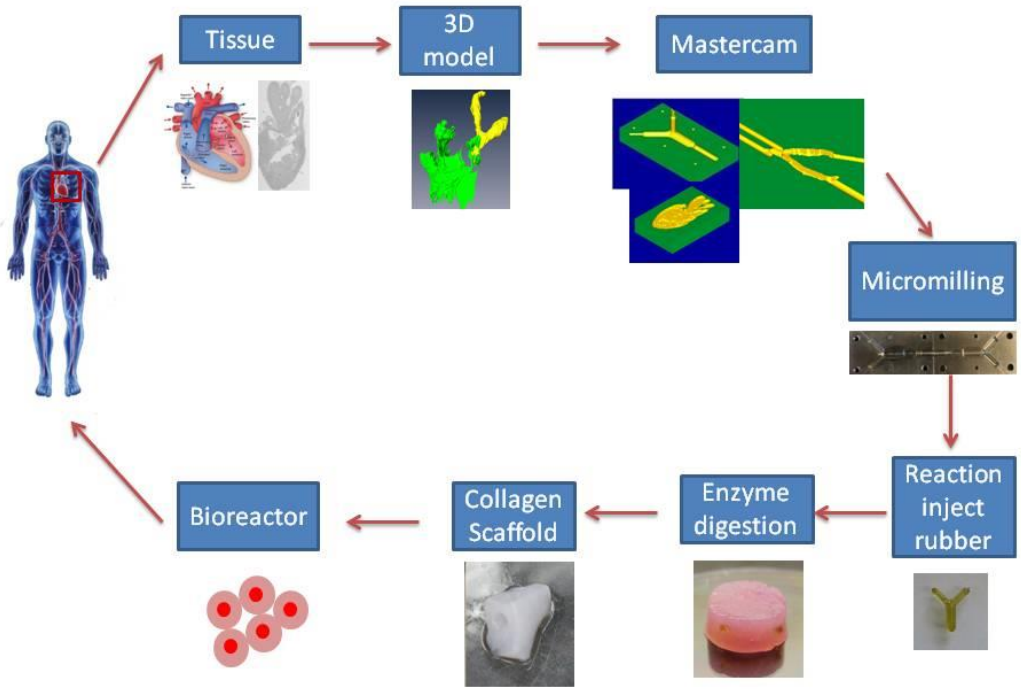

Figure 6.1. Biofabrication scheme. The goal of this technique is to engineer 3D collagen scaffolds that are representative of the composition and architectural features of the *in vivo* tissue. The first step is the selection of the vasculature or tissue of interest and imaging it. As soon as it is imaged, we can obtain the specific architecture and transfer it to a solid mold which in combination with the biodegradable rubber, will serve to transfer the instructive to the collagen hydrogel. Then, seeded with autologous cells, can be placed in a bioreactor and transplanted to the patient.

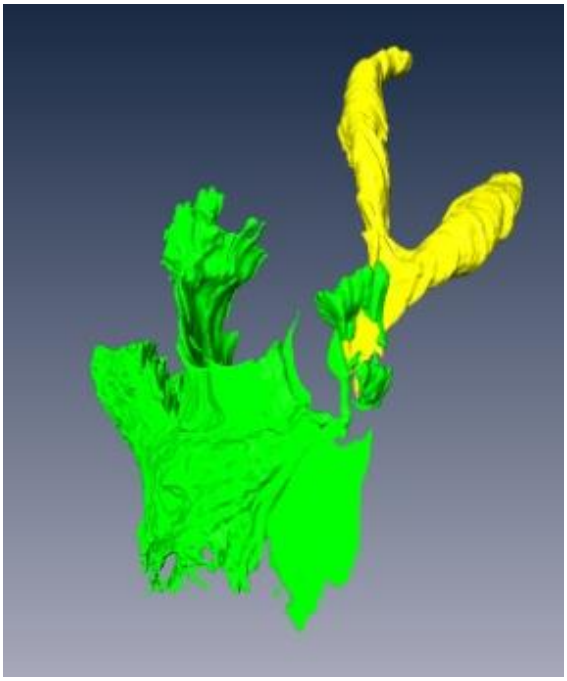

Figure 6.2. Amira® model for stage 40 embryonic heart. High-resolution images were taken from the sliced of the sectioned heart at stage 40. The green area represents the lumen of the right ventricle and the yellow area represent the lumen of the pulmonary truck as it branches to each bronchus

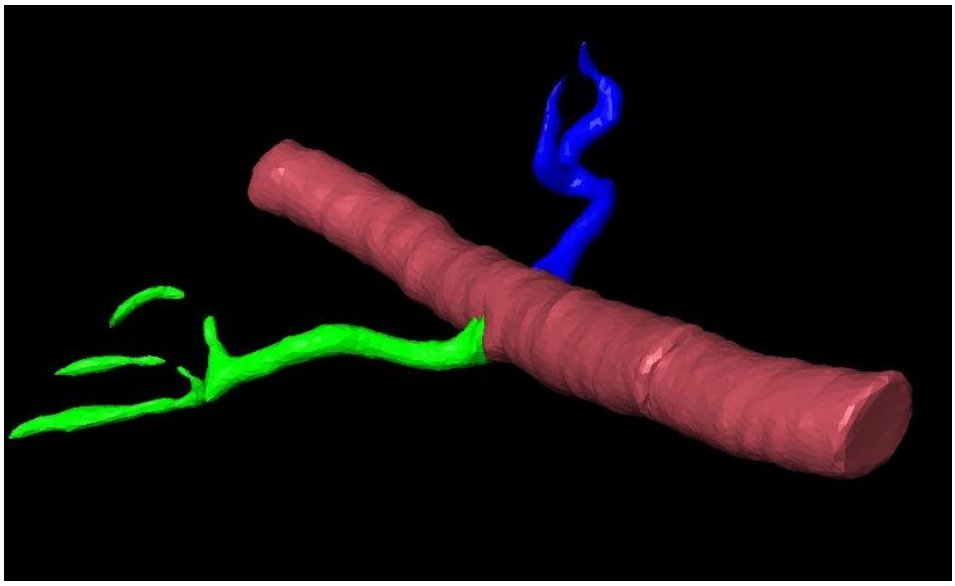

Figure 6.3. Amira 3D Model of the Renal Artery. Using Amira we reconstructed the abdominal arta and the renal artery. The pink, green, and blue area corresponds to the abdominal aorta, right and left renal artery respectively.

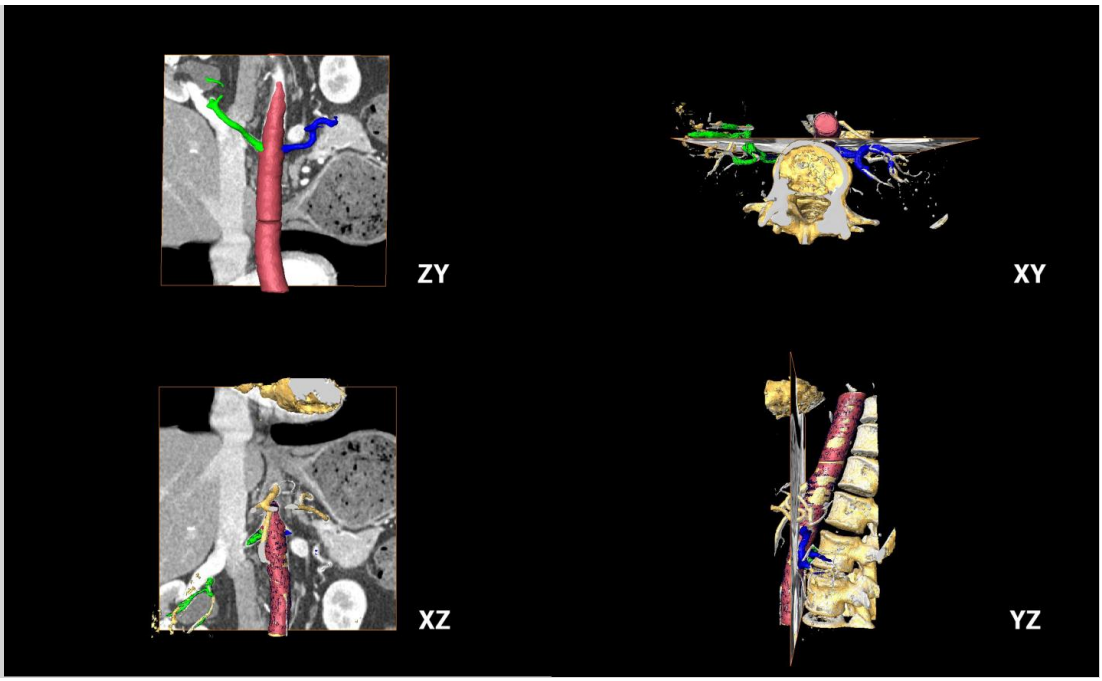

Figure 6.4. Ortho slices of the Renal CT Angiograms with the Amira 3D model reconstruction

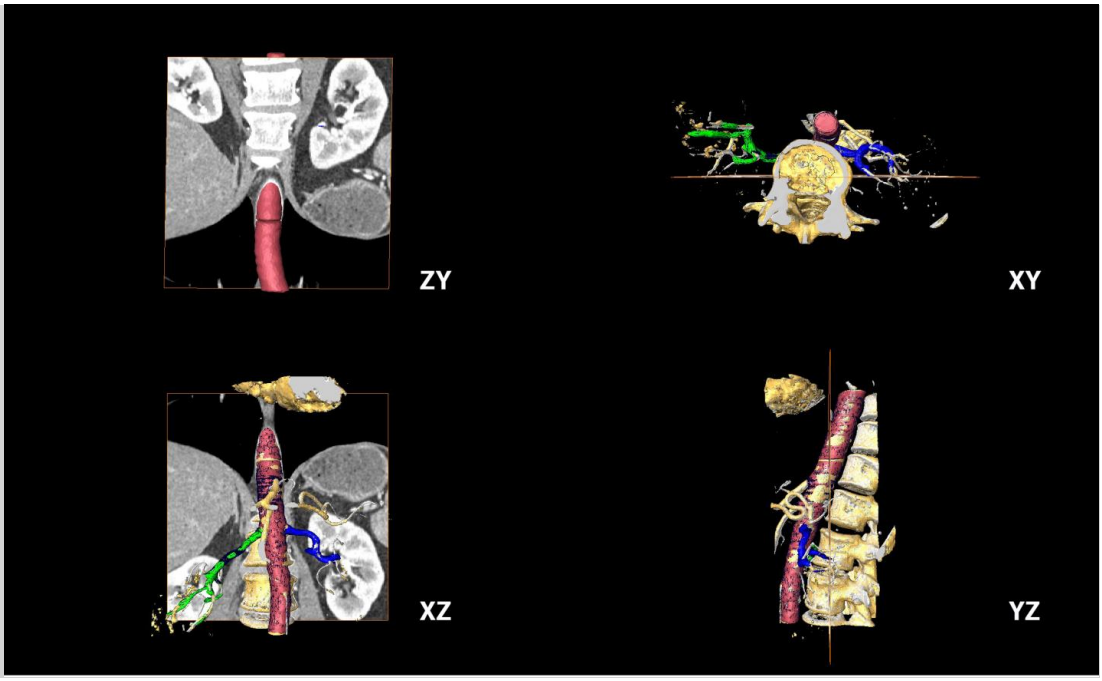

Figure 6.5. Ortho slices of the Renal CT Angiograms with the Amira 3D model reconstruction.

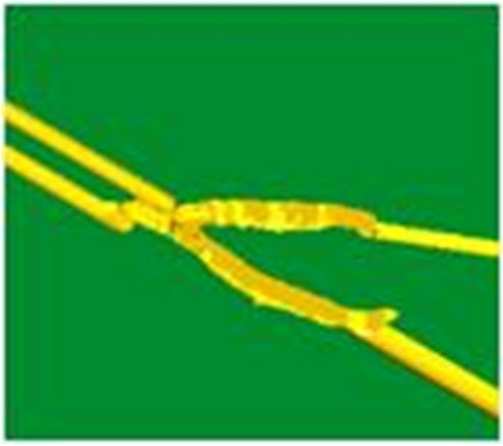

Figure 6.6. Matercam Art images for stage 40 embryonic heart. After obtaining the 3D reconstruction, the architectural features of the pulmonary trunk and its ramification were imported to MastercamArt. After selecting the desired toolpaths, we will generate G code and transfer this data into a stainless steel mold.

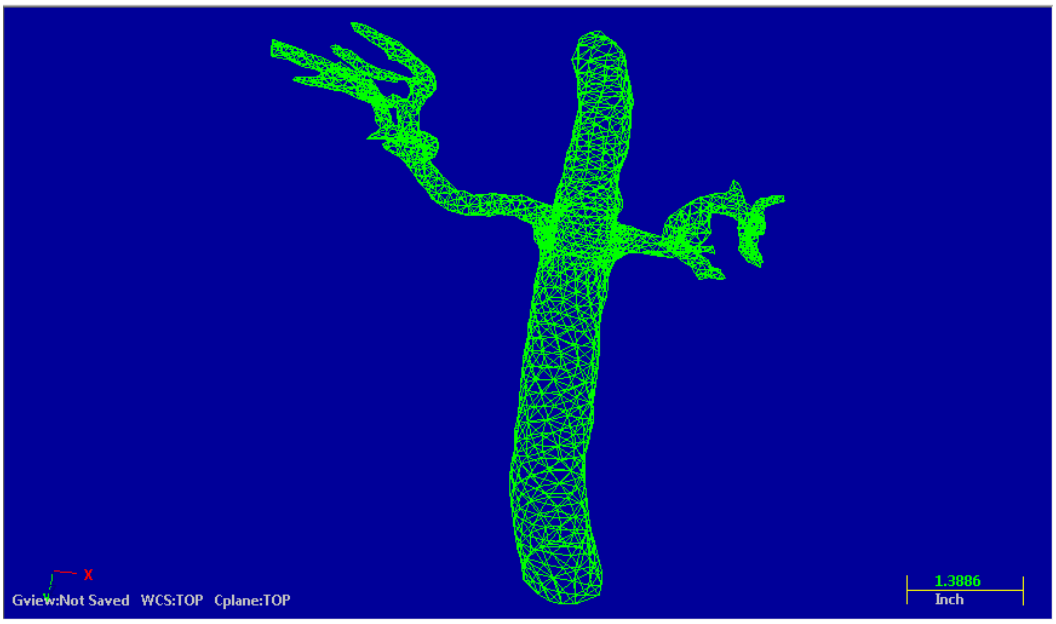

Figure 6.7. Mastercam Art model of the abdominal aorta and renal arteries. Amira model of the renal CT Angiographs were imported to Mastercam.

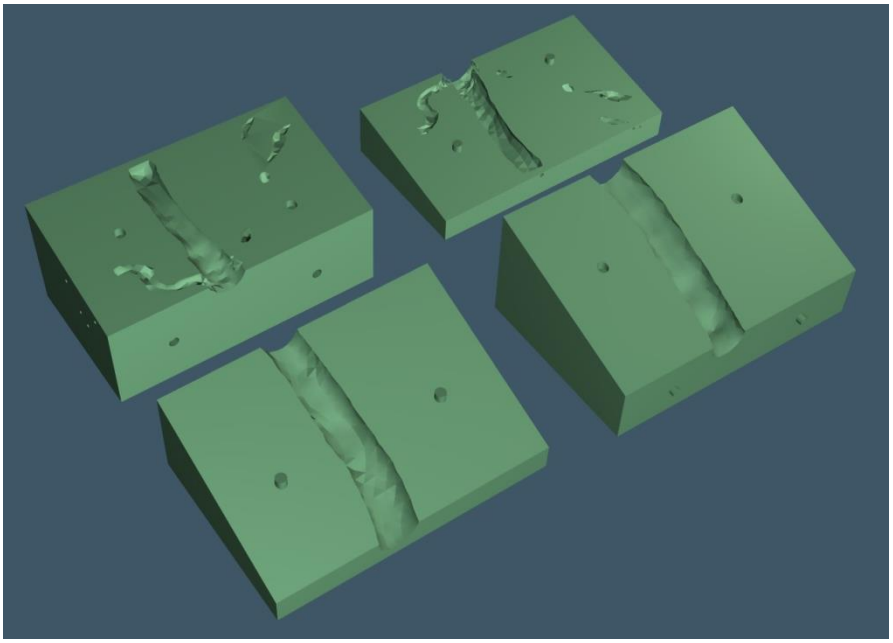

Figure 6.8. Abdominal aorta and renal artery solid using True Space. The 3D model was embeeded into a solid using the True Space software and broken into four pieces to allow the release of the BSA rubber.

Figure 6.9. PLA molds of the renal artery model. The 3D model was cut in four connecting pieces and printed in the 3D printer. This was done to facilitate the removal of the BSA rubber, which will serve as a template for the collagen hydrogel to adopt the geometries.

CHAPTER 7:

SUMMARY OF DISCUSSION

7.1 SUMMARY OF DISCUSSION

The extracellular matrix is responsible for providing adequate balance between physical features, chemical composition, and mechanical forces that influence the cells[1, 2]. Numerous researchers have studied the cell responses to numerous mechanical stimulation *in vitro*. The microenvironment exerts forces that are transmitted through focal adhesion causing changes in the cell behavior from maintaining quiescence to inducing activation of cells.

The studies presented here had five main objectives. First, the development of a standardize collagen extraction procedure in which we can produce highly purified collagen. Second, use the collagen extracted to create fibrous tissue scaffold. Third, identify the cell response to changes in stiffness of the collagen scaffold. Fourth, develop an enzyme labile material that can deliver specific tissue architectures to a collagen hydrogel. Finally, bring all these components together to development 3D collagen scaffolds using in vivo data and demonstrate their many applications in the regenerative and tissue engineering field.

The optimization of the collagen extraction protocol came due to the variability encounter between batch to batch of the collagen solution. Up to date, the collagen extraction protocol has not been well documented. The series of step that starts with the calf hide to the purifying of the collagen involve a series of modifications to the collagen structure in order to remove all the non collagenous materials and allow the collagen to be manipulated for numerous tissue engineering applications. Several extraction techniques are acid, enzyme, and salt extraction[3]. Each technique modifies the collagen

in a particular way. For example, the enzyme extraction protocol partially or completely removes the telopeptides at the end of the triple helix domain. This induces changes in the fibrillogenesis kinetics compared to the other procedures. Also, the presence of other molecules in the end product can have an effect in the fibrillogenesis[4, 5]. The incomplete removal of these materials, especially residual DNA can cause ECM rejection or an acute immune response when place in the body [6]. In our studies, we tested each step of the extraction protocol to determine the complete removal of noncollagenous material such as fats and proteoglycans. We determined that in the initial steps of the extraction, the protocol is effective in the removal of noncollagenous materials and maintaining the integrity of the collagen molecule without degrading based on the results of the enzymatic assay.

The extracellular matrix is a dynamic environment for cells that is mainly composed by collagen fibrils and form a highly organized 3D scaffold that surrounds the cells. Electrospinning is one of the most successful techniques in the production of fibrous tissue scaffolds [7, 8]. Currently used solvents for the electrospinning of collagen fibers has been shown to denature the structure of the collagen[9]. The end product was a soluble fiber mat that needed to be severely crosslink in order to mimic the mechanical stability shown in the native collagen. We wanted to preserve the molecular structure of the collagen that makes it biocompatible, biodegradable, mechanical stable, and porous. The development of reaction electrospinning which combines the process of electrospinnning and fibrillogenesis, allows the fabrication of fibrous collagen scaffolds that mimic the dimensions of fibrils in the *in vivo* tissueThese fibers were not soluble in

aqueous environment and were resistant to enzymatic attack. The fibrous nature of these scaffolds mimics the state that the collagen is *in vivo* tissues.

Cell behavior including morphology, function and fate depends strongly on the substrate stiffness. The elastic modulus is tissue dependent, ranging from 0.1 – 100 KPa for brain tissue and bone, respectively[10]. In order to create tunable collagen hydrogels, we established the relationship between collagen concentration and elastic modulus. We showed that by tuning the collagen hydrogel to the elasticity of the *in vivo* niche of satellite cells (12 KPa), we maintained the quiescent phenotype. In stiffer substrates, it drove the cell to differentiation pathways. Interesting, unsorted muscle cells culture in an environment of 12 KPa seem to cause changes from activation to quiescent. This needs to be further investigated. We showed that we can control the stiffness of a collagen matrix in a simpler way compared to other researches that have developed crosslinking mechanisms for synthetic substrates to modulate cell potential[11]. Also, the use of collagen, which is natural extracellular material, provides the necessary cues for cells to behave as they do *in vivo*[12, 13].

Previously, researches have shown the effects of the topography by mechanotransduction influence the cell behavior. These cues provide the necessary information for cells to proliferate, differentiate or drive the cells to specific lineage[2, 14]. We developed the technology in which we can transfer *in vivo* tissue geometries to a collagen scaffold. To create a 3D scaffold, we developed a sacrificial material called "BSA rubber". This enzyme labile material can be use to transfer specific geometries to scaffold materials. We determined the proper parameters of BSA and glutaraldehyde concentration in order to achieve the best consistency that can sustain loading forces of

casting materials without collapsing and affecting the architectural features.. Using *in vivo* data, we developed a 3D model that can be used to create a PLA mold of the *in vivo* dimensions. This mold can be reaction injected with BSA rubber and serve as a template for collagen to polymerize around it. After the rubber is digested, we can have a true replica of the *in vivo* tissue. This technology is applicable to any type of tissue, making it a versatile true recapitulation of the tissue in an in vitro material.

One of the many applications of this technology is for individuals with kidney disease. Approximately there are about 400,000 individuals that are living with end-stage kidney disease that require hemodialysis[15]. Several approaches based on cell therapy and tissue engineering has been made in constructing devices or tissue scaffolds to replace tissue or organ functions lost due to this disease. Song et al showed that by using an accelular matrix seeded with endothelial and epithelial cells, the construct showed some functionality but not enough to become permanent replacement[16]. Others researchers have used cell therapy by combining a filtration system seeded with porcine renal proximal tubule cells and show improvements compared to conventional hemodialysis[15]. We created a new alternative in which we can combine conventional and advance biofabrication technique to generate tissue scaffolds that provide the adequate tissue geometry preventing immunoresponse. At the same time, collagen provides the ideal characteristics of biocompatability and through the cell-matrix interation not only play a role in adhesion and migration but also regulates and/or promotes cell differentiation promoting functionality of the scaffold. Mimiking architectural features can provide the ideal conditions for the development of funtional

grafts. This can improve the quality of life for patients with renal disease by reducing their need for hemodialysis.

By combining the composition of the substrate, the geometrical features and the elasticity of the substrate, we can recapitulate the microenvironments and see *in vivo* behaviors. Overall, we developed several biofabrication techniques to incorporate the instructive features into a deliver collagen scaffold. These biofabrication techniques combines imaging of tissue of interest, 3D printing, and selective enzymatic activity to create the new generation of 3D biomaterials for research and clinical application. We can use the BSA rubber that contains the intrinsic geometrical features and cast either collagen tuned to a specific elastic modulus or electrospun collagen fibers. After rubber is enzyme digested, we can generate two types of scaffolds: one is composed of a tighter network, while the other has a fibrous nature that it's highly porous. These biofabrication techniques move forward the tissue engineering and regenerative field that aims to restore form and function to tissues that have been lost or damaged due to disease, congenital defect, or trauma. Using this technology we can create custom made constructs that mimic the tissue of interest and can be used to further develop therapeutics alternatives by studying the cell-ECM interactions as well as replace damage tissue.

7.2 REFERENCES

1. Moore, K.A. and I.R. Lemischka, *Stem cells and their niches.* Science, 2006. **311**(5769): p. 1880-5.
2. Kshitiz, et al., *Control of stem cell fate and function by engineering physical microenvironments.* Integrative Biology, 2012. **4**(9): p. 1008.
3. Xiong, X., et al., *A new procedure for rapid, high yield purification of Type I collagen for tissue engineering.* Process Biochemistry, 2009. **44**(11): p. 1200-1212.
4. Obrink, B., *Study of interactions between monomeric tropocollagen and glycosaminoglycans.* European Journal of Biochemistry, 1973. **33**(2): p. 387-400.
5. Vogel, K.G., M. Paulsson, and D. Heinegard, *Specific-inhibition of type-i and type-ii collagen fibrillogenesis by the small proteoglycan of tendon.* Biochemical Journal, 1984. **223**(3): p. 587-597.
6. Badylak, S.F. and T.W. Gilbert, *Immune response to biologic scaffold materials.* Semin Immunol, 2008. **20**(2): p. 109-16.
7. Yang, L., et al., *Mechanical properties of single electrospun collagen type I fibers.* Biomaterials, 2008. **29**(8): p. 955-62.
8. Matthews, J.A., et al., *Electrospinning of Collagen Nanofibers.* Biomacromolecules, 2002. **3**(2): p. 232-238.
9. Zeugolis, D.I., et al., *Electro-spinning of pure collagen nano-fibres – Just an expensive way to make gelatin?* Biomaterials, 2008. **29**(15): p. 2293-2305.
10. Engler, A.J., et al., *Matrix Elasticity Directs Stem Cell Lineage Specification.* Cell, 2006. **126**(4): p. 677-689.

11. Gilbert, P.M., et al., *Substrate elasticity regulates skeletal muscle stem cell self-renewal in culture.* Science (New York, N.Y.), 2010. **329**(5995): p. 1078-81.

12. Yost, M.J., et al., *A novel tubular scaffold for cardiovascular tissue engineering.* Tissue Eng, 2004. **10**(1-2): p. 273-84.

13. Whelan, M.C. and D.R. Senger, *Collagen I initiates endothelial cell morphogenesis by inducing actin polymerization through suppression of cyclic AMP and protein kinase A.* J Biol Chem, 2003. **278**(1): p. 327-34.

14. Gelse, K., *Collagens—structure, function, and biosynthesis.* Advanced Drug Delivery Reviews, 2003. **55**(12): p. 1531-1546.

15. Humes, H.D., et al., *Replacement of renal function in uremic animals with a tissue-engineered kidney.* Nature Biotechnology, 1999. **17**(5): p. 451-455.

16. Song, J.J., et al., *Regeneration and experimental orthotopic transplantation of a bioengineered kidney.* Nature Medicine, 2013. **19**(5): p. 646-651.

CHAPTER 8:

SUGGESTED FUTURE WORK

8.1 SUGGESTED FUTURE WORK

8.1.1Future work for the collagen extraction

8.1.1.1 Molecular testing of the extraction protocol

This work presented here provided insight of the effectiveness of our collagen extraction procedure. To further document the entire collagen extraction process, we need to finish testing each of the steps. In this study, the supernatant for the RIPA, trypsin, and collagenase of the hide and limed processed samples were tested. The collagenase assay needs to be repeated in order to activate the enzyme and further study the collagen degradation. This will provide a more profound insight of the collagen structure and further validate the purified extract. It may prove useful to perform a turbidimetry curve in which the collagen can be polymerize using this media 4 after neutralizing it and study the causes of the difference between the buffer. This media showed larger values of absorbance, which can be indicative of larger aggregates but created a highly acidic hydrogel.

8.1.2 Future work for the biofabrication techniques

8.1.2.1 Investigation of skeletal muscle cells

The work presented here shows that the stiffness of the matrix play a crucial role in the control of the phenotype expression of cells. We found that by mimicking the stiffness of the satellite cells niche, we maintain the quiescent phenotype. To further characterize the effects of the stiffness of the matrix as the driving force affecting the cells behavior, we need to do PCR analysis to quantify the changes in expression of each

of the transcription factors. This should be done for the satellite cells and the unsorted cells. For the sorted cells it will serve as a validation of what we can see in the immunofluorescence analysis, indicative that the quiescent phenotype of the cells is maintain in an environment that mimics the *in vivo* elasticity of the satellite cells. For the unsorted cells, a detail quantification of the transcription factors will help identify if the cell after being exposed to a matrix of 12 KPa reacts as we can see in the immunofluorescent analysis, by upregulating Pax7 that is characteristic of quiescent and downregulating MyoD which is indicative of cell activation. Also, these gels should be tested after they are seeded with cells to identify how the cells remodel their surrounding substrates to their liking.

8.1.2.2 Investigations of reaction electrospinning

The experiments presented here show a random fibrous collagen scaffold made by combining electrospinning and fibrillogenesis processes. In order to further develop this technique, we should test electrospinning with higher collagen concentrations. Higher collagen concentration may help making a more manageable construct that can maintain specific 3D features. Also, we should test the for the elasticity of the fibers, which can be done by Atomic Force Microscopy (AFM), to identify the relationship between the collagen concentration and the elasticity of the fibers. It should be interesting to compare these results with the relationship established earlier with the casted collagen hydrogels. Also, in order to engineer fibrous 3D scaffold that contain specific architectures, we can use the BSA rubber that contains specific architectures and cast collagen electrospun fibers around it. Then, by digesting the rubber, we can obtain a fibrous scaffold that mimic the extracellular matrix, containing a unique hollow structure.

8.1.2.3 Investigation of 3D Collagen Scaffolds

In this work we showed that using *in vivo* data from human renal CT angiograms we can create negative molds of the 3D reconstruction model. The next step would be to reaction inject the BSA rubber. Then, cast collagen around the sacrificial material and enzyme digested it, leaving a true representation of the architectural features in an in vitro. It will be beneficial to analyze the cell response to the topographical cues. The same approach should be done with other types of tissue such as heart to expand the applicability of this technique to a wide range of clinical applications.

REFERENCES

CHAPTER 1

1. Moore, K.A. and I.R. Lemischka, *Stem cells and their niches.* Science, 2006. 311(5769): p. 1880-5.

2. Kshitiz, et al., *Control of stem cell fate and function by engineering physical microenvironments.* Integrative Biology, 2012. 4(9): p. 1008.

3. Yost, M.J., et al., *A novel tubular scaffold for cardiovascular tissue engineering.* Tissue Eng, 2004. 10(1-2): p. 273-84.

4. Whelan, M.C. and D.R. Senger, *Collagen I initiates endothelial cell morphogenesis by inducing actin polymerization through suppression of cyclic AMP and protein kinase A.* J Biol Chem, 2003. 278(1): p. 327-34.

5. Orr, A.W., et al., *Mechanisms of Mechanotransduction.* Developmental Cell, 2006. 10(1): p. 11-20.

6. Gelse, K., *Collagens—structure, function, and biosynthesis.* Advanced Drug Delivery Reviews, 2003. 55(12): p. 1531-1546.

7. Ward, D.F., Jr., et al., *Mechanical strain enhances extracellular matrix-induced gene focusing and promotes osteogenic differentiation of human mesenchymal stem cells through an extracellular-related kinase-dependent pathway.* Stem Cells Dev, 2007. 16(3): p. 467-80.

8. Riha, G.M., et al., *Cyclic strain induces vascular smooth muscle cell differentiation from murine embryonic mesenchymal progenitor cells.* Surgery, 2007. 141(3): p. 394-402.

9. Bayati, V., et al., *The evaluation of cyclic uniaxial strain on myogenic differentiation of adipose-derived stem cells.* Tissue Cell, 2011. 43(6): p. 359-66.

10. Park, J.S., et al., *Differential effects of equiaxial and uniaxial strain on mesenchymal stem cells.* Biotechnol Bioeng, 2004. 88(3): p. 359-68.

11. Weinbaum, S., S.C. Cowin, and Y. Zeng, *A model for the excitation of osteocytes by mechanical loading-induced bone fluid shear stresses.* J Biomech, 1994. 27(3): p. 339-60.

12. Partridge, J., et al., *Laminar shear stress acts as a switch to regulate divergent functions of NF-kappaB in endothelial cells.* FASEB J, 2007. 21(13): p. 3553-61.

13. Wang, H., et al., *Shear stress induces endothelial differentiation from a murine embryonic mesenchymal progenitor cell line.* Arterioscler Thromb Vasc Biol, 2005. 25(9): p. 1817-23.

14. Tian, X.F., et al., *Comparison of osteogenesis of human embryonic stem cells within 2D and 3D culture systems.* Scand J Clin Lab Invest, 2008. 68(1): p. 58-67.

15. Cukierman, E., et al., *Taking cell-matrix adhesions to the third dimension.* Science, 2001. 294(5547): p. 1708-12.

16. Baker, B.M. and C.S. Chen, *Deconstructing the third dimension: how 3D culture microenvironments alter cellular cues.* J Cell Sci, 2012. 125(Pt 13): p. 3015-24.

17. Ankam, S., et al., *Substrate topography and size determine the fate of human embryonic stem cells to neuronal or glial lineage.* Acta Biomater, 2013. 9(1): p. 4535-45.

18. Engler, A.J., et al., *Matrix elasticity directs stem cell lineage specification.* Cell, 2006. 126(4): p. 677-89.

19. Gilbert, P.M., et al., *Substrate elasticity regulates skeletal muscle stem cell self-renewal in culture.* Science (New York, N.Y.), 2010. 329(5995): p. 1078-81.

20. Rowlands, A.S., P.A. George, and J.J. Cooper-White, *Directing osteogenic and myogenic differentiation of MSCs: interplay of stiffness and adhesive ligand presentation.* Am J Physiol Cell Physiol, 2008. 295(4): p. C1037-44.

21. Li, D., et al., *Role of mechanical factors in fate decisions of stem cells.* Regen Med, 2011. 6(2): p. 229-40.

22. Chen, S.S., et al., *Cell-cell and cell-extracellular matrix interactions regulate embryonic stem cell differentiation.* Stem Cells, 2007. 25(3): p. 553-61.

23. Kihara, T., et al., *Exogenous type I collagen facilitates osteogenic differentiation and acts as a substrate for mineralization of rat marrow mesenchymal stem cells in vitro.* Biochem Biophys Res Commun, 2006. 341(4): p. 1029-35.

24. Kotch, F.W. and R.T. Raines, *Self-assembly of synthetic collagen triple helices.* Proc Natl Acad Sci U S A, 2006. 103(9): p. 3028-33.

25. Di Lullo, G.A., et al., *Mapping the ligand-binding sites and disease-associated mutations on the most abundant protein in the human, type I collagen.* J Biol Chem, 2002. 277(6): p. 4223-31.

26. Benjakul, S., et al., *Extraction and characterisation of pepsin-solubilised collagens from the skin of bigeye snapper (Priacanthus tayenus and Priacanthus macracanthus).* J Sci Food Agric, 2010. 90(1): p. 132-8.

27. Kadler, K.E., et al., *Collagens at a glance.* Journal of Cell Science, 2007. 120(12): p. 1955-1958.

28. Hofmann, H., P.P. Fietzek, and K. Kuhn, *The role of polar and hydrophobic interactions for the molecular packing of type I collagen: a three-dimensional evaluation of the amino acid sequence.* J Mol Biol, 1978. 125(2): p. 137-65.

29. Shoulders, M.D. and R.T. Raines, *Collagen structure and stability.* Annu Rev Biochem, 2009. 78: p. 929-58.

30. Exposito, J.Y., et al., *The fibrillar collagen family.* Int J Mol Sci, 2010. 11(2): p. 407-26.

31. Malone, J.P., K. Alvares, and A. Veis, *Structure and assembly of the heterotrimeric and homotrimeric C-propeptides of type I collagen: significance of the alpha2(I) chain.* Biochemistry, 2005. 44(46): p. 15269-79.

32. Khoshnoodi, J., et al., *Molecular recognition in the assembly of collagens: terminal noncollagenous domains are key recognition modules in the formation of triple helical protomers.* J Biol Chem, 2006. 281(50): p. 38117-21.

33. Veis, A. and K. Payne, *Collagen fibrillogenesis*. Collagen. Biochemistry. 1988, Boca Raton: CRC Press. 113.

34. Kadler, K.E., et al., *Collagen fibril formation.* Biochemical Journal, 1996. 316: p. 1-11.

35. Holmes, D.F., M.J. Capaldi, and J.A. Chapman, *Reconstitution of collagen fibrils in vitro; the assembly process depends on the initiating procedure.* International Journal of Biological Macromolecules, 1986. 8(3): p. 161-166.

36. Wenstrup, R.J., et al., *Regulation of collagen fibril nucleation and initial fibril assembly involves coordinate interactions with collagens V and XI in developing tendon.* J Biol Chem, 2011. 286(23): p. 20455-65.

37. Wenstrup, R.J., et al., *Murine model of the Ehlers-Danlos syndrome. col5a1 haploinsufficiency disrupts collagen fibril assembly at multiple stages.* J Biol Chem, 2006. 281(18): p. 12888-95.

38. Li, Y., et al., *A fibrillar collagen gene, Col11a1, is essential for skeletal morphogenesis.* Cell, 1995. 80(3): p. 423-430.

39. Kadler, K.E., A. Hill, and E.G. Canty-Laird, *Collagen fibrillogenesis: fibronectin, integrins, and minor collagens as organizers and nucleators.* Curr Opin Cell Biol, 2008. 20(5): p. 495-501.

40. Cao, H. and N. Kuboyama, *A biodegradable porous composite scaffold of PGA/beta-TCP for bone tissue engineering.* Bone, 2010. 46(2): p. 386-95.

41. Bose, S., S. Vahabzadeh, and A. Bandyopadhyay, *Bone tissue engineering using 3D printing.* Materials Today, 2013. 16(12): p. 496-504.

42. Kolesky, D.B., et al., *3D bioprinting of vascularized, heterogeneous cell-laden tissue constructs.* Adv Mater, 2014. 26(19): p. 3124-30.

43. Hasan, A., et al., *Electrospun scaffolds for tissue engineering of vascular grafts.* Acta Biomater, 2014. 10(1): p. 11-25.

44. Zheng, W., W. Zhang, and X. Jiang, *Biomimetic Collagen Nanofibrous Materials for Bone Tissue Engineering.* Advanced Engineering Materials, 2010. 12(9): p. B451-B466.

45. Zhu, N. and X. Chen, *Biofabrication of Tissue Scaffolds*. Advances in Biomaterials Science and Biomedical Applications. 2013.

46. Kundu, J., et al., *Chapter 2 - Biomaterials for Biofabrication of 3D Tissue Scaffolds*, in *Biofabrication*, G. Forgacs and W. Sun, Editors. 2013, William Andrew Publishing: Boston. p. 23-46.

CHAPTER 2

1. Doillon, C.J., *Skin replacement using collagen extracted from bovine hide.* Clin Mater, 1992. 9(3-4): p. 189-93.

2. Oliveira, M.R., et al., *Tissue Engineering: Using Collagen Type I Matrix for Bone Healing of Bone Defects.* Journal of Craniofacial Surgery, 2013. 24(4): p. E394-E396.

3. Pritikin, W.B., *Microscopic structure of small diameter reconstituted collagen sausage casings.* Microscope, 1975. 23(2): p. 103-108.

4. Beghetto, V., et al., *The Leather Industry: A Chemistry Insight Part 1: an Overview of the Industrial Process.* Science at Ca'Foscari, 2013: p. 13-22.

5. Rauterbe.J, R. Timpl, and Furthmay.H, *Structural characterization of n-terminal antigenic determinants in calf and human collagen.* European Journal of Biochemistry, 1972. 27(2): p. 231-&.

6. Bunyaratavej, P. and H.L. Wang, *Collagen membranes: A review.* Journal of Periodontology, 2001. 72(2): p. 215-229.

7. Berglund, J.D., et al., *A biological hybrid model for collagen-based tissue engineered vascular constructs.* Biomaterials, 2003. 24(7): p. 1241-1254.

8. Kadler, K.E., et al., *Collagens at a glance.* Journal of Cell Science, 2007. 120(12): p. 1955-1958.

9. Xiong, X., et al., *A new procedure for rapid, high yield purification of Type I collagen for tissue engineering.* Process Biochemistry, 2009. 44(11): p. 1200-1212.

10. Benjakul, S., et al., *Extraction and characterisation of pepsin-solubilised collagens from the skin of bigeye snapper (Priacanthus tayenus and Priacanthus macracanthus).* J Sci Food Agric, 2010. 90(1): p. 132-8.

11. Kadler, K.E., Y. Hojima, and D.J. Prockop, *Assembly of type-I collagen fibrils denovo - between 37-degrees and 41-degrees-C the process is limited by micro-unfolding of monomers.* Journal of Biological Chemistry, 1988. 263(21): p. 10517-10523.

12. Li, D., W. Yang, and G.Y. Li, *Extraction of native collagen from limed bovine split wastes through improved pretreatment methods.* Journal of Chemical Technology and Biotechnology, 2008. 83(7): p. 1041-1048.

13. Badylak, S.F. and T.W. Gilbert, *Immune response to biologic scaffold materials.* Semin Immunol, 2008. 20(2): p. 109-16.

14. Michael, J.Y., T. Louis, and L.P. Robert, *Collagen Processing*, in *Encyclopedia of Biomaterials and Biomedical Engineering*. 2013, Taylor & Francis. p. 348-354.

15. Zhang, Z.K., G.Y. Li, and B. Shi, *Physicochemical properties of collagen, gelatin and collagen hydrolysate derived from bovine limed split wastes.* Journal of the Society of Leather Technologists and Chemists, 2006. 90(1): p. 23-28.

16. Keech, M.K., *The effect of collagenase and trypsin on collagen-an electron microscopic study* Anatomical Record, 1954. 119(2): p. 139-159.

17. Drake, M.P., et al., *Action of proteolytic enzymes on tropocollagen and insoluble collagen.* Biochemistry, 1966. 5(1): p. 301-312.

18. Elsdale, T. and J. Bard, *Collagen substrata for studies on cell behavior.* J Cell Biol, 1972. 54(3): p. 626-37.

19. Yost, M.J., L. Terracio, and R.L. Price, *Collagen Processing*, in *Encyclopedia of Biomaterials and Biomedical Engineering*. 2013, Taylor & Francis. p. 348-354.

20. Veis, A. and K. Payne, *Collagen fibrillogenesis*. Collagen. Biochemistry. 1988, Boca Raton: CRC Press. 113.

21. Kadler, K.E., et al., *Collagen fibril formation.* Biochemical Journal, 1996. 316: p. 1-11.

22. Holmes, D.F., M.J. Capaldi, and J.A. Chapman, *Reconstitution of collagen fibrils in vitro; the assembly process depends on the initiating procedure.* International Journal of Biological Macromolecules, 1986. 8(3): p. 161-166.

23. Kreger, S.T., et al., *Polymerization and matrix physical properties as important design considerations for soluble collagen formulations.* Biopolymers, 2010. 93(8): p. 690-707.

24. Kuznetsova, N. and S. Leikin, *Does the triple helical domain of type I collagen encode molecular recognition and fiber assembly while telopeptides serve as catalytic domains? Effect of proteolytic cleavage on fibrillogenesis and on collagen-collagen interaction in fibers.* J Biol Chem, 1999. 274(51): p. 36083-8.

25. Harris, J.R., A. Soliakov, and R.J. Lewis, *In vitro fibrillogenesis of collagen type I in varying ionic and pH conditions.* Micron, 2013. 49: p. 60-8.

26. Trelstad, R.L., D.E. Birk, and F.H. Silver, *Collagen fibrillogenesis in tissues, in solution and from modeling - a synthesis.* Journal of Investigative Dermatology, 1982. 79: p. S109-S112.

CHAPTER 3

1. Huang, Z.-M., et al., *A review on polymer nanofibers by electrospinning and their applications in nanocomposites.* Composites Science and Technology, 2003. **63**(15): p. 2223-2253.
2. Matthews, J.A., et al., *Electrospinning of Collagen Nanofibers.* Biomacromolecules, 2002. **3**(2): p. 232-238.
3. Hasan, A., et al., *Electrospun scaffolds for tissue engineering of vascular grafts.* Acta Biomater, 2014. **10**(1): p. 11-25.
4. Liu, T., et al., *Nanofibrous collagen nerve conduits for spinal cord repair.* Tissue Eng Part A, 2012. **18**(9-10): p. 1057-66.
5. Prabhakaran, M.P., J. Venugopal, and S. Ramakrishna, *Electrospun nanostructured scaffolds for bone tissue engineering.* Acta Biomaterialia, 2009. **5**(8): p. 2884-2893.
6. Jeong, S.I., et al., *In vivo biocompatibilty and degradation behavior of elastic poly(L-lactide-co-epsilon-caprolactone) scaffolds.* Biomaterials, 2004. **25**(28): p. 5939-46.
7. Kretlow, J.D., L. Klouda, and A.G. Mikos, *Injectable matrices and scaffolds for drug delivery in tissue engineering.* Adv Drug Deliv Rev, 2007. **59**(4-5): p. 263-73.
8. Oh, S., *Fabrication and characterization of hydrophilic poly(lactic-co-glycolic acid)/poly(vinyl alcohol) blend cell scaffolds by melt-molding particulate-leaching method.* Biomaterials, 2003. **24**(22): p. 4011-4021.

9. Nugent, H.M. and E.R. Edelman, *Tissue engineering therapy for cardiovascular disease.* Circ Res, 2003. **92**(10): p. 1068-78.

10. Yost, M.J., et al., *A novel tubular scaffold for cardiovascular tissue engineering.* Tissue Eng, 2004. **10**(1-2): p. 273-84.

11. Whelan, M.C. and D.R. Senger, *Collagen I initiates endothelial cell morphogenesis by inducing actin polymerization through suppression of cyclic AMP and protein kinase A.* J Biol Chem, 2003. **278**(1): p. 327-34.

12. Mason, B.N., et al., *Tuning three-dimensional collagen matrix stiffness independently of collagen concentration modulates endothelial cell behavior.* Acta Biomater, 2013. **9**(1): p. 4635-44.

13. Zheng, W., W. Zhang, and X. Jiang, *Biomimetic Collagen Nanofibrous Materials for Bone Tissue Engineering.* Advanced Engineering Materials, 2010. **12**(9): p. B451-B466.

14. Fann, S.A., et al., *A model of tissue-engineering ventral hernia repairs.* Journal of Investigative Surgery, 2006: p. 193-205.

15. Hofman, K., et al., *Effects of the molecular format of collagen on characteristics of electrospun fibres.* Journal of Materials Science, 2011. **47**(3): p. 1148-1155.

16. Guarino, V., et al., *Polylactic acid fibre-reinforced polycaprolactone scaffolds for bone tissue engineering.* Biomaterials, 2008. **29**(27): p. 3662-3670.

17. Khadka, D.B. and D.T. Haynie, *Protein- and peptide-based electrospun nanofibers in medical biomaterials.* Nanomedicine, 2012. **8**(8): p. 1242-62.

18. Shin, Y.M., et al., *Electrospinning: A whipping fluid jet generates submicron polymer fibers.* Applied Physics Letters, 2001. **78**(8): p. 1149.

19. Yang, L., et al., *Mechanical properties of single electrospun collagen type I fibers.* Biomaterials, 2008. **29**(8): p. 955-962.

20. Dong, B., et al., *Electrospinning of Collagen Nanofiber Scaffolds from Benign Solvents.* Macromolecular Rapid Communications, 2009. **30**(7): p. 539-542.

21. Zeugolis, D.I., et al., *Electro-spinning of pure collagen nano-fibres – Just an expensive way to make gelatin?* Biomaterials, 2008. **29**(15): p. 2293-2305.

22. Hanaichi, T., et al., *A stable lead by modification of sato method.* Journal of Electron Microscopy, 1986. **35**(3): p. 304-306.

23. Zhang, Z.K., G.Y. Li, and B. Shi, *Physicochemical properties of collagen, gelatin and collagen hydrolysate derived from bovine limed split wastes.* Journal of the Society of Leather Technologists and Chemists, 2006. **90**(1): p. 23-28.

24. Keech, M.K., *The effect of collagenase and trypsin on collagen-an electron microscopic study* Anatomical Record, 1954. **119**(2): p. 139-159.

25. Drake, M.P., et al., *Action of proteolytic enzymes on tropocollagen and insoluble collagen.* Biochemistry, 1966. **5**(1): p. 301-312.

26. Czajka, C.A. and C.J. Drake, *Self-Assembly of Prevascular Tissues from Endothelial and Fibroblast Cells under Scaffold-Free, Non-adherent Conditions.* Tissue Eng Part A, 2014.

27. Reznikov, N., R. Shahar, and S. Weiner, *Three-dimensional structure of human lamellar bone: the presence of two different materials and new insights into the hierarchical organization.* Bone, 2014. **59**: p. 93-104.

28. Liu, T., et al., *Photochemical crosslinked electrospun collagen nanofibers: synthesis, characterization and neural stem cell interactions.* J Biomed Mater Res A, 2010. **95**(1): p. 276-82.

29. Trelstad, R.L., K. Hayashi, and J. Gross, *Collagen fibrillogenesis: intermediate aggregates and suprafibrillar order.* Proc Natl Acad Sci U S A, 1976. **73**(11): p. 4027-31.

30. Harris, J.R., A. Soliakov, and R.J. Lewis, *In vitro fibrillogenesis of collagen type I in varying ionic and pH conditions.* Micron, 2013. **49**: p. 60-8.

31. Holmes, D.F., M.J. Capaldi, and J.A. Chapman, *Reconstitution of collagen fibrils in vitro; the assembly process depends on the initiating procedure.* International Journal of Biological Macromolecules, 1986. **8**(3): p. 161-166.

32. Hartman, O., et al., *Microfabricated electrospun collagen membranes for 3-D cancer models and drug screening applications.* Biomacromolecules, 2009. **10**(8): p. 2019-32.

33. Shih, Y.R., et al., *Growth of mesenchymal stem cells on electrospun type I collagen nanofibers.* Stem Cells, 2006. **24**(11): p. 2391-7.

34. Yang, L., et al., *Mechanical properties of single electrospun collagen type I fibers.* Biomaterials, 2008. **29**(8): p. 955-62.

35. MacKinnon, P.A., et al., *Electron microscopy study of refractory ceramic fibers.* Appl Occup Environ Hyg, 2001. **16**(10): p. 944-51.

CHAPTER 4

1. Usas, A. and J. Huard, *Muscle-derived stem cells for tissue engineering and regenerative therapy.* Biomaterials, 2007. **28**(36): p. 5401-5406.
2. Grefte, S., et al., *Model for Muscle Regeneration around Fibrotic Lesions in Recurrent Strain Injuries.* Medicine and Science in Sports and Exercise, 2010. **42**(4): p. 813-819.
3. Abedi, G., et al., *A Collagen-Poly(vinyl alcohol) Nanofiber Scaffold for Cartilage Repair.* 2010: p. 1-11.
4. De Coppi, P., et al., *Myoblast-acellular skeletal muscle matrix constructs guarantee a long-term repair of experimental full-thickness abdominal wall defects.* Tissue Engineering, 2006. **12**(7): p. 1929-1936.
5. Gilbert, P.M., et al., *Substrate Elasticity Regulates Skeletal Muscle Stem Cell Self-Renewal in Culture.* Science, 2010. **329**(5995): p. 1078-1081.
6. Levenberg, S., et al., *Engineering vascularized skeletal muscle tissue.* Nature Biotechnology, 2005. **23**(7): p. 879-884.
7. Boonen, K.J.M. and M.J. Post, *The Muscle Stem Cell Niche: Regulation of Satellite Cells During Regeneration.* Tissue Engineering Part B-Reviews, 2008. **14**(4): p. 419-431.
8. Lutolf, M.P. and J.A. Hubbell, *Synthesis and Physicochemical Characterization of End-Linked Poly(ethylene glycol)-co-peptide Hydrogels Formed by Michael-Type Addition.* Biomacromolecules, 2003. **4**(3): p. 713-722.

9. Bott, K., et al., *The effect of matrix characteristics on fibroblast proliferation in 3D gels.* Biomaterials, 2010. **31**(32): p. 8454-8464.

10. Yost, M.J.B.C.F.S., Charles E.; Goodwin, Richard L.; Price, Robert L.; Davis, Jeffrey M.; Evans, Heather; Watson, Phillip D.; Gore, Michael; Sweet, Janet; Creech, Laura; Zile, Michael R.; Terracio, Louis, *A Novel Tubular Scaffold for Cardiovascular Tissue Engineering.* Tissue Engineering, 2004. **10**(1/2): p. 273-284.

11. Seale, P., et al., *Pax7 Is Required for the Specification of Myogenic Satellite Cells.* Cell, 2000. **102**(6): p. 777-786.

12. Megeney, L.A., et al., *MyoD is required for myogenic stem cell function in adult skeletal muscle.* Genes & Development, 1996. **10**: p. 1173-1183.

13. Zammit, P.S., et al., *Kinetics of Myoblast Proliferation Show That Resident Satellite Cells Are Competent to Fully Regenerate Skeletal Muscle Fibers.* Experimental Cell Research, 2002. **281**(1): p. 39-49.

14. Zammit, P.S., et al., *Pax7 and myogenic progression in skeletal muscle satellite cells.* Journal of Cell Science, 2006. **119**(9): p. 1824-1832.

15. Blanco-Bose, W.E., et al., *Purification of Mouse Primary Myoblasts Based on α7 Integrin Expression.* Experimental Cell Research, 2001. **265**(2): p. 212-220.

16. Cachaço, A.S., et al., *Integrin Repertoire on Myogenic Cells Changes During the Course of Primary Myogenesis in the Mouse.* Developmental Dynamics, 2005. **232**: p. 1069-1078.

17. Ozeki, N., et al., *α7 integrin expressing human fetal myogenic progenitors have stem cell-like properties and are capable of osteogenic differentiation.* Experimental Cell Research, 2006. **312**(20): p. 4162-4180.

18. Zammit, P.S., et al., *Pax7 and myogenic progression in skeletal muscle satellite cells.* Journal of Cell Science, 2006. **119**: p. 1824-1832.

19. Bott, K., et al., *The effect of matrix characteristics on fibroblast proliferation in 3D gels.* Biomaterials, 2010. **31**: p. 8454-8464.

20. Collins, C.A., et al., *Stem Cell Function, Self-Renewal, and Behavioral Heterogeneity of Cells from the Adult Muscle Satellite Cell Niche.* Cell, 2005. **122**: p. 289-301.

CHAPTER 5

1. Kundu, J., et al., *Chapter 2 - Biomaterials for Biofabrication of 3D Tissue Scaffolds,* in *Biofabrication,* G. Forgacs and W. Sun, Editors. 2013, William Andrew Publishing: Boston. p. 23-46.

2. Vats, A., et al., *Scaffolds and biomaterials for tissue engineering: a review of clinical applications.* Clinical Otolaryngology, 2003. **28**(3): p. 165-172.

3. Chan, B.P. and K.W. Leong, *Scaffolding in tissue engineering: general approaches and tissue-specific considerations.* Eur Spine J, 2008. **17 Suppl 4**: p. 467-79.

4. Salerno, A., et al., *Tailoring the pore structure of PCL scaffolds for tissue engineering prepared via gas foaming of multi-phase blends.* Journal of Porous Materials, 2011. **19**(2): p. 181-188.

5. Hasan, A., et al., *Electrospun scaffolds for tissue engineering of vascular grafts.* Acta Biomater, 2014. **10**(1): p. 11-25.

6. Huang, Z.-M., et al., *A review on polymer nanofibers by electrospinning and their applications in nanocomposites.* Composites Science and Technology, 2003. **63**(15): p. 2223-2253.

7. Sell, S.A., et al., *Electrospinning of collagen/biopolymers for regenerative medicine and cardiovascular tissue engineering.* Advanced Drug Delivery Reviews, 2009. **61**(12): p. 1007-1019.

8. Zheng, W., W. Zhang, and X. Jiang, *Biomimetic Collagen Nanofibrous Materials for Bone Tissue Engineering.* Advanced Engineering Materials, 2010. **12**(9): p. B451-B466.

9. Cao, H. and N. Kuboyama, *A biodegradable porous composite scaffold of PGA/beta-TCP for bone tissue engineering.* Bone, 2010. **46**(2): p. 386-95.

10. Ankam, S., et al., *Substrate topography and size determine the fate of human embryonic stem cells to neuronal or glial lineage.* Acta Biomater, 2013. **9**(1): p. 4535-45.

11. Bose, S., S. Vahabzadeh, and A. Bandyopadhyay, *Bone tissue engineering using 3D printing.* Materials Today, 2013. **16**(12): p. 496-504.

12. Yost, M.J., et al., *A novel tubular scaffold for cardiovascular tissue engineering.* Tissue Eng, 2004. **10**(1-2): p. 273-84.

13. Lundgren, E., et al., *Extracellular matrix components influence the survival of adult cardiac myocytes in vitro.* Exp Cell Res, 1985. **158**(2): p. 371-81.

14. Tanford, C. and J.G. Buzzell, *The Viscosity of Aqueous Solutions of Bovine Serum Albumin between pH 4.3 and 10.5.* The Journal of Physical Chemistry, 1956. **60**(2): p. 225-231.

15. Yadav, S., S.J. Shire, and D.S. Kalonia, *Viscosity analysis of high concentration bovine serum albumin aqueous solutions.* Pharm Res, 2011. **28**(8): p. 1973-83.

16. Tobitani, A. and S.B. Ross-Murphy, *The intrinsic viscosity of polyelectrolytes revisited.* Polymer International, 1997. **44**(3): p. 338-347.

17. Arakawa, T. and S.N. Timasheff, *Theory of protein solubility.* Methods in Enzymology, 1985. **114**: p. 49-77.

18. Habeeb, A.F.S.A. and R. Hiramoto, *Reaction of proteins with glutaraldehyde.* Archives of Biochemistry and Biophysics, 1968. **126**(1): p. 16-26.

19. Migneault, I., et al., *Glutaraldehyde: behavior in aqueous solution, reaction with proteins, and application to enzyme crosslinking.* Biotechniques, 2004. **37**(5): p. 790-6, 798-802.

20. Burmeister, J.J., et al., *Glutaraldehyde cross-linked glutamate oxidase coated microelectrode arrays: selectivity and resting levels of glutamate in the CNS.* ACS Chem Neurosci, 2013. **4**(5): p. 721-8.

21. Chatterji, P.R., *Gelatin with hydrophilic/hydrophobic grafts and glutaraldehyde crosslinks.* Journal of Applied Polymer Science, 1989. **37**(8): p. 2203-2212.

22. Silva, C., et al., *Chemical modifications on proteins using glutaraldehyde.* Food Technology and Biotechnology, 2004. **42**(1): p. 51-56.

23. Peters, T., Jr. and A.J. Stewart, *Albumin research in the 21st century.* Biochim Biophys Acta, 2013. **1830**(12): p. 5351-3.

24. Masuelli, M.A., *Study of Bovine Serum Albumin Solubility in Aqueous Solutions by Intrinsic Viscosity Measurements.* Advances in Physical Chemistry, 2013. **2013**: p. 1-8.

25. Habeeb, A.J. and R. Hiramoto, *Reaction of proteins with glutaraldehyde.* Arch Biochem Biophys, 1968. **126**(1): p. 16-26.

26. Freije, J.R., et al., *Chemically modified, immobilized trypsin reactor with improved digestion efficiency.* J Proteome Res, 2005. **4**(5): p. 1805-13.

27. Lemaire, S.A., et al., *Nerve and conduction tissue injury caused by contact with BioGlue.* J Surg Res, 2007. **143**(2): p. 286-93.

28. Furst, W. and A. Banerjee, *Release of glutaraldehyde from an albumin-glutaraldehyde tissue adhesive causes significant in vitro and in vivo toxicity.* Ann Thorac Surg, 2005. **79**(5): p. 1522-8; discussion 1529.

CHAPTER 6

1. Cleary, M.A., et al., *Vascular tissue engineering: the next generation.* Trends Mol Med, 2012. **18**(7): p. 394-404.

2. Ott, H.C., et al., *Perfusion-decellularized matrix: using nature's platform to engineer a bioartificial heart.* Nat Med, 2008. **14**(2): p. 213-21.

3. Ankam, S., et al., *Substrate topography and size determine the fate of human embryonic stem cells to neuronal or glial lineage.* Acta Biomater, 2013. **9**(1): p. 4535-45.

4. Yim, E.K., S.W. Pang, and K.W. Leong, *Synthetic nanostructures inducing differentiation of human mesenchymal stem cells into neuronal lineage.* Exp Cell Res, 2007. **313**(9): p. 1820-9.

5. Zhao, Y., et al., *Fabrication of skeletal muscle constructs by topographic activation of cell alignment.* Biotechnol Bioeng, 2009. **102**(2): p. 624-31.

6. Yost, M.J., et al., *A novel tubular scaffold for cardiovascular tissue engineering.* Tissue engineering, 2004. **10**(1-2): p. 273-84.

7. Badylak, S.F., et al., *Engineered whole organs and complex tissues.* Lancet, 2012. **379**(9819): p. 943-952.

8. Song, J.J., et al., *Regeneration and experimental orthotopic transplantation of a bioengineered kidney.* Nature Medicine, 2013. **19**(5): p. 646-651.

9. Badylak, S.F. and T.W. Gilbert, *Immune response to biologic scaffold materials.* Semin Immunol, 2008. **20**(2): p. 109-16.

10. Tobita, K., et al., *Engineered early embryonic cardiac tissue retains proliferative and contractile properties of developing embryonic myocardium.* American Journal of Physiology - Heart and Circulatory Physiology, 2006. **291**(4): p. H1829-H1837.

11. LERMAN, L.O., et al., *Noninvasive Evaluation of a Novel Swine Model of Renal Artery Stenosis.* Journal of the American Society of Nephrology, 1999. **10**(7): p. 1455-1465.

12. Clyman, R.I., K.A. McDonald, and R.H. Kramer, *Integrin receptors on aortic smooth muscle cells mediate adhesion to fibronectin, laminin, and collagen.* Circulation Research, 1990. **67**(1): p. 175-186.
13. Briggs, J.D., *Causes of death after renal transplantation.* Nephrology Dialysis Transplantation, 2001. **16**(8): p. 1545-1549.
14. O'Connor, K.J. and F.L. Delmonico, *Increasing the supply of kidneys for transplantation.* Seminars in Dialysis, 2005. **18**(6): p. 460-462.
15. Peloso, A., et al., *Considerations on the development of a model of kidney bioengineering and regeneration in rats.* Expert Review of Medical Devices, 2013. **10**(5): p. 597-601.

CHAPTER 7

1. Moore, K.A. and I.R. Lemischka, *Stem cells and their niches.* Science, 2006. **311**(5769): p. 1880-5.
2. Kshitiz, et al., *Control of stem cell fate and function by engineering physical microenvironments.* Integrative Biology, 2012. **4**(9): p. 1008.
3. Xiong, X., et al., *A new procedure for rapid, high yield purification of Type I collagen for tissue engineering.* Process Biochemistry, 2009. **44**(11): p. 1200-1212.
4. Obrink, B., *Study of interactions between monomeric tropocollagen and glycosaminoglycans.* European Journal of Biochemistry, 1973. **33**(2): p. 387-400.

5. Vogel, K.G., M. Paulsson, and D. Heinegard, *Specific-inhibition of type-i and type-ii collagen fibrillogenesis by the small proteoglycan of tendon.* Biochemical Journal, 1984. **223**(3): p. 587-597.

6. Badylak, S.F. and T.W. Gilbert, *Immune response to biologic scaffold materials.* Semin Immunol, 2008. **20**(2): p. 109-16.

7. Yang, L., et al., *Mechanical properties of single electrospun collagen type I fibers.* Biomaterials, 2008. **29**(8): p. 955-62.

8. Matthews, J.A., et al., *Electrospinning of Collagen Nanofibers.* Biomacromolecules, 2002. **3**(2): p. 232-238.

9. Zeugolis, D.I., et al., *Electro-spinning of pure collagen nano-fibres – Just an expensive way to make gelatin?* Biomaterials, 2008. **29**(15): p. 2293-2305.

10. Engler, A.J., et al., *Matrix Elasticity Directs Stem Cell Lineage Specification.* Cell, 2006. **126**(4): p. 677-689.

11. Gilbert, P.M., et al., *Substrate elasticity regulates skeletal muscle stem cell self-renewal in culture.* Science (New York, N.Y.), 2010. **329**(5995): p. 1078-81.

12. Yost, M.J., et al., *A novel tubular scaffold for cardiovascular tissue engineering.* Tissue Eng, 2004. **10**(1-2): p. 273-84.

13. Whelan, M.C. and D.R. Senger, *Collagen I initiates endothelial cell morphogenesis by inducing actin polymerization through suppression of cyclic AMP and protein kinase A.* J Biol Chem, 2003. **278**(1): p. 327-34.

14. Gelse, K., *Collagens—structure, function, and biosynthesis.* Advanced Drug Delivery Reviews, 2003. **55**(12): p. 1531-1546.

15. Humes, H.D., et al., *Replacement of renal function in uremic animals with a tissue-engineered kidney.* Nature Biotechnology, 1999. **17**(5): p. 451-455.

16. Song, J.J., et al., *Regeneration and experimental orthotopic transplantation of a bioengineered kidney.* Nature Medicine, 2013. **19**(5): p. 646-651.

APPEDIX A:

SUPPLEMENTAL FIGURES AND TABLE FOR CHAPTER 3

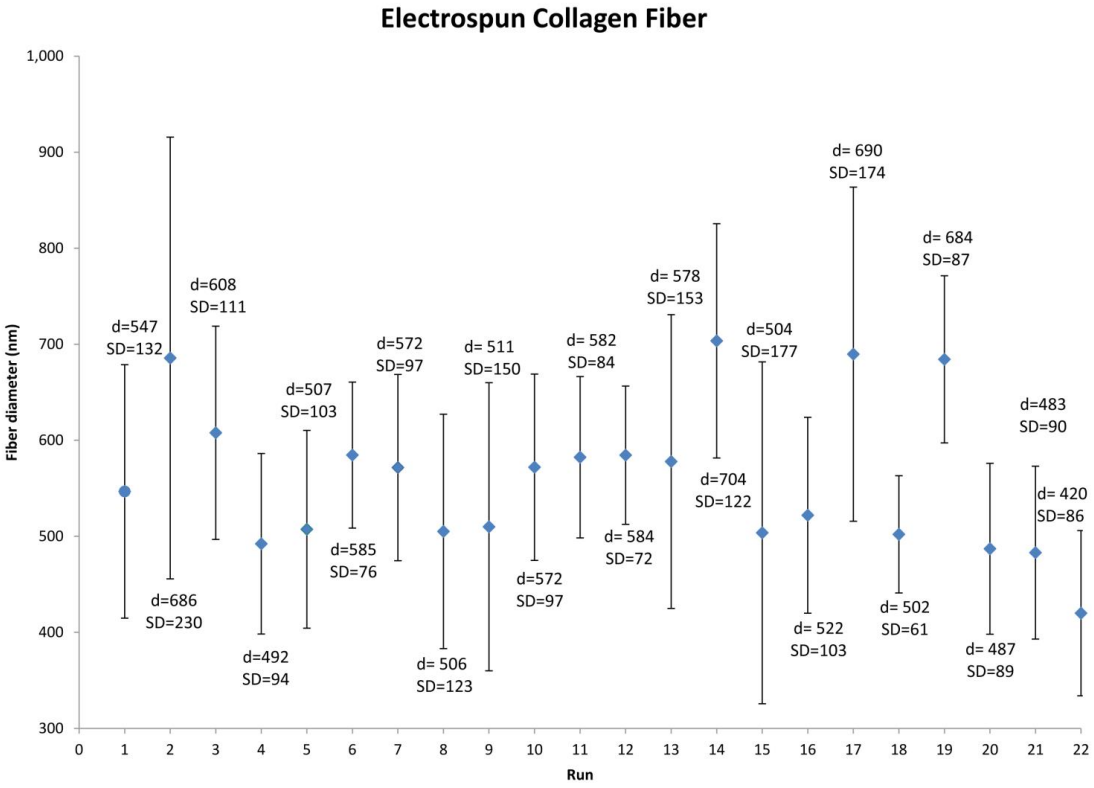

Figure A.1. Fiber diameter distribution for 2% electrospun collagen fibers using the parameters described in Table A.1. Nine fibers were randomly selected and measured. (d = average diameter of the nine fibers per run; SD = standard deviation per run).

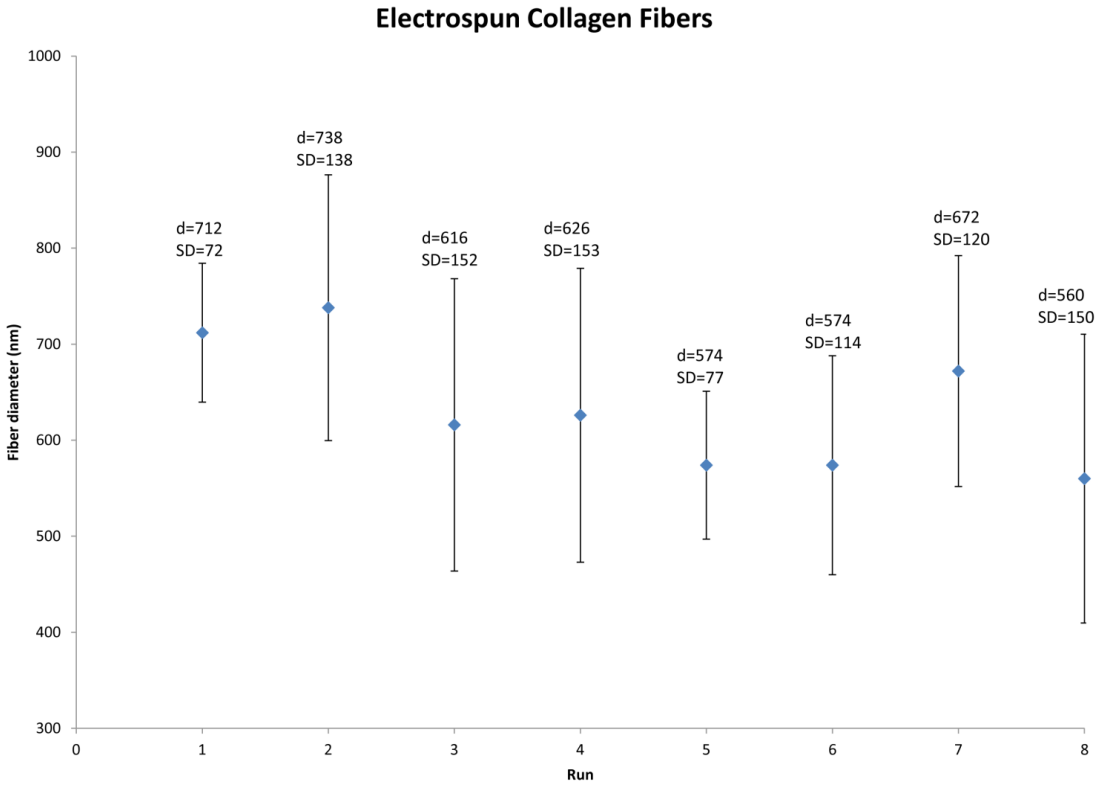

Figure A.2. Fiber diameter distribution of 1 and 2.5% electrospun collagen fibers is shown using the parameters in Table A.4. Nine fibers were randomly selected and measured. (d = average diameter of the nine fibers per run; SD = standard deviation per run).

Table A.1. Electrospinning parameters for 2% collagen.

Run	Field Strength (KV)	Flow Rate (cc/min)	Gap (cm)	Gauge
1	20	0.5	5	20
2	15	1	5	20
3	15	0.5	7	20
4	20	0.5	7	20
5	20	1	7	21
6	20	0.5	7	21
7	20	0.5	5	20
8	15	0.5	7	21
9	20	1	5	21
10	15	0.5	7	21
11	15	1	5	21
12	20	1	5	20
13	15	1	7	20
14	15	1	7	21
15	20	0.5	5	20
16	15	0.5	5	21
17	15	1	5	21
18	20	1	7	21
19	15	1	7	20
20	15	0.5	5	20
21	20	1	7	20
22	20	0.5	5	21

Table A.2. Statistical analysis of the effect of field, flow rate, gap, and needle gauge on the fiber diameter of 2% electrospun collagen (Table A.1). The gap and needle gauge are not significant in the fiber diameter outcome.

ANOVA Results					
	df	***SS***	***MS***	***F***	***Significance F***
Regression	4	5.82E+04	1.46E+04	3.70E+00	2.43E-02
Residual	17	6.69E+04	3.94E+03		
Total	21	1.25E+05			

Regression Analysis				
	Coefficients	***Standard Error***	***t Stat***	***P-value***
Intercept	5.60E+02	1.34E+01	4.19E+01	1.36E-18
Field	-3.99E+01	1.35E+01	-2.95E+00	8.99E-03
Flow rate	2.92E+01	1.35E+01	2.16E+00	4.56E-02
Gap	1.24E-01	1.35E+01	9.17E-03	9.93E-01
Gauge	1.20E+01	1.35E+01	8.89E-01	3.87E-01

Table A.3. Statistical analysis of the effect of field and flow rate on the fiber diameter of 2% electrospun collagen (Table A.1). The field and the flow rate significantly affect the fiber diameter of the spun fibers.

ANOVA Results					
	df	***SS***	***MS***	***F***	***Significance F***
Regression	2	5.51E+04	2.75E+04	7.47E+00	4.04E-03
Residual	19	7.01E+04	3.69E+03		
Total	21	1.25E+05			

Regression Analysis				
	Coefficients	***Standard Error***	***t Stat***	***P-value***
Intercept	5.60E+02	1.29E+01	4.33E+01	1.90E-20
Field	-3.89E+01	1.30E+01	-2.99E+00	7.52E-03
Flow rate	2.82E+01	1.30E+01	2.17E+00	4.32E-02

Table A.4. Electrospinning parameters tested with 1 and 2.5% collagen solutions.

Runs	Concentration (%)	Field (KV)	Flow Rate (cc/min)
1	2.5	15	1
2	1	15	1
3	2.5	15	0.5
4	1	20	1
5	2.5	20	0.5
6	1	15	0.5
7	2.5	20	1
8	1	20	0.5

Table A.5. Statistical analysis of the effect of field, flow rate, and collagen concentration (1% and 2.5%) on the fiber diameter of electrospun collagen (Table A.4). The collagen concentration did not significantly affect the fiber diameter of the collagen fibers.

ANOVA Results					
	df	***SS***	***MS***	***F***	***Significance F***
Regression	3	2.86E+04	9.53E+03	1.36E+01	1.45E-02
Residual	4	2.81E+03	7.02E+02		
Total	7	3.14E+04			

Regression Analysis				
	Coefficients	***Standard Error***	***t Stat***	***P-value***
Intercept	6.34E+02	9.36E+00	6.77E+01	2.85E-07
Concentration	9.50E+00	9.36E+00	1.01E+00	3.68E-01
Field	-2.60E+01	9.36E+00	-2.78E+00	5.00E-02
Flow Rate	5.30E+01	9.36E+00	5.66E+00	4.80E-03

Table A.6. Statistical analysis of the effect of field and flow rate on the fiber diameter of 1% and 2.5% electrospun collagen fibers (Table A.4). As with the conditions used in the previous experiment (Table A.1), the field and the flow rate significantly affected the fiber diameter of the electrospun collagen fibers.

ANOVA Results					
	df	***SS***	***MS***	***F***	***Significance F***
Regression	2	2.79E+04	1.39E+04	1.98E+01	4.23E-03
Residual	5	3.53E+03	7.06E+02		
Total	7	3.14E+04			

Regression Analysis				
	Coefficients	***Standard Error***	***t Stat***	***P-value***
Intercept	6.34E+02	9.39E+00	6.75E+01	1.35E-08
Field	-2.60E+01	9.39E+00	-2.77E+00	3.94E-02
Flow Rate	5.30E+01	9.39E+00	5.64E+00	2.42E-03

Table A.7. Trypsin digestion assay for the electrospun collagen fibers. The amount of protein that was dissolved by trypsin digestion was quantified using a BCA assay. Using mass balance analysis, we quantify the soluble protein distribution.

Sample	**In (mg)**		**Out (mg)**			
	Fibers	**Enzyme**	**BCA (soluble)**		**Fibers**	
	Collagen	*Trypsin*	*Collagen*	*Trypsin*	*Collagen*	*Trypsin*
1	14.50	10.00	1.10	3.29	13.40	6.71
2	16.90	10.00	1.36	3.49	15.54	6.51
3	12.80	10.00	2.50	4.45	10.30	5.55

APPEDIX B:

SUPPLEMENTAL FIGURES AND TABLE FOR CHAPTER 5

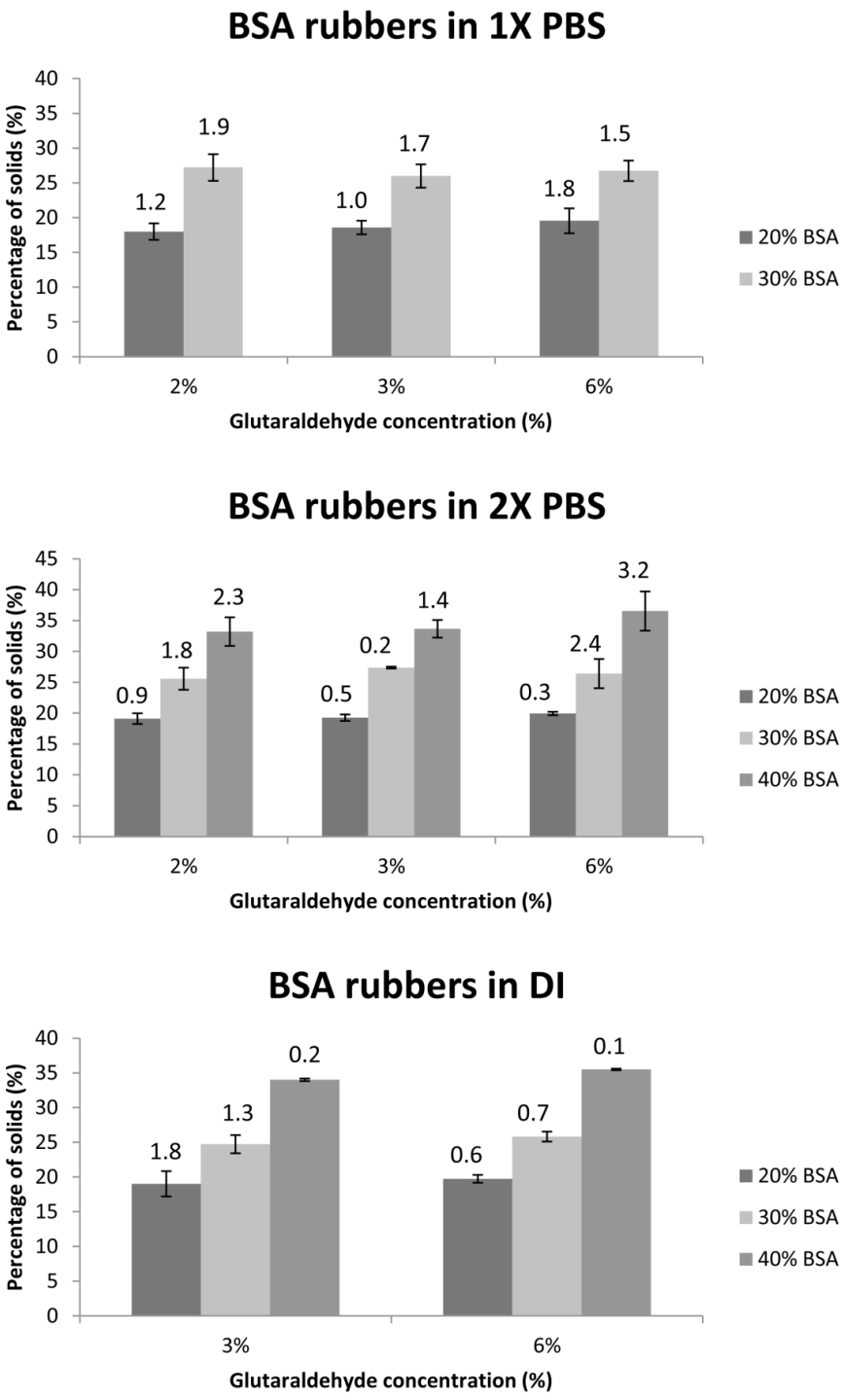

Figure B.1: Solid percentage. We determined the percentage of solids from a wet rubber and determine the solid percentage (dry weight/wet weight). The solvent did not affect the percentage of solids ($p>0.05$).

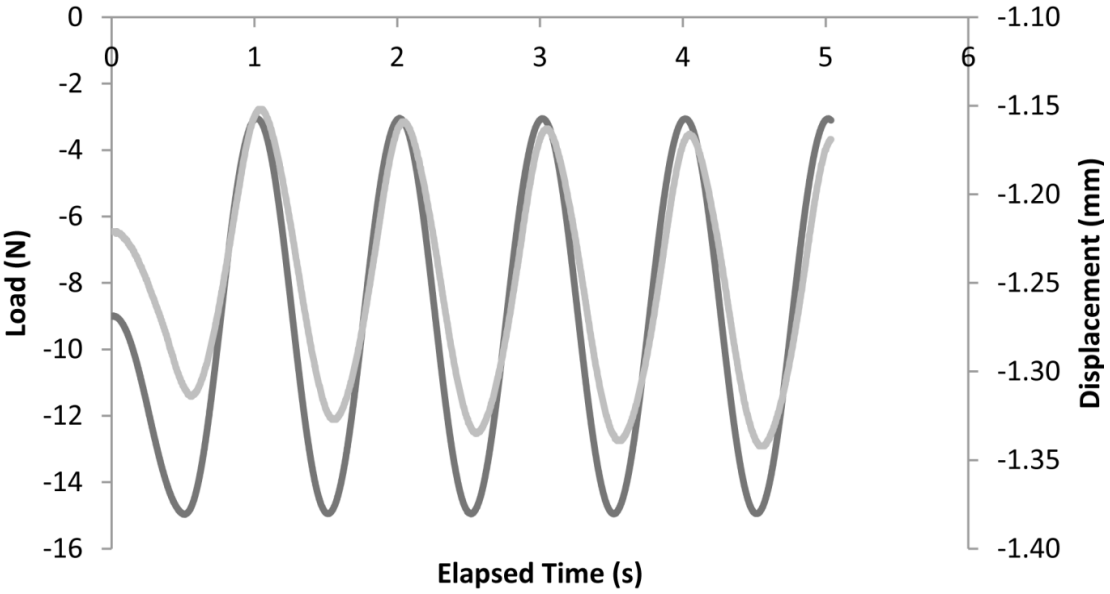

Figure B.2: Sine wave of 30% BSA 3% glutaraldehyde 2× PBS. The compressive load and displacement of the sample are shown as functions of the elapsed time..

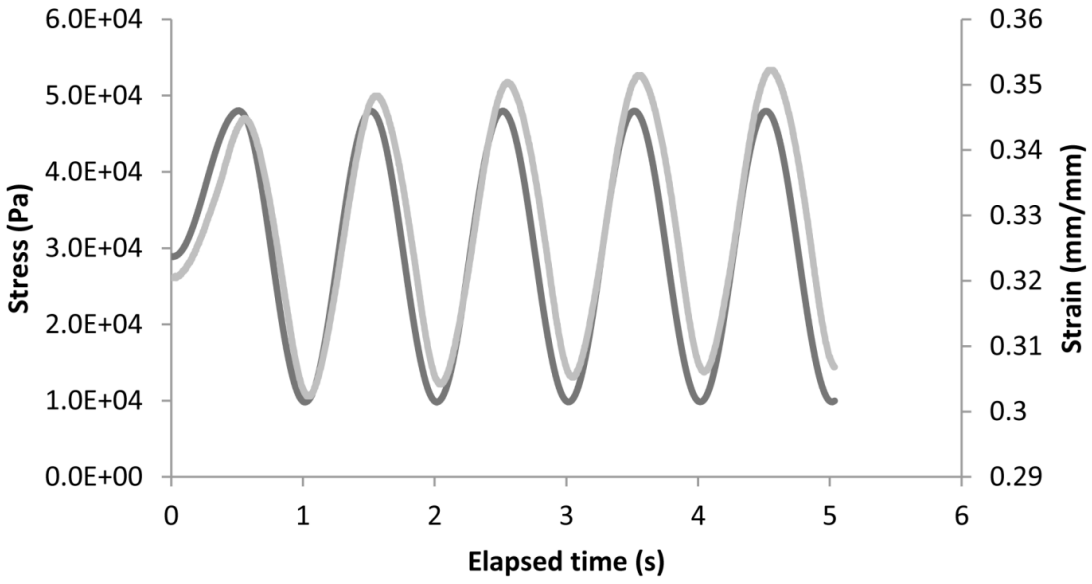

Figure B.3: Sine wave of 30% BSA 3% glutaraldehyde 2× PBS. The stress and strain of the sample were calculated and plotted as a function of elapsed time. There is a small phase shift, indicative of the viscoelastic behavior of the rubber.

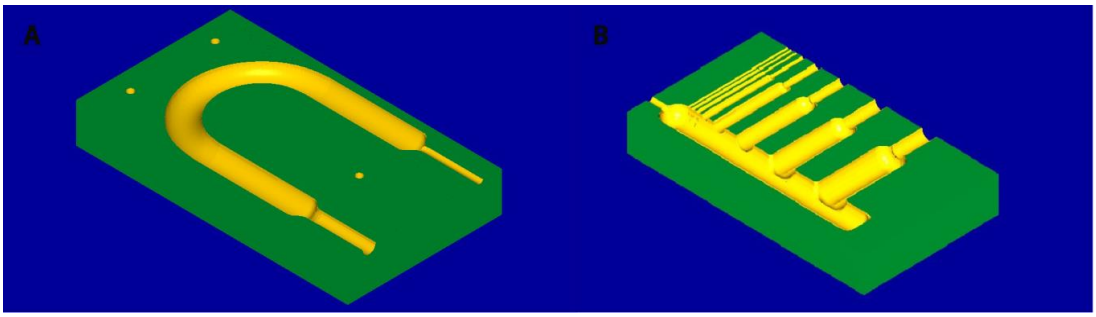

Figure B.4: Mastercam solids. (A) Loop and (B) stability pieces. After designing them using Mastercam, we can import the G code and create a stainless steel or brass piece using the Microlution machine or a PLA piece using the Makerbot.

Table B.1: Compression testing parameters. Using a sine wave, we determined the displacement and the force exerted by four types of rubber.

Limits	Min	Max
Load (N)	-17	3
Displacement (mm)	-1.5	0.3

Wave	Level 1	Level 2	Frequency (Hz)	Cycle
Sine	-15	-3	1	5000

Data Acquisition	
Scan time	1.008
Scan points	360
Number of Scans	5
Subsequent Scan	1.008 sec between scan

Table B.2: Statistical analysis of the percentage of solids in the BSA rubber. The BSA and glutaraldehyde significantly affected the percentage of solids. The solvent did not influence the percentage of solids.

ANOVA Results					
	df	***SS***	***MS***	***F***	***Significance F***
Regression	3	9.85E+02	3.28E+02	4.70E+02	1.06E-18
Residual	20	1.40E+01	6.99E-01		
Total	23	9.99E+02			

Regression Analysis				
	Coefficients	***Standard Error***	***t Stat***	***P-value***
Intercept	1.74E+00	8.23E-01	2.12E+00	4.70E-02
% BSA	7.82E-01	2.09E-02	3.74E+01	5.49E-20
% Glutaraldehyde	3.17E-01	1.03E-01	3.09E+00	5.71E-03
Solvent	2.61E+01	2.22E+01	1.18E+00	2.53E-01

Table B.3: Statistical analysis of the elastic modulus related to the PBS concentration. The PBS concentration significantly affected the elastic modulus. The increase of salts in the solvent caused an increase in the elastic modulus.

ANOVA Results					
	df	***SS***	***MS***	***F***	***Significance F***
Regression	3	3.06E+05	1.02E+05	1.18E+01	4.00E-03
Residual	7	6.07E+04	8.67E+03		
Total	10	3.67E+05			

Regression Analysis				
	Coefficients	***Standard Error***	***t Stat***	***P-value***
Intercept	6.50E+02	4.25E+01	1.53E+01	1.23E-06
BSA (%)	4.67E+00	3.80E+01	1.23E-01	9.06E-01
Solvent	1.02E+02	3.80E+01	2.67E+00	3.20E-02
Glutaraldehyde (%)	1.16E+02	5.70E+01	2.03E+00	8.21E-02

Table B.4: Statistical analysis of the reaction rate after 15 hr of enzyme digestion. The glutaraldehyde concentration significantly affected the reaction rate of the digestion of the rubber by decreasing at higher glutaraldehyde concentrations.

ANOVA Result					
	df	***SS***	***MS***	***F***	***Significance F***
Regression	3	6.15E-15	2.05E-15	3.68E+00	1.67E-02
Residual	60	3.34E-14	5.57E-16		
Total	63	3.96E-14			

Regression Analysis				
	Coefficients	***Standard Error***	***t Stat***	***P-value***
Intercept	3.74E-08	1.37E-08	2.74E+00	8.03E-03
BSA	3.89E-10	3.62E-10	1.07E+00	2.88E-01
Glutaraldehyde	-5.92E-09	1.83E-09	-3.23E+00	2.02E-03
Solvent	-6.78E-08	3.76E-07	-1.80E-01	8.58E-01

Table B.5: Statistical analysis of the reaction rate after 24 hr of enzyme digestion. The BSA and glutaraldehyde concentration significantly affected the reaction rate of the digestion of the rubber. At higher glutaraldehyde concentrations, there is a decrease in the reaction rate. At higher BSA concentrations, there is an increase in the reaction rate.

ANOVA Results					
	df	***SS***	***MS***	***F***	***Significance F***
Regression	3	7.36E-15	2.45E-15	3.62E+01	1.21E-13
Residual	62	4.20E-15	6.78E-17		
Total	65	1.16E-14			

Regression Analysis				
	Coefficients	***Standard Error***	***t Stat***	***P-value***
Intercept	2.98E-08	4.77E-09	6.25E+00	4.22E-08
BSA	4.56E-10	1.26E-10	3.62E+00	6.03E-04
Glutaraldehyde	-6.04E-09	6.15E-10	-9.82E+00	3.00E-14
Solvent	-6.57E-08	1.31E-07	-5.02E-01	6.17E-01

Table B.6: Statistical analysis of the reaction rate after 48 hr of enzyme digestion. The BSA and glutaraldehyde concentration significantly affected the reaction rate of the digestion of the rubber. At higher glutaraldehyde concentrations, there is a decrease in the reaction rate.

ANOVA Results					
	df	***SS***	***MS***	***F***	***Significance F***
Regression	3	3.10E-15	1.03E-15	2.74E+01	1.64E-11
Residual	64	2.42E-15	3.78E-17		
Total	67	5.52E-15			

Regression Analysis				
	Coefficients	***Standard Error***	***t Stat***	***P-value***
Intercept	2.17E-08	3.50E-09	6.20E+00	4.55E-08
BSA	2.13E-10	9.20E-11	2.31E+00	2.39E-02
Glutaraldehyde	-3.94E-09	4.53E-10	-8.70E+00	1.90E-12
Solvent	3.04E-08	9.57E-08	3.18E-01	7.51E-01

Table B.7: Statistical analysis of the reaction rate after 72 hr of enzyme digestion. The BSA and glutaraldehyde concentration significantly affected the reaction rate of the digestion of the rubber. At higher glutaraldehyde concentrations, there is a decrease in the reaction rate. At higher BSA concentrations, there is an increase in the reaction rate.

ANOVA Results					
	df	***SS***	***MS***	***F***	***Significance F***
Regression	3	2.19E-15	7.29E-16	3.05E+01	3.56E-12
Residual	61	1.46E-15	2.39E-17		
Total	64	3.64E-15			

Regression Analysis				
	Coefficients	***Standard Error***	***t Stat***	***P-value***
Intercept	1.05E-08	2.84E-09	3.69E+00	4.80E-04
BSA	3.61E-10	7.48E-11	4.83E+00	9.48E-06
Glutaraldehyde	-3.07E-09	3.69E-10	-8.33E+00	1.21E-11
Solvent	3.97E-08	7.80E-08	5.09E-01	6.12E-01